

7-2018

Fuzzy-Model-Based (FMB) Control of a Spacecraft with Fuel Sloshing Dynamics

Lilit Mazmanyanyan

Santa Clara University, lmazmanyanyan@scu.edu

Follow this and additional works at: https://scholarcommons.scu.edu/eng_phd_theses



Part of the [Mechanical Engineering Commons](#)

Recommended Citation

Mazmanyanyan, Lilit, "Fuzzy-Model-Based (FMB) Control of a Spacecraft with Fuel Sloshing Dynamics" (2018). *Engineering Ph.D. Theses*. 17.

https://scholarcommons.scu.edu/eng_phd_theses/17

This Dissertation is brought to you for free and open access by the Student Scholarship at Scholar Commons. It has been accepted for inclusion in Engineering Ph.D. Theses by an authorized administrator of Scholar Commons. For more information, please contact rsccroggin@scu.edu.

Santa Clara University

Department of Mechanical Engineering

Date: July 2, 2018

I HEREBY RECOMMEND THAT THE THESIS PREPARED UNDER MY
SUPERVISION BY

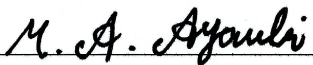
Lilit Mazmanyán

ENTITLED

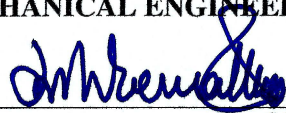
**Fuzzy-Model-Based (FMB) Control of a Spacecraft
with Fuel Sloshing Dynamics**

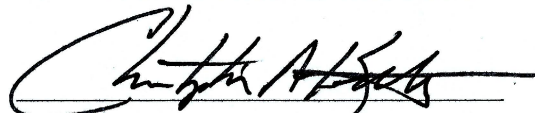
BE ACCEPTED IN PARTIAL FULFILLMENT OF THE REQUIREMENTS FOR
THE DEGREE OF


DOCTOR OF PHILOSOPHY IN MECHANICAL ENGINEERING


Thesis Advisor
Dr. Mohammad A. Ayoubi


Chairman of Department
Dr. Drazen Fabris


Thesis Reader Dr. Mahantesh Hiremath


Thesis Reader Dr. Christopher Kitts


Thesis Reader Dr. On Shun Pak


Thesis Reader Dr. Aleksandar Zecevic

**Fuzzy-Model-Based (FMB) Control of a Spacecraft
with Fuel Sloshing Dynamics**

By

Lilit Mazmanyán

Dissertation

Submitted in Partial Fulfillment of the Requirements
for the Degree of Doctor of Philosophy
in Mechanical Engineering
in the School of Engineering at
Santa Clara University, 2018

Santa Clara, California

To my husband, Michael Okuji and my parents

Acknowledgments

I would like to express my gratitude to my advisor, Professor Mohammad Ayoubi, for his guidance, encouragement, and supervision throughout the various stages of this dissertation. Our stimulating discussions on research problems and his unwavering support during the arduous hours of preparation made it possible for me to complete the work.

I wish to acknowledge the dissertation committee members, Dr. Mahantesh Hiremath, Dr. Christopher Kitts, Dr. On Shun Pak and Dr. Aleksandar Zecevic, for their invaluable feedback that improved my work. I wish to thank Dr. James Longuski and the many anonymous reviewers for their comments which improved my work. A special thank you to my teachers, particularly Dr. Nhan Nguyen and Dr. Arun Banerjee, who inspired me during my course of study.

My thank you, as well, to Dr. Aaron Melman, Dr. Stephen Chiappari, and Heidi Williams, for reviewing some of the published articles, and to department chair Dr. Drazen Fabris for reviewing the thesis; their feedback was extremely valuable.

I am grateful for the opportunity and support provided by the Department of Mechanical Engineering. A portion of my research was supported by the Faculty Summer Scholarship Grant, Santa Clara University. The Packard Research Fellowship in the School of Engineering supported most of my research that was conducted during the 2012-2016 academic years. My heartfelt gratitude goes to the Packard Research Fellowship donors for their generosity without which my work would not have been possible.

I must also acknowledge many friends, particularly Chokri Sendi, for their helpful conversations during the long days of study.

A special thank you goes to my family, particularly my husband, Michael Okuji, for their unwavering support, patience and encouragement throughout my entire effort to write this dissertation.

Fuzzy-Model-Based (FMB) Control of a Spacecraft with Fuel Sloshing Dynamics

Lilit Mazmanyanyan

Department of Mechanical Engineering
Santa Clara University
Santa Clara, California
2018

ABSTRACT

During the upper-stage separation and orbit injection, orbital control, and attitude maneuver, propellant slosh in partially-filled fuel tanks can cause dynamical instability or pointing errors. The spacecraft dynamics combined with propellant sloshing results in a highly nonlinear and coupled dynamic system that requires a complicated control law. This problem has been a long-standing concern for space missions. The purpose of this research is two fold. The first part is to investigate and develop nonlinear Takagi-Sugeno (T-S) fuzzy model-based controllers for a spacecraft with fuel sloshing considering the input constraints on the actuators. It includes i) a fuzzy controller/observer with a minimum upper-bound control input based on the parallel-distributed compensation (PDC) technique, ii) a fuzzy controller/observer based on the linear quadratic regulator (LQR) that uses the premises of the T-S model, and iii) a robust-optimal fuzzy-model-based controller/observer. The designed controllers are globally asymptotically stable and have a satisfactory performance and robustness. The second part of the research is to develop a mathematical model of a spinning spacecraft with fuel sloshing during high-g maneuvers. The equations of motion of a spacecraft with partially-filled multiple-tanks are derived using the Kane's method. To do this, two spherical pendulums as an equivalent mechanical model of the fuel sloshing are adopted. The effect of the slosh model parameters on the spacecraft nutation angle is studied. The developed model is validated via several numerical simulations.

Table of Contents

1	Introduction	1
1.1	Motivation	1
1.2	Spacecraft Anomalies and Failures	1
1.3	Mission Phases	3
1.4	Literature Review	7
1.5	Research Objectives and Thesis Overview	12
2	Dynamics of Spacecraft with Fuel Sloshing	15
2.1	Introduction	15
2.2	Review of Kane’s Method or Virtual Power	15
2.3	Slosh Modeling Techniques	18
2.4	Mathematical Model of Spacecraft with Fuel Sloshing	22
2.4.1	Equations of Motion	22
2.4.2	The Kinematic Equations	25
3	Takagi-Sugeno Fuzzy Modeling	27
3.1	Introduction	27
3.2	T-S Fuzzy Modeling	27

3.3	T-S Fuzzy Observer	30
3.4	T-S Fuzzy Model with Uncertainty	31
3.5	T-S Fuzzy Model Validation	33
4	Fuzzy Controller Design	36
4.1	Introduction	36
4.2	Fuzzy PDC Controller Design	37
4.3	Robust-Optimal Fuzzy Control	41
4.4	Fuzzy LQR Controller Design	45
4.5	PID Controller Design	47
4.6	Numerical Simulation	48
4.6.1	A note on the Interior-Point Method	48
4.6.2	Closed-Loop Simulation	48
4.6.3	Robustness Evaluation	52
4.6.4	Robust-Optimal Simulation	53
4.6.5	Performance Evaluation	56
4.7	Design Case Studies	59
5	Modeling and Analysis of Spacecraft with Fuel Sloshing in High-G Maneuvers	63
5.1	Introduction	63
5.2	Modeling of Spacecraft with Fuel Sloshing	64
5.2.1	Model Description	64

5.2.2	Equations of Motion	67
5.2.3	The Kinematic Equations	74
5.3	Analysis of Spacecraft with Fuel Sloshing in High-G Maneuvers	76
5.3.1	Nutation Angle	76
5.3.2	Dynamic Analysis	77
6	Conclusions and Future Work	85
6.1	Conclusions	85
6.2	Recommendations for Future Work	86
	Appendices	86
A	87
A.1	The Elements of Matrix M and Vectors E and F in case of one tank with one pendulum	87
A.2	The Elements of Matrix M and Vectors C and F in case of one tank with two pendulums	90
	References	96

List of Figures

1.1	Delta launch vehicle [11], Courtesy: NASA/JPL-Caltech.	4
1.2	Launch boost phase [11], Courtesy: NASA/JPL-Caltech.	5
1.3	Launch injection phase [11], Courtesy: NASA/JPL-Caltech.	6
2.1	A spacecraft model with spherical pendulum.	22
3.1	Fuzzy membership functions and universe of discourse for the premise variables: a) $\mu_{ij}[z_j(\omega)]$ ($i = 1, \dots, 128; j = 1, 2, 3$) and b) $\mu_{ij}[z_j(q)]$ ($i = 1, \dots, 128; j = 4, 5, 6, 7$).	30
3.2	Time response of the selected states for the open-loop validation.	34
4.1	Schematic diagram of the fuzzy PDC observer-based feedback control.	40
4.2	Schematic diagram of the robust-optimal T-S fuzzy observer-based feedback control.	43
4.3	Schematic diagram of the fuzzy LQR observer-based feedback control.	46
4.4	Time responses of the spacecraft angular velocities using fuzzy PDC and fuzzy LQR controllers.	49
4.5	Time responses of the quaternions using fuzzy PDC and fuzzy LQR controllers.	50
4.6	Actual and estimated responses of the pendulum angles.	50
4.7	Time responses of the control inputs using fuzzy PDC and fuzzy LQR controllers.	51

4.8	The effect of uncertainty in the mass-moment-of-inertia on the time responses of quaternions using Fuzzy PDC controller.	52
4.9	The effect of uncertainty in the mass-moment-of-inertia on the time responses of quaternions using Fuzzy LQR controller.	53
4.10	Time response of the spacecraft angular velocity components.	55
4.11	Time response of the quaternions.	55
4.12	Actual and estimated response of the pendulum angles.	56
4.13	Control inputs, $ u_i(t) \leq 79 \text{ N.m}$, ($i = 1, 2, 3$).	56
4.14	Time responses of the spacecraft angular velocities using fuzzy PDC, robust-optimal fuzzy PDC and PID controllers.	57
4.15	Time responses of the quaternions using fuzzy PDC, robust-optimal fuzzy PDC and PID controllers.	58
4.16	Time responses of the control inputs using fuzzy PDC, robust-optimal fuzzy PDC and PID controllers.	59
4.17	Design on the responses of quaternions: Nominal, Case 1– $\max(\beta^2)$, Case 2– $\min(\alpha^2)$, Case 3– $\max(d)$	60
4.18	Design on the responses of input control: Nominal, Case 1– $\max(\beta^2)$, Case 2– $\min(\alpha^2)$, Case 3– $\max(d)$	61
5.1	A gyrostat model with multiple, partially-filled, spherical tanks.	65
5.2	Equivalent model of fuel sloshing in spherical tank j for high-g environment.	66
5.3	Angles α_{ij} and β_{ij} represent the relative orientation of the spherical pendulum with respect to the G -frame.	67

5.4 The time history of spacecraft angular velocity components with spherical-spherical pendulum model (Case 1). 79

5.5 Nutation angle for spherical-spherical pendulum model (Case 1). 79

5.6 The time history of spacecraft angular velocity components with spherical-spherical pendulum model (Case 2). 80

5.7 Nutation angle for spherical-spherical pendulum model (Case 2). 80

5.8 Case 2-The time history of spacecraft angular velocity components with an empty tank and without nutation damper. 81

5.9 Case 2-The time history of spacecraft angular velocity components with an empty tank and with nutation damper. 81

5.10 Case 2-The effect of nutation damper on spacecraft nutation angle with empty tank. 82

5.11 Case 2-The time history of spacecraft angular velocity components with partially-filled tank and without nutation damper. 82

5.12 Case 2-The time history of spacecraft angular velocity components with partially-filled tank and with nutation damper. 83

5.13 Case 2-The effect of nutation damper on spacecraft nutation angle with partially-filled tank. 83

5.14 Case 1-The effect of pendulum mass-ratio on the spacecraft nutation angle. 84

List of Tables

3.1	Fuzzy Rule Table (<i>Negative = N, Positive = P</i>)	29
3.2	The spherical pendulum and spring-damper parameters	34
3.3	Initial Conditions	35
4.1	Observer Initial Conditions	51
4.2	RMSE for states and control inputs using Fuzzy PDC and Fuzzy LQR	53
4.3	PID gains using closed-loop Ziegler-Nichols method	57
4.4	RMSE for states and control inputs	58
5.1	The spherical pendulum and nutation damper parameters	77
5.2	Initial Conditions for spherical-spherical pendulum case	78

CHAPTER 1

Introduction

1.1 Motivation

During the upper-stage separation and orbit injection, orbital control, and attitude maneuver, propellant slosh in partially filled fuel tanks can cause dynamical instability or pointing errors. The spacecraft dynamics combined with propellant sloshing results in a highly nonlinear and coupled dynamic system that requires complicated control law. This problem has been a long-standing concern for space missions. The aim of this research is to model and propose a robust, optimal fuzzy-model-based (FMB) controller for attitude stabilization of a rigid spacecraft with fuel sloshing. The motivation for this research arose from induced attitude anomalous motions caused by the effects of propellant slosh on spacecraft dynamics that resulted in delays or failures of space missions.

1.2 Spacecraft Anomalies and Failures

Numerous spacecraft, presented below, experienced anomalous motions which resulted in mission delay or even catastrophic failure of the mission with one possible cause being fuel sloshing in spacecraft. Here are some examples in a chronological order:

1. Apollo 11 Lunar Module, during the last seconds of the first lunar landing in 1969, had a problem with control of the landing maneuver because of sloshing of the remaining propellant [1].

2. Even small amounts of liquid can cause a mission failure. In 1969, ATS-V spacecraft of 452 kg carrying only 1.2 kg liquid, experienced an uncontrollable 11-second divergent nutation time constant after upper stage burnout. The mission was lost after the spacecraft entered flat spin [2].
3. Some attitude nutation instability effects were determined from an extensive series of in-orbit tests in INTELSAT IV series spacecraft in 1974 which carried liquid hydrazine in four conispheric propellant tanks mounted on the spinning rotor section [3].
4. During transfer orbit operations of the first LEASAT mission in 1984, control system instability developed during the preapogee injection phase that immediately followed activation of the despin control system [4]. Similar instability was observed again during transfer orbit operations of the second LEASAT launched two months later. The investigations pointed to propellant oscillations as the most probable cause of the instability. Propellant dynamics had not been originally considered in the design.
5. During the NEAR (Near Earth Asteroid Rendezvous) mission to the asteroid Eros in 1998, the spacecraft's reorientation maneuver experienced anomalous series of attitude motions and went into safety mode that lead to a 13-month delay of mission [5]. Fuel slosh was identified as the probable cause.
6. DemoSat failed to reach targeted orbit due to fuel sloshing in 2007 [6]. After second stage ignition, a circular coning oscillation began that increased in amplitude.
7. Solar Dynamics Observatory, which is a three-axis controlled, single-fault tolerant spacecraft, was successfully launched and deployed from its Atlas V launch vehicle in 2010 [7]. It had two large tanks with propellant which comprised almost half of its launch mass. During the second apogee motor firing the anomalous attitude motion was discovered and the cause for the anomaly was determined to be the fuel slosh.
8. Chang'e 3 lunar probe, launched in 2013, was designed to achieve soft-landing and roving exploration on the lunar surface. During soft landing to avoid an obstacle, the Chang'e 3

experienced motion instability because of fuel sloshing in the liquid propellant. The lander kept vertical attitude and moved back and forth horizontally while approaching the moon [8].

1.3 Mission Phases

Most missions have a few common distinct phases: 1) launch into geosynchronous transfer orbit (GTO) with perigee (low altitude of 200 km) and apogee (high altitude of 35,786 km); 2) transfer from GTO to geostationary orbit (GEO) with both perigee and apogee at 35,786 km, and the orbit inclination and eccentricity close to null; 3) preparation and calibration of the attitude and orbit control system (AOCS) before the start of the GEO mission; and 4) GEO mission operations [9]. Many missions consist of some phases in which space craft is spin-stabilized and some phases in which it is three-axis stabilized [10]. During the spin stabilization the angular momentum of the spacecraft remains approximately fixed in inertial space for extended periods. For spin-stabilized spacecraft the rotational orientation of the spacecraft about the spin axis is not controlled. For three-axis stabilized spacecraft the three mutually perpendicular axes are controlled to achieve the required orientation and pointing accuracy during on-orbit operation.

Numerous spacecraft, flown on launch vehicles such as Delta and Atlas Centaur, feature spin stabilized upper stage injection using apogee kick motors (AKM) following de-spin to an on-orbit three-axis stabilized operation [11–13]. Fig. 1.1 presents a typical Delta launch vehicle [11] carrying a Deep Space 1 spacecraft. This typical Delta launch vehicle employs three stages and Figures 1.2 and 1.3 demonstrate the launch boost and injection phases [11].

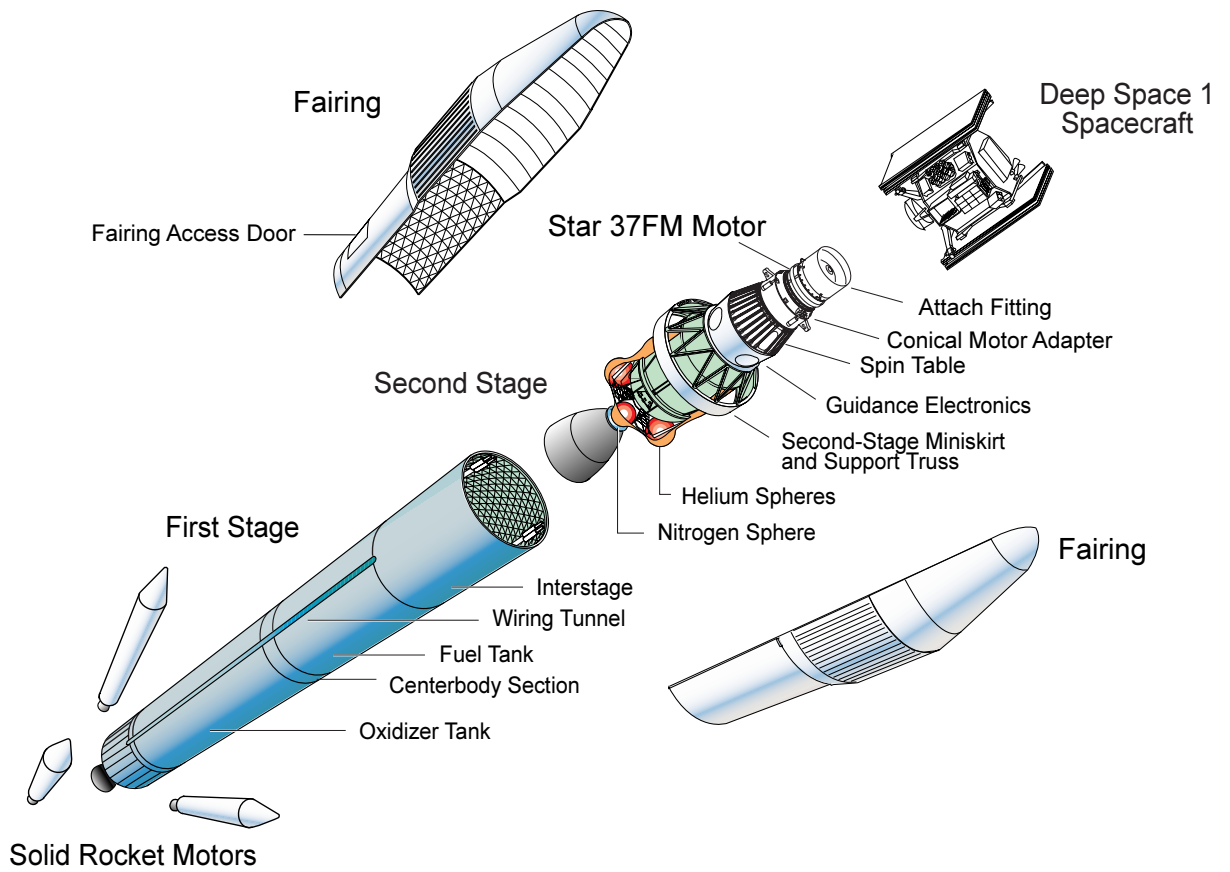


Fig. 1.1: Delta launch vehicle [11], Courtesy: NASA/JPL-Caltech.

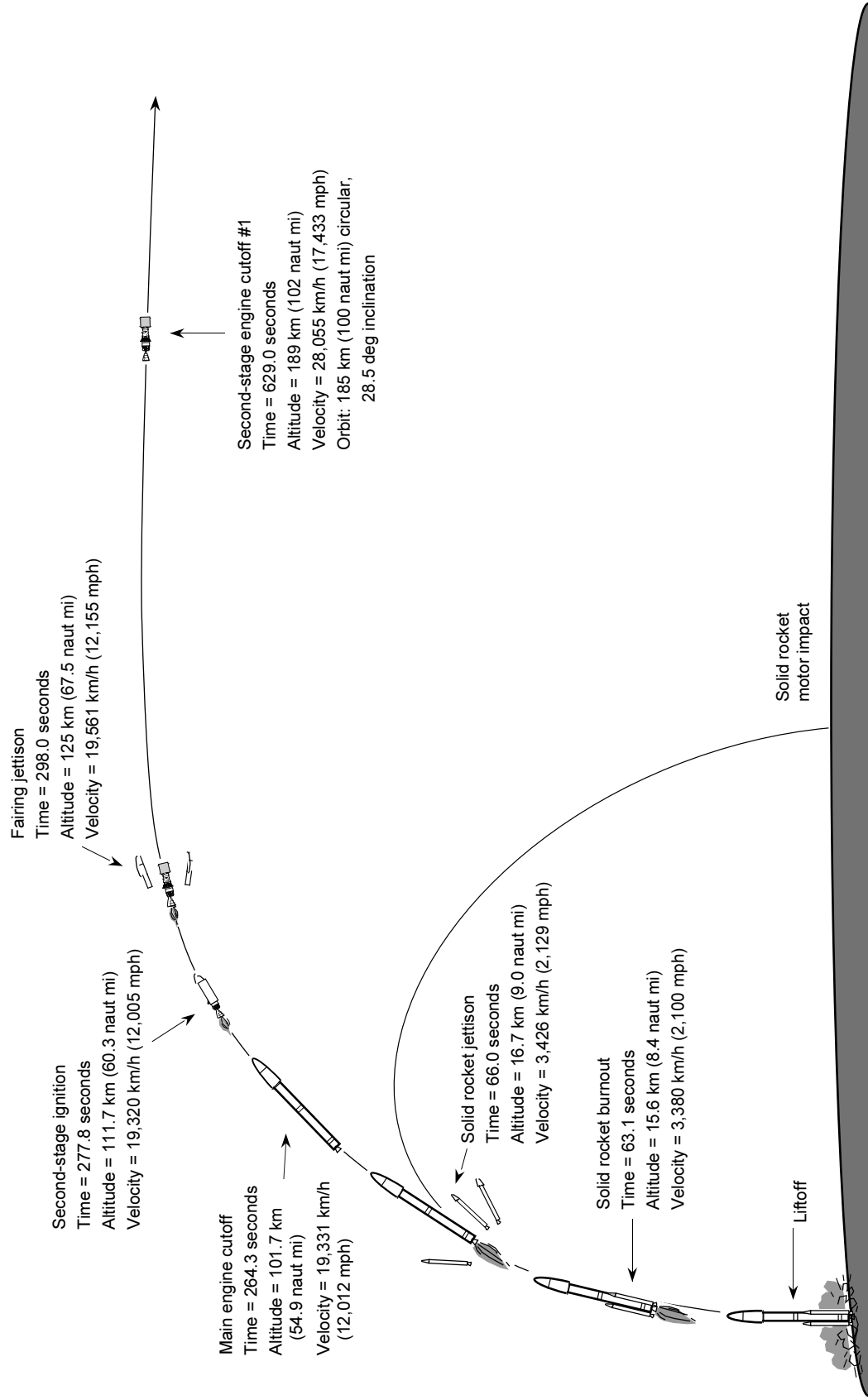


Fig. 1.2: Launch boost phase [11], Courtesy: NASA/JPL-Caltech.

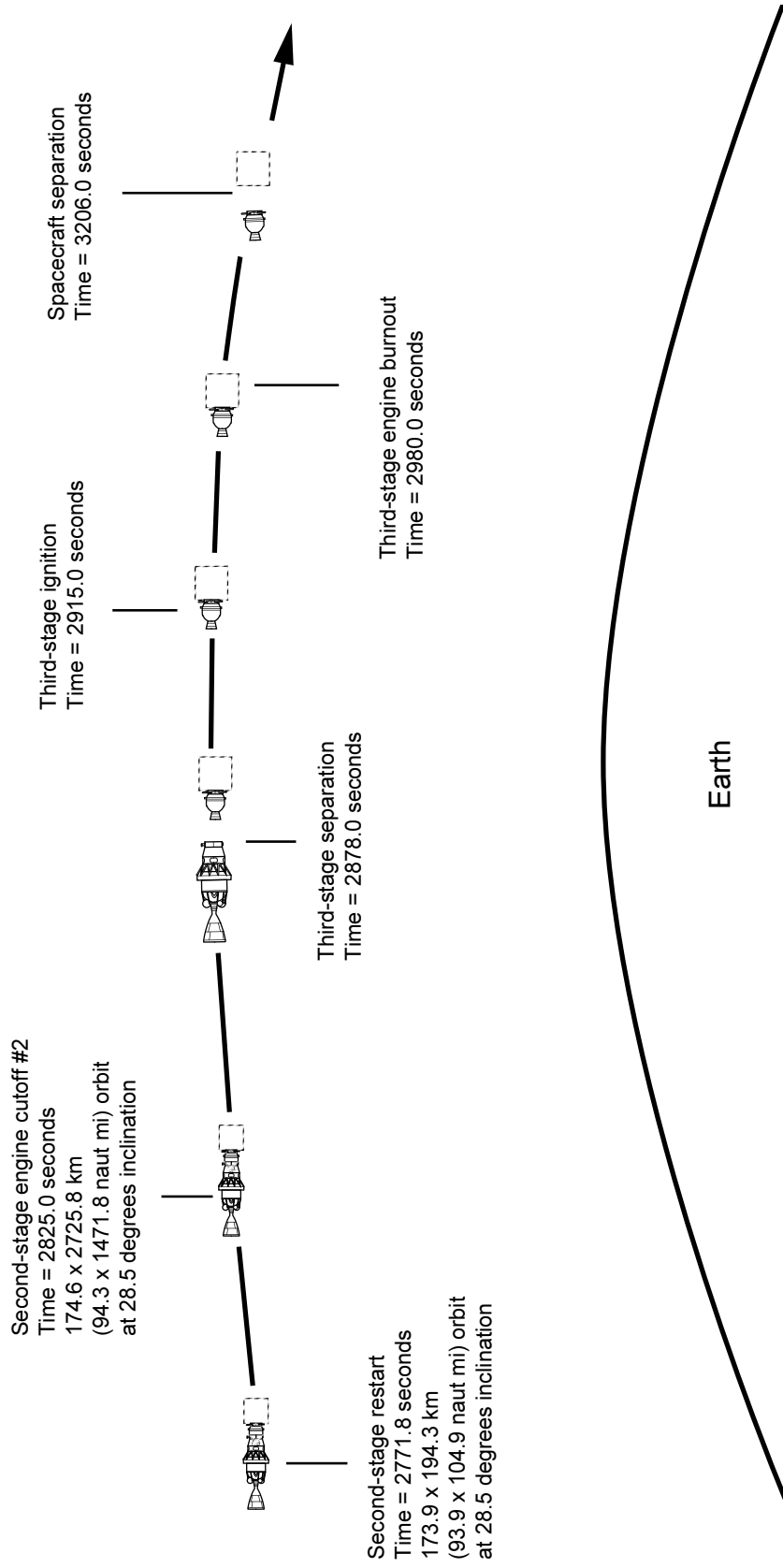


Fig. 1.3: Launch injection phase [11], Courtesy: NASA/JPL-Caltech.

The first stage of the launch vehicle lifts the spacecraft and launch vehicle off the ground to sky. The second stage sends the spacecraft into the space. Each stage has its own fuel source. The third stage, an upper stage connected to the spacecraft covered by the fairing, transfers the spacecraft out of the Earth's atmosphere where separation of the spacecraft from the upper stage follows and the spacecraft is sent to the desirable orbit to complete its mission. The third stage is spin stabilized, a spin table supporting small rockets which are used to spin up the third stage itself and the attached spacecraft. To spin the third stage is to keep it in the proper orientation before being released from the second stage. Further, spinning third stage needs to be de-spun before the spacecraft separates and acquires its proper cruise orientation. The attitude control problem of spacecraft in the presence of propellant sloshing is important in different phases of mission.

1.4 Literature Review

The problem of propellant slosh in partially filled fuel tanks of spacecraft has been studied since the early 1960s. A substantial mass of fuel is necessary to transfer the spacecraft from the geosynchronous transfer orbit (GTO) to geostationary orbit (GEO). Uncontrollable movement of partially filled fuel in tanks can cause attitude instability. This attracted the attention of many engineers and scientists who were motivated to design control system for various aerospace vehicles with the dynamic interaction of propellant sloshing [9, 14, 15]. In the past, a considerable amount of analytical and experimental work was done to study the nutation stability of spinning solid propellant rockets [16] and spacecraft [17–19] taking into account the effect of propellant slosh, see Refs. [20–23, 25–27]. The development of multi-body dynamics led to the successful prediction of attitude motions of space vehicles [28–30]. Because the exact formulation and solution for propellant sloshing in various tanks is complex, the dynamically equivalent mechanical models were adopted to model the fuel motion. In order to

approximate the sloshing liquid behavior, equivalent mechanical models were proposed and implemented by various investigators. Abramson and Dodge et al. [14,31–33] studied the dynamic behavior of liquids in moving containers with applications to space vehicles. Roberts et al. described different equivalent mechanical models in their slosh design handbook [34]. Hill and Baumgarten [20] investigated dynamics of spin stabilized satellites carrying sloshing liquid stores. To study interaction of fluid motion and spinning body, the test rig was designed, built and instrumented. Kana [35] proposed a compound pendulum model, which included both spherical and planar pendulums, to model the liquid slosh motion in a rotary tank. Cochran and Kang discussed attitude motion of a spinning asymmetric rigid body with a spherical pendulum included in their article [22]. Enright, Wong, and Breckenridge [36,37] studied propellant slosh models for the Cassini spacecraft. They proposed two spherical pendulums model for "high-g" maneuver. The spacecraft is said to be in a "high-g" environment when it is under high acceleration provided by the main engine and the surface tension forces of liquid in tanks do not significantly affect the propellant motion during main engine burns. Supported by extensive literature review, Ibrahim [15] presented liquid sloshing dynamics from the basic theory through advanced analytical and experimental results. In 2008, Kang and Lee [26] investigated the attitude motion of a rigid spacecraft with a momentum wheel along the spin axis and a spherical pendulum. Mason and Starin studied the effects of propellant slosh dynamics on the Solar Dynamics Observatory [7], which is a three axis controlled, single fault tolerant spacecraft. Anomaly caused by the slosh during the first apogee motor firing which caused the spacecraft to transition into Sun Acquisition mode was determined. Agrawal [4] discussed attitude control motion instabilities caused by liquid slosh in fuel tanks. Recently, a composite equivalent mechanical model was considered to predict the slosh forces and moments exerted on a spherical propellant tank in a spacecraft by Nan et al. [38]. Navabi et al. [39] presented a three-dimensional model for maneuvering of a spacecraft with unactuated fuel slosh dynamics using Lagrange method. They adopted a multi-pendulum model to

characterize the fuel slosh.

The spacecraft combined with propellant slosh in partially filled fuel tanks results a highly nonlinear and coupled dynamic system that requires complicated control law. The complicated control system analysis has been a long-standing concern for space missions. Baumgarten et al. [21] developed a control law using an equivalent mechanical model of the liquid slosh—a two-degree of freedom pendulum—which resulted in stability of the system dynamics. Hill and Baumgarten [40] designed a time varying linear feedback control law for a spin-stabilized spacecraft with sloshing fluid stores. Wong et al. [37] proposed an attitude controller for the Cassini spacecraft using thrust vector for precision pointing and stabilization for science missions. Cho et al. [41] studied feedback control of a space vehicle with unactuated fuel slosh dynamics. Shageer and Tao [42] conducted a study of adaptive control of spacecraft with fuel slosh. They linearized dynamical equations of motion of spacecraft combined with a pendulum and then developed an adaptive control law for stability and tracking objectives. Reyhanoglu and Hervas [43] presented a multi-pendulum model and control of a spacecraft with fuel sloshing which is an extended work of their previous model where only the lowest frequency slosh mode was included [44]. Ayoubi et al. [27] developed equations of motion of a spinning spacecraft with fuel sloshing, three momentum wheels, and a nutation damper. Hervas and Reyhanoglu [45] designed a Lyapunov-based nonlinear feedback controller for a spacecraft with fuel slosh to control the translational velocity and the attitude of the spacecraft. They considered a multi-mass-spring model to represent the fuel slosh in the tank. In their paper [45], the observer-based control of space vehicles with fuel slosh dynamics in a zero gravity environment was studied. Zhang and Wang [46] proposed a controller to stabilize the attitude of the spacecraft with liquid sloshing in the presence of low frequency periodic disturbance. The controller is composed of active disturbance rejection control, positive position feedback, extended state observer and singular spectrum analysis.

Recently, studies started to combine spacecraft as a rigid body with flexible appendage and fuel slosh. For example, Deng and Yue [47] presented nonlinear modeling and attitude dynamics of spacecraft coupled with liquid sloshing dynamics and flexible appendage vibration. In their previous work [48], the authors studied dynamics and control of spacecraft with multiple liquid propellant tanks. In both studies, improved moving pulsating ball model was adopted to characterize the slosh. Attitude reorientation of the spacecraft is implemented by a feedback control strategy based on Lyapunov theory.

In the last three decades, intelligent control systems such as fuzzy logic and neuro-fuzzy systems have been used to control aerospace vehicles including spacecraft attitude stabilization. Most work has been done for rigid spacecraft. Recent research has been conducted on fuzzy-model-based control systems that guarantee both stability and performance of a closed-loop system. Takagi and Sugeno introduced the T-S fuzzy-model fuzzy system in 1985 [49]. The T-S fuzzy-model-based system is based on a set of fuzzy rules to describe a global nonlinear system in terms of a set of local linear models that are smoothly connected by fuzzy membership functions. Using the Lyapunov approach, the stability conditions can be formed in terms of linear matrix inequalities (LMIs) that can be solved numerically and efficiently using convex programming techniques. LMIs based approach has received significant attention in design control [52–54]. Wang et al. presented the Parallel Distributed Compensation (PDC) nonlinear control technique [55]. The basic idea behind PDC is to design a feedback controller for each local model and then to construct a globally asymptotic stable controller from the local controllers. Li et al. [56] presented a framework for designing a dynamic feedback controller for nonlinear systems described by T-S models. A nonlinear dynamic feedback controller in the form of dynamic parallel distributed compensation (DPDC) was used, the parameters of which are obtained from a set of linear matrix inequality problems. Feng [57] presented a comprehensive survey on state of the art of analysis and design of fuzzy-model-

based control systems that focused on the Takagi-Sugeno (T-S) fuzzy model. Song et al. studied the quaternion based, fuzzy attitude regulation of a rigid spacecraft in the presence of external disturbances [58]. Recently, Ayoubi and Sendi [59] presented a T-S fuzzy model with full-state feedback, control input constraint, and disturbance rejection objective to stabilize a rigid spacecraft with flexible antenna. Further, they [60] presented T-S fuzzy-model-based control of spacecraft with flexible appendage and studied the robust-optimal fuzzy controller for position and attitude stabilization and vibration suppression of a flexible spacecraft during antenna retargeting maneuvers [61]. Recently, Baculi and Ayoubi [62] designed a Takagi-Sugeno type fuzzy attitude controller for solar sail spacecraft with reaction wheels and translating masses. In our previous paper [63], we presented the T-S fuzzy model for a spacecraft with fuel sloshing and we designed a full-state feedback fuzzy PDC with control input constraint to stabilize the attitude motion of a non-spinning spacecraft.

Some research was conducted to integrate the fuzzy controller with a linear quadratic regulator (LQR). The standard LQR was proposed on linearized models for attitude control of rigid spacecraft and spacecraft with fuel sloshing [40,64]. To apply the LQR to nonlinear systems, Driankov et al. [65] proposed a fuzzy gain scheduler based on LQR and applied it to the problem of tracking a reference trajectory of a nonlinear autonomous system. Li et al. introduced an attitude controller for Reusable Launch Vehicle (RLV) within a large operating envelope, combining LQR with fuzzy gain scheduling based on the Takagi-Sugeno fuzzy model [67]. The T-S fuzzy model with LQR keeps the asymptotic stability performance provided by the optimal feedback gain approach.

The control performance robustness and optimality in the control system design has been continuously studied. Chen et al. introduced fuzzy linear control of the robustness design of nonlinear dynamic systems [69]. Tanaka et al. [70] presented a mixed control design via

linear matrix inequalities that combined robust fuzzy and optimal fuzzy controllers. The optimal fuzzy control is based on quadratic performance functions. Later, Park et al. [71] proposed a new design methodology for the optimal stabilization of a T-S fuzzy system. Their proposed model was validated via application to the rigid spacecraft attitude control. Ousailoo [72] proposed an attitude controller using fuzzy logic for a small satellite with model uncertainty. He claimed that the presented controller increased robustness for automatic control reconfiguration and model uncertainty, and reduces development and production cost for flight control systems and autonomous on-board control features. Zhang et al. proposed a multi-objective control based on the T-S fuzzy model and PDC scheme for a rigid spacecraft maneuver [73]. Sendi and Ayoubi [61] introduced robust-optimal fuzzy-model-based control of flexible spacecraft with actuator constraints.

1.5 Research Objectives and Thesis Overview

The aim of this research is modeling and fuzzy control of spacecraft with fuel sloshing. For the first part of the research (Chapters 2,3,&4), equations of motions are derived for the spacecraft with fuel sloshing in one spherical tank. Further, fuzzy controllers are designed which stabilize the attitude motion of a spacecraft with fuel sloshing considering the input constraints on the actuators. The designs are for three-axis stabilization. An observer is introduced to estimate the unmeasurable states. We designed a Fuzzy controller/observer based on the parallel-distributed compensation (PDC) technique and a fuzzy controller/observer based on the linear quadratic regulator (LQR). Both controllers/observer designs are built from the Takagi-Sugeno (T-S) model of the spacecraft. Using the Lyapunov stability theorem, the fuzzy PDC controller design problem was cast as a minimization problem for the upper bound of control input in the form of linear matrix inequalities. The efficacy and robustness of each controller are compared via numerical simulations. The design is extended to robust and

optimal fuzzy-model-based attitude controller. The advantages of the proposed fuzzy controllers are: i) globally asymptotically stable; ii) robust to model uncertainties; iii) satisfies the actuator amplitude constraint; iv) simple structure and therefore easy to implement; and v) the design procedure is formulated in terms of linear matrix inequalities (LMIs), which can address stability, performance, and robustness of the closed loop system at the same time. Designing an active attitude control system for a spacecraft with partially filled tank is a challenging task because of the highly nonlinear and coupled dynamics of the system. To the best of our knowledge, this is the first attempt to apply fuzzy PDC and fuzzy LQR controllers to this problem.

For the second part of the research (Chapter 5), a mathematical model of a thrusting, spinning spacecraft with partially filled multiple-tanks, a nutation damper, and momentum wheels in the high-g environment is developed. Equations of motion of spacecraft are derived using the Kane's method with two spherical pendulums to represent fuel sloshing in spinning spacecraft. Torsional viscous dashpots are added to the pendulum hinges to simulate the damping effect. Three momentum wheels included in the model are used as attitude control actuators. The numerical simulation for the model, including pre and post Payload Assist Module (PAM) motor burnout phases, is conducted and the dynamical behavior of the spacecraft with fuel sloshing is investigated. The effect of the slosh model parameters on the spacecraft nutation angle is studied.

This is presented in the following order: In Chapter 2, Kane's method for the derivation of a system's equations of motion and slosh modeling techniques is reviewed and applied to derive the nonlinear equations of motion for spacecraft with fuel sloshing. In Chapter 3, T-S fuzzy model with uncertainty, fuzzy observer, and T-S model validation are presented. In Chapter 4, the fuzzy controller design procedure including fuzzy PDC, fuzzy LQR and

robust-optimal fuzzy controllers and LMI based formulation of the problem is presented. It includes the stability, performance, and robustness of the proposed controllers with some design case studies. In Chapter 5, modeling and analysis of spacecraft with fuel sloshing in high-g maneuvers are discussed. In Chapter 6, conclusions and future work recommendations are presented. Appendix A lists some parameters of the mathematical model.

CHAPTER 2

Dynamics of Spacecraft with Fuel Sloshing

2.1 Introduction

In this chapter, Kane's method is first reviewed to derive dynamic equations for a multi-body system, then, slosh modeling techniques are studied. The equations of motion of spacecraft with a partially filled fuel tank are derived, where fuel sloshing is modeled by the means of a spherical pendulum with spring-torsional damper at hinge point.

2.2 Review of Kane's Method or Virtual Power

In this section, we briefly review the Kane's method [28, 29] to formulate the dynamic equations of the motion of a system. In 1961, Thomas Kane of Stanford University formulated a variation of the virtual power principle explicitly for rigid body systems [74]. This method originated from the Jourdain's Principle [75]. The Kane's method has advantages over Newton- Euler, Lagrange, D'Alembert's principle, Hamilton, Boltzmann-Hamel, and Gibbs-Appell methods and provides an easy and systematic way to formulate equations of motions for complex, multi-body systems. Kane's method, using generalized forces, eliminates the noncontributing forces and torques between bodies from the equations of motion unlike in the Newton-Euler method. Kane's method does not employ energy functions and, therefore, overpasses the differentiations of energy functions unlike in the Lagrange and Gibbs-Appell

methods. Kane's method is applicable to both the holonomic and nonholonomic systems. Kane's equations may be interpreted as follows: if the partial velocity vectors define the directions of motion of a mechanical system, then Kane's equations represent a projection of the applied and inertia forces along those directions. Detail comparison and advantages and disadvantages of Kane's method to other mentioned methods can be found in numerous works [30, 76–78].

We note that the Kane's method is based on developed new kinematic quantities as partial angular velocities and partial velocities, first discovered in Kane's work, in 1960 [79]. It allows, with a minimum amount of labor, derivation of equations of motion formulating expressions for generalized forces using generalized speeds, partial angular velocities, and partial velocities. Generalized speeds are generalization of the generalized velocities. For a mechanical system S having n degrees of freedom, represented by generalized coordinates, q_r ($r = 1, \dots, n$), the generalized speeds, u_r ($r = 1, \dots, n$), for S in a reference frame N are defined as linear combinations of the generalized velocities, \dot{q}_r ($r = 1, \dots, n$) as [28, 29]

$$u_r = \sum_{s=1}^n Y_{rs} \dot{q}_s + Z_r, \quad (r = 1, \dots, n), \quad (2.1)$$

where Y_{rs} and Z_r are functions of q_r ($r = 1, \dots, n$), and t , and Y_{rs} ($r, s = 1, \dots, n$) must be chosen such that Eq. (2.1) can be solved uniquely for \dot{q}_r ($r = 1, \dots, n$). Thereafter, the angular velocity, ω , of a rigid body B in N , and the velocity, V , of a particle P in N , can be expressed uniquely as

$$\omega = \sum_{r=1}^n \omega_r u_r + \omega_t, \quad (2.2)$$

$$V = \sum_{r=1}^n V_r u_r + V_t, \quad (2.3)$$

where ω_r , V_r ($r = 1, \dots, n$), ω_t , and V_t are functions of q_r ($r = 1, \dots, n$) and t . The vectors ω_r and V_r are called partial angular velocities of ω and partial velocities of V , respectively.

Having partial angular velocities and partial velocities, we can formulate the generalized forces.

The generalized active and inertia forces for a system S in N consisting of particles P_i ($i = 1, \dots, n_P$) are defined, respectively, as

$$(F_r)_P = \sum_{i=1}^{n_P} {}^N V_r^{P_i} \cdot R_i, \quad (r = 1, \dots, n_P), \quad (2.4)$$

$$(F_r^*)_P = \sum_{i=1}^{n_P} {}^N V_r^{P_i} \cdot R_i^*, \quad (r = 1, \dots, n_P), \quad (2.5)$$

where ${}^N V_r^{P_i}$ is the r th partial velocity of P_i in N , and R_i is the resultant of all external (contact and body) forces acting on particle P_i . R_i^* is the inertia force for P_i in N defined as

$$R_i^* = -m_i a_i, \quad (r = 1, \dots, n), \quad (2.6)$$

where m_i is the mass of particle P_i , and a_i is its acceleration in N .

The generalized active and inertia forces for a rigid body B in N are defined, respectively, as

$$(F_r)_B = {}^N \omega_r^B \cdot T + {}^N V_r^Q \cdot R, \quad (r = 1, \dots, n), \quad (2.7)$$

$$(F_r^*)_B = {}^N \omega_r^B \cdot T^* + {}^N V_r^{B^*} \cdot R^*, \quad (r = 1, \dots, n), \quad (2.8)$$

where ${}^N \omega_r^B$ and ${}^N V_r^Q$ are the r th partial angular velocity of B in N and the r th partial velocity of Q in N , respectively. Q is a point in B . ${}^N V_r^{B^*}$ is the r th partial velocity of the mass center B^* of B in N . R is the resultant of all external forces acting on B , and T is the resultant external torque acting on B . R^* and T^* are the inertia force and inertia torque, respectively,

acting on B in N defined as

$$R_i^* = -M^N a^{B*}, \quad (r = 1, \dots, n), \quad (2.9)$$

$$T_i^* = -{}^N\alpha^B \cdot I - {}^N\omega^B \times I \cdot {}^N\omega^B, \quad (r = 1, \dots, n), \quad (2.10)$$

where M is the mass of B , and a^{B*} is the acceleration of the mass center B^* of B in N . ${}^N\alpha^B$ and ${}^N\omega^B$ are the angular acceleration and angular velocity of B in N , respectively. I is the central inertia dyadic of B in N .

For a mechanical system S having n degrees of freedom, represented by generalized coordinates, q_r ($r = 1, \dots, n$), Kane's equations simply state that the sum of the generalized inertia and active forces is zero for each generalized coordinate:

$$F_r + F_r^* = 0, \quad (r = 1, \dots, n), \quad (2.11)$$

where F_r and F_r^* are the generalized active and inertia forces, respectively.

2.3 Slosh Modeling Techniques

Sloshing is defined as any motion of the free liquid surface inside a partially filled container due to any disturbance [15]. There are different types of motion that free liquid surface can experience such as simple planar, nonplanar, rotational, irregular beating, symmetric, asymmetric, quasi-periodic and chaotic. In general, the motion of sloshing systems can be influenced by capillary forces (surface forces), gravitational (body) forces, inertia forces, and viscous forces. Often, some forces are much smaller compared to other forces and, therefore,

they can be ignored resulting in simplified analysis of liquid sloshing. Dimensionless numbers such as the Bond number, Weber number, and Froude number characterize the relative importance of different forces. These dimensionless numbers separate the hydrodynamic behavior into gravity, inertia and capillary dominated regimes [14].

Gravity dominated regime: The gravitational forces are larger compared to capillary forces and, therefore, capillary forces can be disregarded. In this regime, the Bond number defined as the ratio of gravitational to surface tension forces is $Bo = \rho g L^2 / \sigma \gg 1$. For rotational sloshing, the centrifugal Bond number defined as the ratio of centrifugal and surface tension forces is $Bo = \rho R L^2 \Omega^2 / \sigma \gg 1$.

Inertia dominated regime: The inertia forces are larger compared to capillary forces and, therefore, capillary forces can be disregarded. In this regime, the Weber number defined as the ratio of inertia to surface tension forces is $We = \rho V^2 L / \sigma \gg 1$, and the Froude number defined as the ratio of inertia to gravitational forces is $Fr = We / Bo = V^2 / g L \gg 1$; inertia forces dominate the behavior.

Capillary dominated regime: The gravitational and inertia forces are small compared to capillary forces and, therefore, they can be disregarded.

The Reynolds number defined as the ratio of inertia to viscous forces is $Re = LV / \nu$ characterizes the importance of viscous effects. It must be determined separately for each regime.

Above mentioned, ρ is the density of the fluid, g is the gravitational acceleration, L is the characteristic dimension of the tank such as diameter, σ is the surface tension, Ω is the spin rate, R is the radius, where equivalent gravity is calculated, V is the characteristic velocity, and ν is the kinematic viscosity.

Based on the hydrodynamic regimes, the slosh models are defined as low-g and high-g [14, 36]:

Low-g: Surface tension forces are critical to the determination of the behavior of the propellant. Generally, the low-g slosh frequency is smaller than it is in normal gravity. The Bond

number is much less than 1, $Bo \ll 1$.

High-g: The spacecraft acceleration that is provided by the main engine is large enough so that surface tension forces do not significantly affect the propellant motion during main engine burn. The Bond number is much higher than 1, $Bo \gg 1$.

These dimensionless numbers can be determined experimentally with air bearing tests, spin drop tests, or energy dissipation tests [24], which are not conducted in this research.

To mimic the behavior of liquid sloshing, fluid dynamics modeling and equivalent mechanical modeling can be utilized. Fluid dynamics modeling uses partial differential equations to describe the fluid behavior in a given environment and an exact solution for sloshing dynamics in a moving container is extremely difficult to derive [7]. Instead, they are solved numerically using computational fluid dynamics (CFD) techniques. However, for complex dynamical systems, CFD takes computationally longer time to solve and instead, especially for incorporating the dynamic effects of sloshing in the spacecraft control and stability analysis, equivalent mechanical models were employed.

Various types of equivalent mechanical models such as planar and spherical pendulum, spring mass models are discussed and derived in Abramson's work "The Dynamic Behavior of Liquids in Moving Containers with Applications to Space Vehicle Technology" [32]. We note that if there is no free surface, which means the tank is fully filled, the liquid can be replaced by an equivalent rigid body [80]. Some masses of liquid with free surface, which are free to oscillate, are replaced by equivalent mechanical models, and the rest is replaced by rigid body [81]. The mechanical models should duplicate the static and dynamic properties of liquid, which are presented below [14]

Static properties. To preserve the static properties of the liquid, the sum of all the masses must be the same as the liquid mass m_{liq} , and the center of mass of the model must be at the

same elevation as the liquid. These constraints are expressed analytically by:

$$m_0 + \sum_{n=1}^{\infty} m_n = m_{liq}, \quad (2.12)$$

$$m_0 h_0 + \sum_{n=1}^{\infty} m_n h_n = 0, \quad (2.13)$$

where m_0 is the rigidly-attached mass, h_0 is the location of m_0 referenced to the center of mass, the other parameters are for moving masses of the model.

Dynamic properties. Equations Eq. (2.12) and Eq. (2.13) are not sufficient to fix the values of the model parameters. To do that, the model must also duplicate the sloshing forces, torques, and natural frequencies.

The equivalent model parameters depend on the fuel tank shape such as rectangular, cylindrical, spherical et al. and the liquid properties. They can be calculated from the sloshing force and moment analysis or from the experimental analysis. Spherical tanks are the most often used in the aerospace industry because of their high volume to weight ratio. The liquid motions in a spherical tank are inherently more nonlinear than in other tanks, and, therefore, the slosh characteristics are obtained numerically using SLOSH code [14]. The predicted natural frequency for the first two anti-symmetric modes and the pendulum model parameters of the first mode for a spherical tank in the result of SLOSH code can found in the work of Dodge et al [14]. The use of scale model tanks or modern free surface CFD codes generally determines slosh damping experimentally. The damping in mechanical models can be included via linear viscous dashpots.

2.4 Mathematical Model of Spacecraft with Fuel Sloshing

2.4.1 Equations of Motion

Consider a rigid spacecraft with one spherical pendulum shown in Fig. 2.1. We define inertial and body (spacecraft) fixed-frames as the reference frames by N and S , respectively. The inertial frame N corresponds to the Sun center. S^* is the center-of-mass, and $I^{S^*} \in \mathbb{R}^{3 \times 3}$ is the central principal moment-of-inertia of the spacecraft. We model fuel sloshing by means

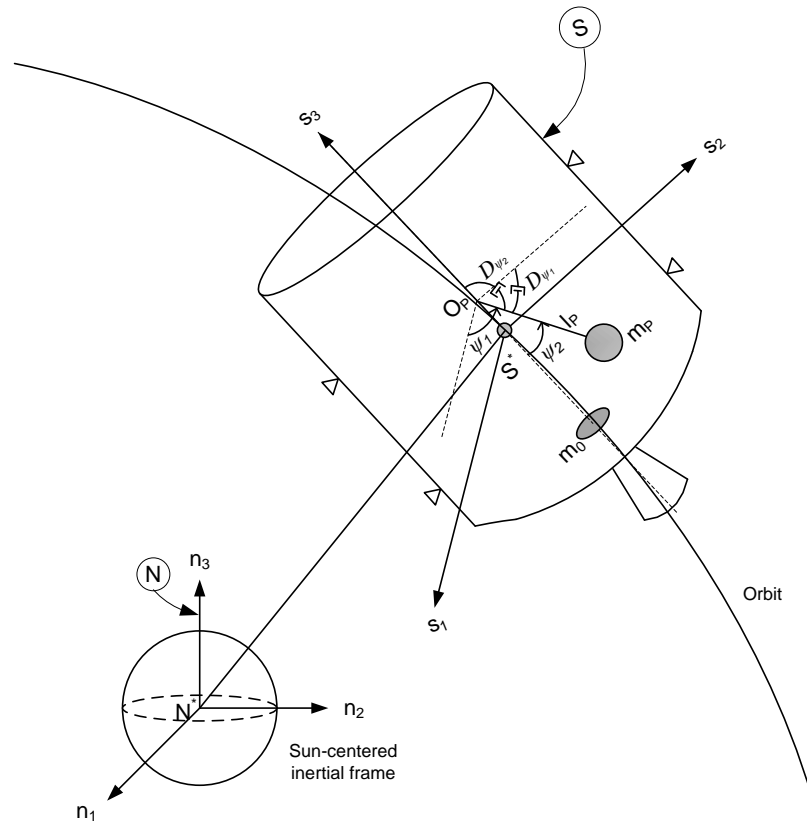


Fig. 2.1: A spacecraft model with spherical pendulum.

of a spherical pendulum of mass m_P with torsional spring damper at the hinge point. The rest of the fuel that is not participating in sloshing is assigned as a static body with mass m_0 . The presented model preserves the static and dynamic properties of the liquid [32]. In other

words, the total fuel mass in the tank must be equal to the sum of all masses in the pendulum model, Eq. (2.12), and the center of mass of the model must be at the same elevation as the liquid, sEq. (2.13).

We choose the generalized speeds, g_k , as follows:

$$g_k = \omega_k, \quad (k = 1, 2, 3), \quad (2.14)$$

$$g_{3+k} = \dot{\psi}_k, \quad (k = 1, 2), \quad (2.15)$$

where ω_1, ω_2 , and ω_3 are the components of the angular velocity of the spacecraft with respect to the N frame (${}^N\omega^S$). The angles ψ_k ($k = 1, 2$) represent the relative orientation of the massless rod of the spherical pendulum in the tank, and $\dot{\psi}_k$ ($k = 1, 2$) are the corresponding generalized speeds.

The equations of motion of the spacecraft with spherical pendulum model can be written as [82]:

$$F_l + F_l^* = 0, \quad (l = 1, \dots, 5), \quad (2.16)$$

where F_l and F_l^* are the generalized inertia and active forces, respectively.

The generalized inertia force is determined by

$$F_l^* = -T_S^{*T} {}^N\omega_l^S - F_{m_0}^{*T} {}^N V_l^{m_0} - F_{m_P}^{*T} {}^N V_l^{m_P}, \quad (l = 1, \dots, 5), \quad (2.17)$$

where

$$F_{m_0}^* = m_0 {}^N a^{m_0}, \quad (2.18)$$

$$F_{m_P}^* = m_P {}^N a^{m_P}, \quad (2.19)$$

$$T_{S^*}^* = I^{S^*} {}^N \alpha^S + {}^N \tilde{\omega}^S I^{S^*} {}^N \omega^S. \quad (2.20)$$

The skew-symmetric matrix ${}^N \tilde{\omega}^S$ is defined as:

$${}^N \tilde{\omega}^S = \begin{bmatrix} 0 & -\omega_3 & \omega_2 \\ \omega_3 & 0 & -\omega_1 \\ -\omega_2 & \omega_1 & 0 \end{bmatrix}, \quad (2.21)$$

and the detailed calculations of the partial velocities and partial angular velocities can be found in Ref. [82].

The generalized active force is of the form

$$F_l = -T_{f m_P}^T {}^N \omega_l^S + T_{f m_P}^T {}^N \omega_l^P + T^{S^*} {}^N \omega_l^S, \quad (l = 1, \dots, 5), \quad (2.22)$$

where $T^{S^*} \in \mathbb{R}^{1 \times 3}$ is the thrust torque on the spacecraft with respect to S^* and $T_{f m_P}$ is the linear viscous torque model on the pendulum m_P given by

$$T_{f m_P} = [-(D_{\psi_2} + K_{\psi_2})l_P^2 \dot{\psi}_2 s \psi_1, (D_{\psi_2} + K_{\psi_2})l_P^2 \dot{\psi}_2 c \psi_1, -(D_{\psi_1} + K_{\psi_1})l_P^2 \dot{\psi}_1 s^2 \psi_2]^T, \quad (2.23)$$

where D_{ψ_k} and K_{ψ_k} ($k = 1, 2$) are damping and stiffness coefficients, respectively. l_P is the length of the pendulum. We note that the pendulum is spring-restrained too as the spring represents the surface tension forces, which are not zero in low-g environment. As described in section 2.3, the model is in low-g then the surface tension forces are critical to the determination of the behavior of the propellant.

Taking into consideration generalized active and inertia forces, Eq. (2.16) can be written in matrix form as:

$$\dot{G} = M^{-1}(F - E), \quad (2.24)$$

where $G \in \mathbb{R}^{5 \times 1}$, and the elements of the vectors $E, F \in \mathbb{R}^{5 \times 1}$ and matrix $M \in \mathbb{R}^{5 \times 5}$ are listed in the Appendix.

2.4.2 The Kinematic Equations

We use a unit quaternion to describe the attitude motion of the spacecraft in the inertial frame. Let's define $q_0 \in \mathbb{R}$ and $\bar{q} = [q_1, q_2, q_3]^T \in \mathbb{R}^{3 \times 1}$ as the scalar and vector components of a unit quaternion. The kinematic equations in terms of this unit quaternion are given by [83]

$${}^N \dot{q}^S = \frac{1}{2} B(q) {}^N \omega^S, \quad (2.25)$$

where

$$B(q) = \begin{bmatrix} -\bar{q}^T \\ q_0 \mathbb{I}_3 + \tilde{q} \end{bmatrix}, \quad (2.26)$$

where $\mathbb{I}_3 \in \mathbb{R}^{3 \times 3}$ is the identity matrix, $\omega = [\omega_1, \omega_2, \omega_3]^T$ and $q = [q_0, \bar{q}^T]^T \in \mathbb{R}^{4 \times 1}$ satisfying the constraint $q_0^2 + \bar{q}^T \bar{q} = 1$. We note that q_0 has the value $+1$ and -1 if the attitude of the spacecraft is zero. \tilde{q} is a skew-symmetric matrix.

The set of Eq. (5.54) along with the kinematic equations, Eq. (2.25), constitute a mathematical model of the system.

Mathematical model of the system can be written in the form of nonlinear systems as:

$$\Sigma_{NL} : \begin{cases} \dot{x} = f(x) + g(x)u, \\ y = Cx, \end{cases} \quad (2.27)$$

where the state vector, $x(t) \in \mathbb{R}^{11 \times 1}$, and the control vector, $u(t) \in \mathbb{R}^{3 \times 1}$, are defined as:

$$x = [\omega_1, \omega_2, \omega_3, \dot{\psi}_1, \dot{\psi}_2, \psi_1, \psi_2, q_0, q_1, q_2, q_3]^T, \quad (2.28)$$

$$u = [u_1, u_2, u_3]^T, \quad (2.29)$$

where u_1 , u_2 , and u_3 are the components of the control torque produced by the actuators. We assume that angular rates and attitude of the spacecraft are available for measurement through rate gyros and horizon sensors [10] and $C = [\mathbb{I}_{3 \times 3} \ 0_{3 \times 8}; 0_{4 \times 7} \ \mathbb{I}_{4 \times 4}]$. The slosh parameters as of pendulum positions and angular rates are difficult or impossible to measure and, therefore, they will be estimated. Details are described in section 3.3. $f(x)$ and $g(x)$ are obtained in the following forms:

$$f(x) = (M')^{-1}E', \quad (2.30)$$

$$g(x) = (M')^{-1}\mathbb{I}'. \quad (2.31)$$

The block matrix $M' \in \mathbb{R}^{11 \times 11}$ is defined as:

$$M' = \begin{bmatrix} M & 0 \\ 0 & \mathbb{I} \end{bmatrix}, \quad (2.32)$$

where $M \in \mathbb{R}^{5 \times 5}$, $\mathbb{I} \in \mathbb{R}^{6 \times 6}$. The block matrix $\mathbb{I}' \in \mathbb{R}^{11 \times 3}$ is defined as $\mathbb{I}' = [\mathbb{I}_1, 0]^T$ with identity matrix $\mathbb{I}_1 \in \mathbb{R}^{3 \times 3}$. The elements of the matrix M and vector $E' \in \mathbb{R}^{11 \times 1}$ are presented in the Appendix (A.1).

CHAPTER 3

Takagi-Sugeno Fuzzy Modeling

3.1 Introduction

Takagi-Sugeno (T-S) fuzzy model was proposed by Tomohiro Takagi and Michio Sugeno in 1985 [49]. The basic idea of the T-S model is to approximate the complex nonlinear systems by fuzzy blending of the local linear models in different state regions. Furthermore, the obtained fuzzy model can be used to control and study the stability of the system using the Lyapunov method [52]. The T-S fuzzy model is a universal approximator of any smooth nonlinear control system. In recent years, there has been great interest in using the T-S model to approximate the complex nonlinear dynamical system of spacecraft for stability analysis and control [58–62, 71–73].

In this chapter, T-S fuzzy model is constructed to approximate the nonlinear system of spacecraft with fuel sloshing. The T-S fuzzy observer is constructed to estimate the unmeasurable states. Further, the T-S model with uncertainties are constructed. In the end, the presented T-S model is validated.

3.2 T-S Fuzzy Modeling

To construct the T-S fuzzy model, we consider the nonlinear system in Eq. (2.27) and use the local approximation method [52]. The fuzzy linear model approximates the nonlinear system around the selected parameter values (or premise variables) and uses membership functions

in the universe of discourse of each premise variable and IF-THEN rules corresponding to each point.

The i^{th} rule of the T-S fuzzy model can be described in the following form:

Plant Rule i :

IF z_1 is μ_{i1} AND ... AND z_p is μ_{ip} ,

THEN

$$\Sigma_i : \begin{cases} \dot{x}(t) = A_i x(t) + B_i u(t), & (i = 1, \dots, r), \\ y(t) = C_i x(t), \end{cases} \quad (3.1)$$

where z_j is the premise variables and $\mu_{ij}[z_j]$ is the grade of membership of z_j in the fuzzy set μ_{ij} , r is the number of model rules, and $x(t) \in \mathbb{R}^{n \times 1}$, $u(t) \in \mathbb{R}^{m \times 1}$, and $y(t) \in \mathbb{R}^{q \times 1}$ are the state, input and output vectors, respectively. $A_i \in \mathbb{R}^{n \times n}$, $B_i \in \mathbb{R}^{n \times m}$, and $C_i \in \mathbb{R}^{q \times n}$ are the system, input and output matrices, respectively, for each rule. Furthermore, we show that Σ_i is controllable and observable.

Combining all the rules of T-S models, the nonlinear system Eq. (2.27) can be approximated by the following form:

$$\Sigma_{TS} : \begin{cases} \dot{x}(t) = \sum_{i=1}^r h_i[z] \{A_i x(t) + B_i u(t)\}, \\ y(t) = \sum_{i=1}^r h_i[z] C_i x(t), \end{cases} \quad (3.2)$$

where the nonnegative fuzzy basis functions are

$$h_i[z] = \frac{w_i[z]}{\sum_{i=1}^r w_i[z]}, \quad (3.3)$$

and their summation equals one. The firing strength of each model rule is determined using

the T – norm product as follows:

$$w_i[z] = \prod_{j=1}^p \mu_{ij}[z_j], \quad (3.4)$$

where

$$\sum_{i=1}^p \mu_{ij}[z_j] = 1, \quad 0 \leq \mu_{ij}[z_j] \leq 1. \quad (3.5)$$

To apply the T-S fuzzy model to the nonlinear system Eq. (2.27), we choose the fuzzy premise variables to be the angular velocities of the spacecraft and the unit quaternion from the state vector Eq. (2.28):

$$z_1 \triangleq \omega_1, z_2 \triangleq \omega_2, z_3 \triangleq \omega_3, z_4 \triangleq q_0, z_5 \triangleq q_1, z_6 \triangleq q_2, z_7 \triangleq q_3. \quad (3.6)$$

For each fuzzy premise variable we choose their possible minimum and maximum values

Table 3.1: Fuzzy Rule Table (*Negative = N, Positive = P*)

Rules	z_1	z_2	z_3	z_4	z_5	z_6	z_7
R1	<i>N</i>	<i>N</i>	<i>N</i>	<i>N</i>	<i>N</i>	<i>N</i>	<i>N</i>
R2	<i>N</i>	<i>N</i>	<i>N</i>	<i>N</i>	<i>N</i>	<i>N</i>	<i>P</i>
R3	<i>N</i>	<i>N</i>	<i>N</i>	<i>N</i>	<i>N</i>	<i>P</i>	<i>N</i>
R4	<i>N</i>	<i>N</i>	<i>N</i>	<i>N</i>	<i>N</i>	<i>P</i>	<i>P</i>
\vdots	\vdots	\vdots	\vdots	\vdots	\vdots	\vdots	\vdots
R127	<i>P</i>	<i>P</i>	<i>P</i>	<i>P</i>	<i>P</i>	<i>P</i>	<i>N</i>
R128	<i>P</i>	<i>P</i>	<i>P</i>	<i>P</i>	<i>P</i>	<i>P</i>	<i>P</i>

representing as $z_j \in \{Negative, Positive\}$, ($j = 1, \dots, 7$) and construct $2^7 = 128$ rules. Below we describe the third plant rule, and all possible combinations for 128 rules are described in Table 3.1.

Plant Rule 3:

IF z_1 is *Negative* AND z_2 is *Negative* AND z_3 is *Negative* AND

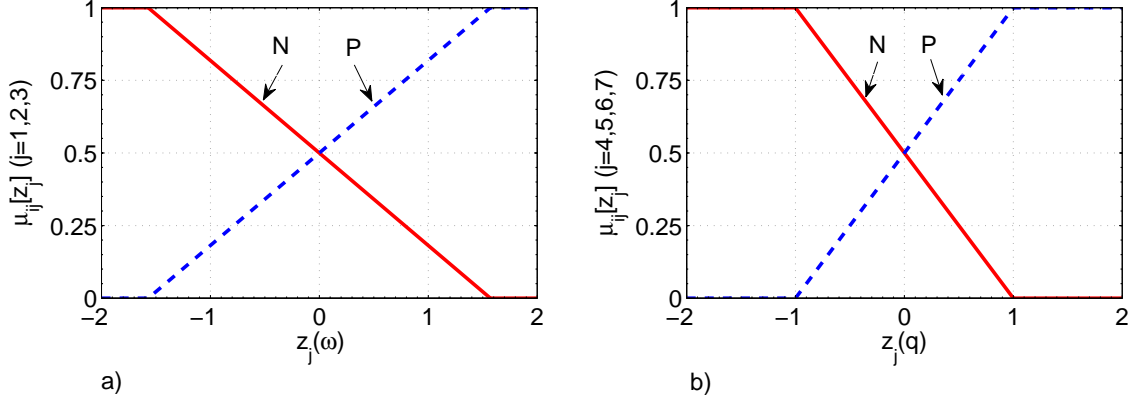


Fig. 3.1: Fuzzy membership functions and universe of discourse for the premise variables: a) $\mu_{ij}[z_j(\omega)]$ ($i = 1, \dots, 128; j = 1, 2, 3$) and b) $\mu_{ij}[z_j(q)]$ ($i = 1, \dots, 128; j = 4, 5, 6, 7$).

z_4 is *Negative* AND z_5 is *Negative* AND z_6 is *Positive* AND z_7 is *Negative*,

THEN

$$\Sigma_3 : \begin{cases} \dot{x}(t) = A_3x(t) + B_3u(t), \\ y(t) = C_3x(t). \end{cases} \quad (3.7)$$

State space matrices can be obtained by linearizing the nonlinear system in Eq. (2.27) around the possible sets from Table 3.1. The membership functions of the fuzzy sets μ_{ij} ($i = 1, \dots, 128; j = 1, \dots, 7$) can be defined through *Negative* and *Positive* sets as shown in Fig. 3.2.

3.3 T-S Fuzzy Observer

In real control problems, all states cannot always be directly measured. Therefore, the fuzzy observer is considered to estimate the unavailable states. Rate gyros and horizon sensors are used to measure the angular rates and attitude of the spacecraft [10] but the slosh parameters as of pendulum positions and angular rates are difficult or impossible to measure. We consider the T-S observer based, output feedback stabilization for the nonlinear system, Eq. (2.27), and

the measurable output is $y(t) = Cx$, where matrix $C = [\mathbb{I}_{3 \times 3} \ 0_{3 \times 8}; 0_{4 \times 7} \ \mathbb{I}_{4 \times 4}]$, assuming that the states of angular velocities and the unit quaternion are available. Thereafter, we consider the case when the premise variables depend on the available state variables. The i^{th} rule of the T-S fuzzy observer can be described in the following form [52]:

Observer Rule i :

IF z_1 is μ_{i1} AND... AND z_p is μ_{ip} ,

THEN

$$\Sigma_{O_i} : \begin{cases} \dot{\hat{x}}(t) = A_i \hat{x}(t) + B_i u(t) + L_i [y(t) - \hat{y}(t)], & (i = 1, \dots, r), \\ \hat{y}(t) = C_i \hat{x}(t), \end{cases} \quad (3.8)$$

where $L_i \in \mathbb{R}^{n \times p}$ is the observer gain for the i^{th} observer rule, $\hat{x}(t)$ is the state vector estimated by a fuzzy observer. $y(t) \in \mathbb{R}^{p \times 1}$ is the measurable output, and $\hat{y}(t) \in \mathbb{R}^{(n-p) \times 1}$ is the estimated output vector.

The overall fuzzy observer can be defined as

$$\Sigma_O : \begin{cases} \dot{\hat{x}}(t) = \sum_{i=1}^r h_i[z] \{A_i \hat{x}(t) + B_i u(t) + L_i [y(t) - \hat{y}(t)]\}, \\ \hat{y}(t) = \sum_{i=1}^r h_i[z] C_i \hat{x}(t). \end{cases} \quad (3.9)$$

The fuzzy observer is required to satisfy $e(t) = [x(t) - \hat{x}(t)] \rightarrow 0$ when $t \rightarrow \infty$, i.e., the steady-state error between $x(t)$ and $\hat{x}(t)$ converges to zero.

3.4 T-S Fuzzy Model with Uncertainty

To construct the T-S fuzzy model with uncertainty, we add uncertainty blocks to the T-S fuzzy model addressing the structure and actuator uncertainties. The i^{th} rule of the T-S fuzzy model with uncertainty can be described in the following form:

Plant Rule i :

IF $z_1(t)$ is μ_{i1} and ... and $z_p(t)$ is μ_{ip} ,

THEN

$$\Sigma_i : \begin{cases} \dot{x}(t) = (A_i + D_{ai}\Delta_{ai}(t)E_{ai})x(t) + (B_i + D_{bi}\Delta_{bi}(t)E_{bi})u(t), & (i = 1, \dots, r), \\ y(t) = C_i x(t), \end{cases} \quad (3.10)$$

where z_j is the premise variables and $\mu_{ij}[z_j]$ is the grade of membership of z_j in the fuzzy set μ_{ij} , r is the number of model rules, and $x(t) \in \mathbb{R}^{n \times 1}$, $u(t) \in \mathbb{R}^{m \times 1}$, and $y(t) \in \mathbb{R}^{q \times 1}$ are the state, input and output vectors, respectively. $A_i \in \mathbb{R}^{n \times n}$, $B_i \in \mathbb{R}^{n \times m}$, and $C_i \in \mathbb{R}^{q \times n}$ are the system, input and output matrices, respectively, for each rule. Furthermore, we show that Σ_i is controllable and observable. $D_{ai} \in \mathbb{R}^{n \times p}$, $E_{ai} \in \mathbb{R}^{p \times n}$, $D_{bi} \in \mathbb{R}^{n \times q}$ and $E_{bi} \in \mathbb{R}^{q \times m}$ are constant row vectors, which characterize the structure of the uncertainty. The uncertain blocks for all i satisfy

$$\|\Delta_{ai}(t)\| \leq \frac{1}{\gamma_{ai}}, \quad \Delta_{ai}(t) = \Delta_{ai}^T(t), \quad (3.11)$$

$$\|\Delta_{bi}(t)\| \leq \frac{1}{\gamma_{bi}}, \quad \Delta_{bi}(t) = \Delta_{bi}^T(t). \quad (3.12)$$

Combining all the rules of T-S models, the nonlinear system (2.27) can be approximated to the following form:

$$\Sigma_{TS} : \begin{cases} \dot{x}(t) = \sum_{i=1}^r h_i[z(t)] \{(A_i + D_{ai}\Delta_{ai}(t)E_{ai})x(t) + (B_i + D_{bi}\Delta_{bi}(t)E_{bi})u(t)\}, \\ y(t) = \sum_{i=1}^r h_i[z(t)] C_i x(t), \end{cases} \quad (3.13)$$

where the fuzzy basis functions are

$$h_i[z(t)] = \frac{w_i[z(t)]}{\sum_{i=1}^r w_i[z(t)]}, \quad (3.14)$$

and the firing strength of each model rule is determined using $T - norm$ product as follows

$$w_i[z(t)] = \prod_{j=1}^p \mu_{ij}[z_j(t)], \quad (3.15)$$

where

$$\sum_{i=1}^p \mu_{ij}[z_j] = 1, \quad 0 \leq \mu_{ij}[z_j] \leq 1. \quad (3.16)$$

To apply the T-S fuzzy model on nonlinear system Eq. (2.27) we choose fuzzy premise variables to be angular velocities of the spacecraft and unit quaternion from state vector Eq. (2.28):

$$z_1 \triangleq \omega_1, z_2 \triangleq \omega_2, z_3 \triangleq \omega_3, z_4 \triangleq q_0, z_5 \triangleq q_1, z_6 \triangleq q_2, z_7 \triangleq q_3. \quad (3.17)$$

For each fuzzy premise variable we choose their possible minimum and maximum values representing as $z_j \in \{Negative, Positive\}$, ($j = 1, \dots, 7$) and construct $2^7 = 128$ rules. All possible combinations for 128 rules are described in Table 3.1. State space matrices can be obtained by linearizing the nonlinear system in Eq. (2.27) around the possible sets from Table 3.1. The membership functions of the fuzzy sets μ_{ij} ($i = 1, \dots, 128; j = 1, \dots, 7$) can be defined through *Negative* and *Positive* sets as shown in Fig. 3.2.

3.5 T-S Fuzzy Model Validation

We use MATLAB/ SIMULINK[®] to model and simulate the response of the open and closed-loop systems. For the numerical simulation, we use the data of the Deep Space One (DS1) spacecraft described in the paper by Quadrelli [25]. The DS1 spacecraft contains a monopro-

pellant hydrazine propulsion system for the attitude control. The system includes one spherical titanium propellant tank with diameter 0.418 m and the center of the tank is attached to the center of the axis of the spacecraft.

Table 3.2: The spherical pendulum and spring-damper parameters

Parameter	Value	Units
m	643.6	kg
m_0	26.6310	kg
m_P	2.0686	kg
l_P	0.07	m
h_0	0	m
h_1	0.10	m
$D_{\psi_1}=D_{\psi_2}$	0.03	$N.s/m$
$K_{\psi_1}=K_{\psi_2}$	0.34	N/m

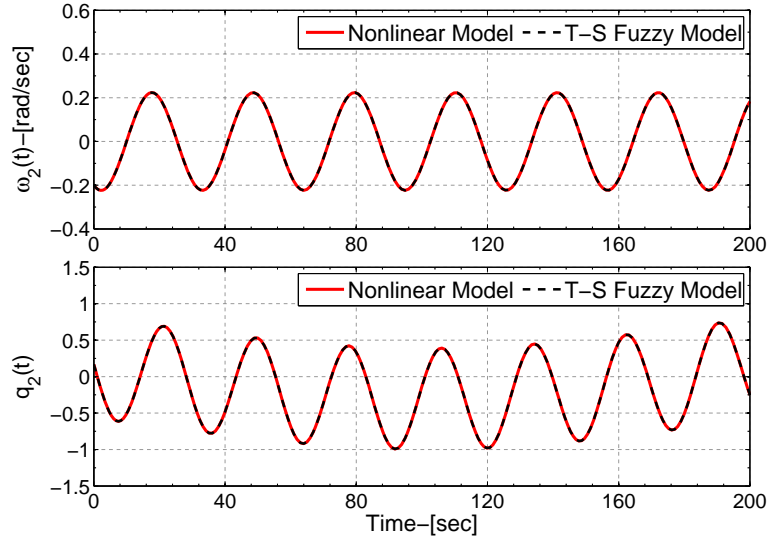


Fig. 3.2: Time response of the selected states for the open-loop validation.

The simulation is conducted for the third-stage vehicle after post-burn. The physical parameters of the whole third-stage vehicle including the STAR 37 FM solid-rocket motor attached to the DS1 spacecraft and the spherical pendulum are given in Table 3.2. The inertia matrix of the spacecraft with respect to its principal axes is $I^{S^*} = \text{diag}(540.97, 540.97, 173.5)\text{ kg.m}^2$, where $\text{diag}(\cdot)$ function denotes a diagonal matrix.

Table 3.3: Initial Conditions

Parameter	Value	Units
$\omega_1(0)$	0.1	<i>rad/s</i>
$\omega_2(0)$	-0.2	<i>rad/s</i>
$\omega_3(0)$	0.3	<i>rad/s</i>
$q_0(0)$	0.720006	
$q_1(0)$	0.411592	
$q_2(0)$	0.170797	
$q_3(0)$	-0.531989	
$\psi_1(0)$	$15\pi/180$	<i>rad</i>
$\psi_2(0)$	$10\pi/180$	<i>rad</i>
$\dot{\psi}_1(0)$	$2\pi/180$	<i>rad/s</i>
$\dot{\psi}_2(0)$	$3\pi/180$	<i>rad/s</i>

Let us define the universe of discourses as: $z_\omega = [z_1, z_2, z_3] \in [-\pi/2, \pi/2]$ *rad/s* and $z_q = [z_4, z_5, z_6, z_7] \in [-1, 1]$. The model rules are constructed based on the strategy presented in Table 3.1. Linearizing the nonlinear system Eq. (2.27) around the possible sets presented in Table 3.1 with given values, including $\psi_1 = \dot{\psi}_1 = \dot{\psi}_2 = 0$, and $\psi_2 = \pi/180$ *rad*, we obtain the local state-space models. Then, we construct the T-S fuzzy model by following the 128 rules described in section (3.2) with the membership functions of the fuzzy sets μ_{ij} ($i = 1, \dots, 128; j = 1, \dots, 7$) shown in Fig. 3.2. We validate the T-S fuzzy model by comparing the open-loop response of all the states of the T-S fuzzy model with the nonlinear model, Eq. (2.27). The time history of $\omega_2(t)$ and $q_2(t)$ are shown in Fig. 3.2 with the initial conditions presented in Table 3.3.

CHAPTER 4

Fuzzy Controller Design

4.1 Introduction

Designing an active attitude control system for a spacecraft with partially filled tank is a challenging task because of the highly nonlinear and coupled dynamics of the system. Different controllers are designed to stabilize the attitude of a spacecraft with fuel sloshing such as PID, LQR, Lyapunov based nonlinear feedback control, adaptive control [37, 40–42, 44, 46, 48]. In this chapter we present and compare fuzzy controllers as fuzzy PDC, fuzzy LQR and robust optimal fuzzy control to stabilize the attitude of spacecraft with a partially filled tank. We introduce an observer to estimate the unmeasurable states.

Fuzzy PDC control design with the actuator amplitude constraint utilizes the Parallel Distributed Compensation (PDC) technique [50, 51, 55] based on T-S fuzzy model described in Chapter 3. The main idea of the PDC controller is to design a linear feedback control for each local model and obtain the overall nonlinear controller by fuzzy blending these linear controllers. The advantage of the PDC controller is the simple structure, and it's easy to implement. Another advantage is the control design procedure can be formulated in terms of linear matrix inequalities (LMIs), which addresses the stability, performance, and robustness of the closed-loop system at the same time. Furthermore, with small modification in the set of LMIs, the design procedure can be easily modified to address the problem of maximizing the size of the reachability set, and maximizing the decay rate.

The proposed robust-optimal fuzzy controller/observer design with the actuator amplitude

constraint for spacecraft with fuel sloshing is based on the PDC technique [52] that simultaneously considers both the robust fuzzy and the optimal fuzzy controller designs. Using Lyapunov stability theory and linear matrix inequalities (LMIs) the problem is formulated as a convex optimization problem. The robust control addresses the uncertainties in the structure and actuators while the optimal fuzzy control addresses the optimality in certain quadratic performance function.

Recently, the fuzzy control was synthesized with classical control designs such as LQR, PID, sliding mode control etc. [65–68]. We propose the fuzzy control synthesized with LQR (fuzzy LQR), which we apply to spacecraft with fuel sloshing. The Linear Quadratic Regulator (LQR), a design method for multivariable system, is known to yield good performance for linear systems while the fuzzy control yield good performance for nonlinear systems.

This chapter presents the controller designs in the following order: the fuzzy PDC; robust optimal fuzzy control; fuzzy LQR; and PID as a baseline controller. It follows with the numerical simulation results of designed controllers including the efficacy and robustness of the proposed fuzzy controllers. In the end, design case studies are presented.

4.2 Fuzzy PDC Controller Design

This section introduces the Parallel Distributed Compensation (PDC) nonlinear control technique in the presence of the T-S fuzzy observer, Eq. (3.9). First, for each model rule the control law is designed by the fuzzy IF-THEN implications. The third control rule is described below, and the other 127 control rules are defined in an analogous way based on the model rules from Table 3.1.

Control Rule 3:

IF z_1 is *Negative* AND z_2 is *Negative* AND z_3 is *Negative* AND

z_4 is Negative AND z_5 is Negative AND z_6 is Positive AND z_7 is Negative,

THEN

$$u_3(t) = -K_3\hat{x}(t), \quad (4.1)$$

and the overall fuzzy controller becomes

$$u(t) = -\sum_{i=1}^r h_i[z]K_i\hat{x}(t), \quad (4.2)$$

where $h_i[z]$ are obtained from Eq. (3.14) and K_i are the feedback gains.

Using a quadratic Lyapunov function, $V(x) = x^T Px$, where $P = P^T > 0$, we can show that the problem of determining the feedback gains K_i ($i = 1, \dots, 128$) and observer gains L_i ($i = 1, \dots, 128$), which stabilize the T-S fuzzy system Eq. (3.2) and fuzzy observer system Eq. (3.9), can be cast into the following linear matrix inequalities form [52] including LMIs of control input constraints:

$$LMI_1 : \begin{cases} P^{-1} = G > 0, \\ -GA_i^T - A_iG + M_i^T B_i^T + B_i M_i - 2dG > 0, \quad (i = 1, \dots, 128), \\ -GA_i^T - A_iG - GA_j^T - A_jG + M_j^T B_i^T + B_i M_j + M_i^T B_j^T + \\ \quad + B_j M_i - 4dG \geq 0, \quad (i, j = 1, \dots, 128), \end{cases} \quad (4.3)$$

and

$$LMI_2 : \begin{cases} R^{-1} = Q > 0, \\ -A_i^T Q - QA_i + C_i^T N_i^T + N_i C_i - 2dG > 0, \quad (i = 1, \dots, 128), \\ -A_i^T Q - QA_i - A_j^T Q - QA_j + C_i^T N_j^T + N_j C_i + C_j^T N_i^T + \\ \quad + N_i C_j - 4dG \geq 0, \quad (i, j = 1, \dots, 128), \end{cases} \quad (4.4)$$

such that $i \leq j$ for $h_i \cap h_j \neq \emptyset$. In Eqs. (4.3) and (4.4), the M_i and N_i matrices are defined

as:

$$M_i = K_i G \text{ or } K_i = M_i G^{-1}, \quad (4.5)$$

and

$$N_i = Q L_i \text{ or } L_i = Q^{-1} N_i. \quad (4.6)$$

d is the decay rate and $d > 0$. We obtain a stable fuzzy controller design when $d = 0$.

We include the control input constraint equations $|u_i(t)| \leq \alpha_i$ ($i = 1, 2, 3$) in the form of the following LMIs:

$$LMI_3 : \begin{bmatrix} G & (M_k)_i^T \\ (M_k)_i & \alpha_k^2 \end{bmatrix} \geq 0, \quad (i = 1, \dots, 128), \text{ and } (k = 1, 2, 3). \quad (4.7)$$

where $(M_k)_i = (K_k)_i G$ and K_k is the k^{th} row of K_i . The initial constraint is defined by the following LMI:

$$LMI_4 : \begin{bmatrix} 1 & x(0)^T \\ x(0) & G \end{bmatrix} \geq 0. \quad (4.8)$$

To make the solution of the system independent of the initial conditions, we assume $\|x(0)\| \leq \beta$ and, therefore, we can replace Eq. (4.8) with

$$LMI_5 : G \geq \beta^2 \mathbb{I}. \quad (4.9)$$

The feasible solution of Eqs. (4.3), (4.4), (4.7), and (4.9)—which is to find the common positive definite matrix G , Q and M_i, N_i ($i = 1, \dots, 128$)—yields the local state-feedback gains, K_i , and observer gains, L_i . We are interested in minimizing the control input upper bound or actuator size while the upper bound on the initial states and decay rate are known. The modified LMIs for input bound constrains $|u_i(t)| \leq \alpha_i$, ($i = 1, 2, 3$) are given in Eq. (4.7). Defining $\alpha = [\alpha_1, \alpha_2, \alpha_3]^T$, the optimization problem is formulated as:

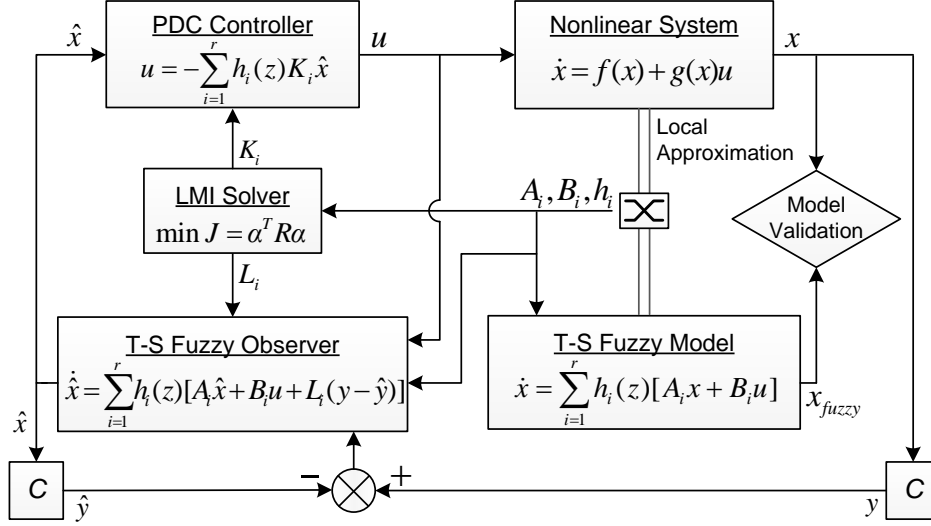


Fig. 4.1: Schematic diagram of the fuzzy PDC observer-based feedback control.

$$\begin{aligned}
 & \text{Minimize:} && J = \alpha^T R \alpha, && R = R^T > 0, \\
 & (G, Q, M_i, N_i) && && \\
 & \text{subject to:} && \text{Eqs. (4.3), (4.4), (4.7), and (4.9)}. &&
 \end{aligned} \tag{4.10}$$

The set of LMIs can be solved by any convex optimization software such as the Matlab LMI Control Toolbox [84], or the Matlab toolbox YALMIP which uses an interior-point solver [85].

The schematic diagram of the T-S fuzzy observer-based feedback control is presented in Fig. 4.1. The design procedure consists of the following steps:

1. Obtain the mathematical model of the plant to be controlled.
2. Design and validate the T-S fuzzy model for the nonlinear system stated in Step 1.
3. Design the fuzzy PDC controller.
4. Design the fuzzy observer for the T-S fuzzy model from Step 2.
5. Solve the LMIs to find feedback gains and observer gains for each rule.
6. Obtain the overall controller in Step 3 and apply to nonlinear system stated in Step 1.

4.3 Robust-Optimal Fuzzy Control

We design a robust-optimal fuzzy controller to stabilize the attitude of spacecraft with fuel slosh. The Parallel Distributed Compensation (PDC) nonlinear control technique [55] based on the T-S fuzzy observer model (3.9) is implied. For each model rule described in section 2 the control law is designed by the fuzzy IF-THEN implications and the overall fuzzy controller results to

$$u(t) = - \sum_{i=1}^r h_i[z] K_i \hat{x}(t), \quad (4.11)$$

where $h_i[z]$ are obtained from Eq. (3.14) and K_i are the feedback gains. Using a quadratic Lyapunov function, $V(x) = x^T P x$, we can show that the problem of determining the feedback gains K_i ($i = 1, \dots, 128$) and observer gains L_i ($i = 1, \dots, 128$) which stabilize the T-S fuzzy system Eq. (3.13) and fuzzy observer system Eq. (3.9) can be cast into the following linear matrix inequalities [52] including LMIs of control input constraints [96]:

$$\begin{array}{ll} \text{Minimize:} & J = \lambda + \sum_{i=1}^r \{\alpha_i \gamma_{ai}^2 + \beta_i \gamma_{bi}^2\}, \\ \lambda, \gamma_{ai}^2, \gamma_{bi}^2, X, M_1, \dots, M_r & \end{array} \quad (4.12)$$

$$\text{Subject to:} \quad \text{Eqs. (4.13)–(4.17)}$$

$$LMI_1 : \begin{cases} P^{-1} = X > 0, \\ S_{ii} < 0, \\ T_{ij} < 0, \end{cases} \quad (4.13)$$

$$LMI_2 : \begin{cases} U_{ii} < 0, \\ V_{ij} < 0, \end{cases} \quad (4.14)$$

$$LMI_3 : \begin{cases} R^{-1} = Q > 0, \\ -A_i^T Q - QA_i + C_i^T N_i^T + N_i C_i - 2dX > 0, \\ -A_i^T Q - QA_i - A_j^T Q - QA_j + C_i^T N_j^T + N_j C_i + C_j^T N_i^T + \\ \quad + N_i C_j - 4dX \geq 0, \end{cases} \quad (4.15)$$

$$LMI_4 : \begin{bmatrix} X & (M_k)_i^T \\ (M_k)_i & \mu_k^2 \end{bmatrix} \geq 0, \quad (4.16)$$

$$LMI_5 : \begin{bmatrix} 1 & x(0)^T \\ x(0) & X \end{bmatrix} \geq 0, \quad (4.17)$$

where $(i = 1, 2, \dots, r)$ and $i < j \leq r$ such that $h_i \cap h_j \neq \emptyset$, and $(k = 1, 2, 3)$. d is the decay rate and $d > 0$. We obtain a stable fuzzy controller design when $d = 0$.

As noted in Eq. (4.12), the objective of the design is to synthesize 1) the robust fuzzy controller design minimizing γ_{ai} and γ_{bi} described in Eq. (3.11) in the class of the PDC controller, Eq. (4.11), while satisfying the robust stability conditions, Eq. (4.13), and 2) the optimal fuzzy controller design minimizing λ , the upper bound of the quadratic performance function, Eq. (4.18), while satisfying the optimal stability conditions, Eq. (4.14). α_i and β_i are the design parameters and λ is the upper bound of the quadratic performance function

$$J_1 = \int_0^\infty y^T(t)W y(t) + u^T(t)R u(t)dt < x^T(0)X x(0) < \lambda, \quad (4.18)$$

where

$$y(t) = \sum_{i=1}^r h_i[z(t)]C_i x(t) \quad (4.19)$$

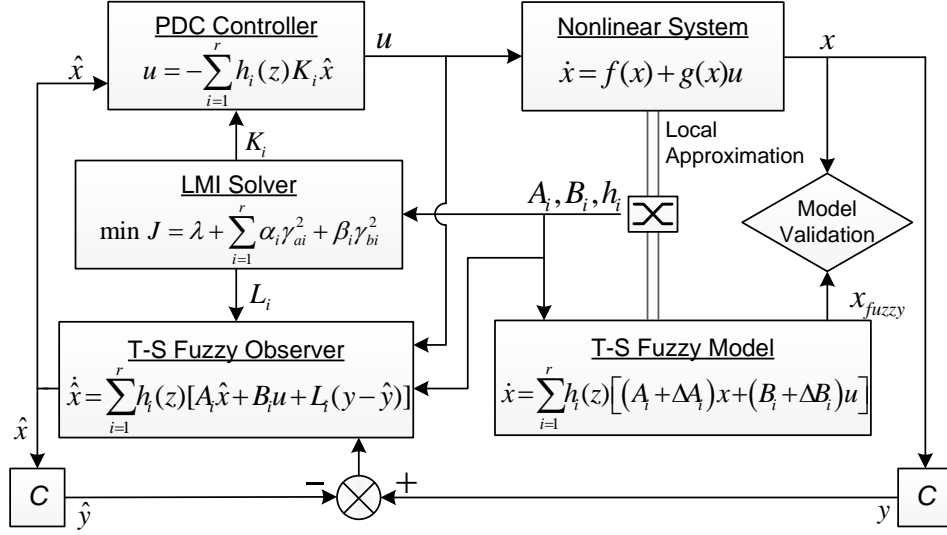


Fig. 4.2: Schematic diagram of the robust-optimal T-S fuzzy observer-based feedback control.

and $W = W^T > 0$ and $R = R^T > 0$ are weighting coefficient matrices.

Note that in the robust-optimal stability conditions, Eq. (4.13) and Eq. (4.14), we have

$$S_{ii} = \begin{bmatrix} X A_i^T + A_i X - B_i M_i - M_i^T B_i^T & * & * & * & * \\ D_{ai}^T & -\mathbb{I} & * & * & * \\ D_{bi}^T & 0 & -\mathbb{I} & * & * \\ E_{ai} X & 0 & 0 & -\gamma_{ai}^2 \mathbb{I} & * \\ -E_{bi} M_i & 0 & 0 & 0 & -\gamma_{bi}^2 \mathbb{I} \end{bmatrix}, \quad (4.20)$$

and

$$U_{ii} = \begin{bmatrix} X A_i^T + A_i X - B_i M_i - M_i^T B_i^T & * & * \\ C_i X & -W^{-1} & * \\ -M_i & 0 & -R^{-1} \end{bmatrix}, \quad (4.21)$$

and

$$T_{ij} = \begin{bmatrix} T_{ij}(1,1) & * & * & * & * & * & * & * & * & * \\ D_{ai}^T & -\mathbb{I} & * & * & * & * & * & * & * & * \\ D_{bi}^T & 0 & -\mathbb{I} & * & * & * & * & * & * & * \\ D_{aj}^T & 0 & 0 & -\mathbb{I} & * & * & * & * & * & * \\ D_{bj}^T & 0 & 0 & 0 & -\mathbb{I} & * & * & * & * & * \\ E_{ai}X & 0 & 0 & 0 & 0 & -\gamma_{ai}^2\mathbb{I} & * & * & * & * \\ -E_{bi}M_j & 0 & 0 & 0 & 0 & 0 & -\gamma_{bi}^2\mathbb{I} & * & * & * \\ E_{aj}X & 0 & 0 & 0 & 0 & 0 & 0 & -\gamma_{aj}^2\mathbb{I} & * & * \\ -E_{bj}M_i & 0 & 0 & 0 & 0 & 0 & 0 & 0 & -\gamma_{bj}^2\mathbb{I} & * \end{bmatrix}, \quad (4.22)$$

and

$$V_{ij} = \begin{bmatrix} V_{ij}(1,1) & * & * & * & * \\ C_iX & -W^{-1} & * & * & * \\ -M_j & 0 & -R^{-1} & * & * \\ C_jX & 0 & 0 & -W^{-1} & * \\ -M_i & 0 & 0 & 0 & -R^{-1} \end{bmatrix}, \quad (4.23)$$

where

$$T_{ij}(1,1) = V_{ij}(1,1) = XA_i^T + A_iX - B_iM_j - M_j^T B_i^T + XA_j^T + A_jX - B_jM_i - M_i^T B_j^T. \quad (4.24)$$

The M_i and N_i matrices are defined as:

$$M_i = K_iX \text{ or } K_i = M_iX^{-1}, \quad (4.25)$$

and

$$N_i = QL_i \text{ or } L_i = Q^{-1}N_i. \quad (4.26)$$

In the above designed optimization problem the LMI constraints include the robust, optimal, observer stability conditions, respectively Eq. (4.13), Eq. (4.14), and Eq. (4.15), the control input constraint equations $|u_i(t)| \leq \mu_i$ ($i = 1, 2, 3$) in the form of LMIs, Eq. (4.16), and the initial constraint defined in the form of LMI, Eq. (4.17). In the result of solving LMIs we can find the feedback gains K_i ($i = 1, \dots, 128$) and observer gains L_i ($i = 1, \dots, 128$), which stabilize the T-S fuzzy system Eq. (3.13) and fuzzy observer system Eq. (3.9).

The schematic diagram of the T-S robust-optimal fuzzy observer-based feedback control is presented in Fig. 4.2. The design procedure consists of the following steps:

1. Obtain the mathematical model of the plant to be controlled.
2. Design and validate the T-S fuzzy model for the nonlinear system stated in Step 1.
3. Design the T-S fuzzy model with uncertainties.
4. Design the robust-optimal fuzzy PDC controller.
5. Design the fuzzy observer for the T-S fuzzy model from Step 2.
6. Solve the LMIs to find feedback gains and observer gains for each rule.
7. Obtain the overall controller in Step 4 and apply to nonlinear system including uncertainties

$$\dot{x} = [f(x) + \Delta f(x)] + [g(x) + \Delta g(x)]u.$$

4.4 Fuzzy LQR Controller Design

A fuzzy LQR controller integrates fuzzy logic with the LQR [65]. First, the nonlinear system in Eq. (2.27) is linearized around some operating points using the T-S fuzzy modeling approach described in subsection 3.2. For each linearized model, we construct the local optimal control law, $u_{LQR} = -K_{i,LQR}\hat{x}$, ($i = 1, \dots, 128$), which minimizes the following cost

where x_{max} is the highest tolerable value for the state x_j ($j = 1, \dots, 11$), and u_{max} is the highest tolerable value for the input u_k ($k = 1, 2, 3$). Q_O and R_O are obtained similarly.

Thereafter, we obtain the overall fuzzy LQR controller as

$$u(t) = - \sum_{i=1}^r h_i[z] K_{i,LQR} \hat{x}(t), \quad (i = 1, \dots, 128), \quad (4.31)$$

where $K_{i,LQR}$ are the feedback gains and $h_i[z]$ are obtained in analogously, as described in subsection 3.2. The schematic diagram of the fuzzy LQR observer-based feedback control is presented in Fig. 4.3. It is analogous to the schematic diagram described in Fig. 4.2, except that to obtain the LQR controller and observer gains we solve the algebraic Riccati equations, Eqs. (4.28)-(4.29), instead of LMIs.

4.5 PID Controller Design

We compare the effectiveness of the robust-optimal fuzzy PDC controller with a fuzzy PDC and proportional-integral-derivative (PID) controllers. Fuzzy PDC was constructed and evaluated in our previous work [86]. The PID controllers have the following form:

$$u_i = -K_{P_i} q_i(t) - K_{I_i} \int q_i(t) dt - K_{D_i} \frac{d}{dt} q_i(t), \quad i = (1, 2, 3), \quad (4.32)$$

where q_i ($i = 1, 2, 3$) are the components of the unit quaternion, and K_{P_i} , K_{I_i} , and K_{D_i} are the proportional, integral and derivative gains for each of the three torque inputs, respectively. These gains can be tuned using the closed-loop Ziegler-Nichols method [88].

4.6 Numerical Simulation

4.6.1 A note on the Interior-Point Method

The class of numerical optimization problems called Linear Matrix Inequality (LMI) has received a significant attention in recent years [52–54, 84, 85]. The stability analysis and the most control design problems can be reduced to LMI problems. LMIs can be solved in polynomial time based on interior-point methods [89]. We use YALMIP, Yet Another LMI Parser, with solver SDPT3 [85] to find the feedback and observer gain matrices in the result of LMI optimization problems described in sections 4.2 and 4.3. YALMIP is a modeling language integrated and developed in the MATLAB environment. The infeasible primal-dual interior-point algorithm [90, 91] that uses the path-following paradigm is implemented in SDPT3. To decrease the duality gap as much as possible, the predictor search direction is computed in each iteration followed by generation of a Mehrotra-type corrector step [92] with the intention to keep the iterates close to the central path. The iteration is terminated if the infeasibility measure and the relative duality gap are sufficiently small, or numerical problems are encountered such as the iterates or the Schur complement matrix are not being positive definite. The search direction uses the HKM direction method, which is a Newton direction found from the linearization of a symmetrized version of the optimality condition.

4.6.2 Closed-Loop Simulation

First, we examine and compare the fuzzy PDC and fuzzy LQR controllers. The MATLAB /SIMULINK[®] software is used to model, simulate and analyze the closed-loop simulations for both controllers following the design procedures presented in the schematic diagrams 4.1 and 4.3. After validation of the T-S fuzzy model, we use the model rules and construct the fuzzy controller, Eq. (4.11), for the Fuzzy PDC controller. The feedback gains

K_i ($i = 1, \dots, 128$) and the observer gains, L_i ($i = 1, \dots, 128$), are found by solving the optimization problem described in Eq. (4.10) using the Matlab toolbox YALMIP [85] with SDPT3 described in subsection 4.6.1, which is a modeling language for solving convex and non-convex optimization problems. We choose the upper bound of the norm of the initial condition $\beta = 3$, and the decay rate parameter $d = 0.01$. Assuming all α_i ($i = 1, 2, 3$) are equal and $R = \text{diag}(1, 1, 1)$, we found that the minimum upper bound value for the control input is 79 $N.m$.

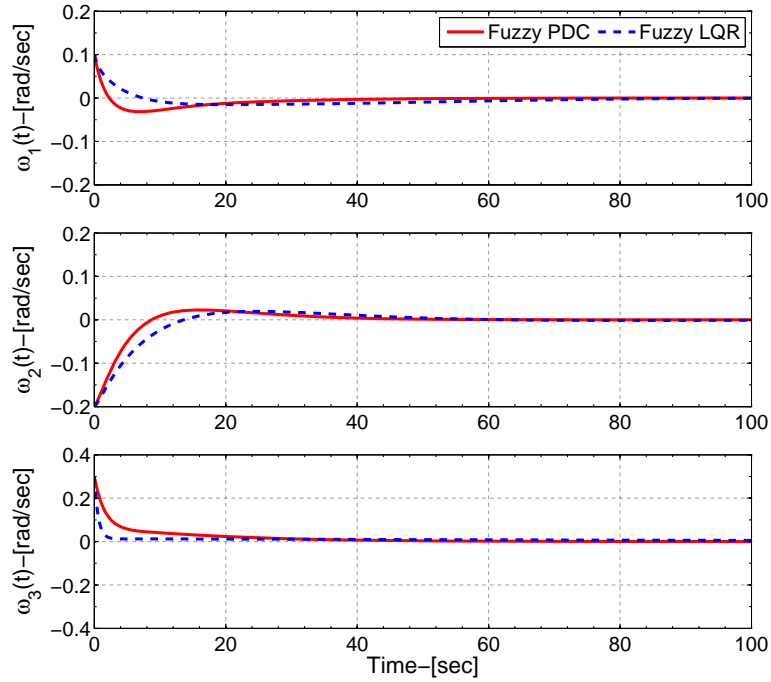


Fig. 4.4: Time responses of the spacecraft angular velocities using fuzzy PDC and fuzzy LQR controllers.

For the fuzzy LQR model, the feedback gain and observer gain matrices are found by solving the algebraic Riccati equations Eqs. (4.28)–(4.29) for each local linearized system. We note that for comparison the highest tolerable value for the control input in Eq. (4.30) is taken to be 79 $N.m$, which is the optimized value of the minimum upper bound value for the control input for the fuzzy PDC model.

The simulations of a closed-loop system for the fuzzy PDC and fuzzy LQR models are con-

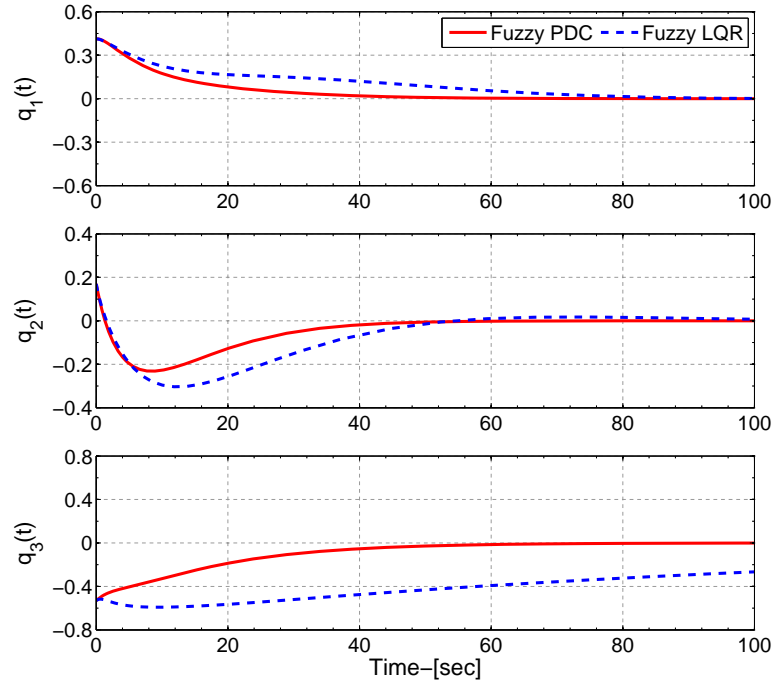


Fig. 4.5: Time responses of the quaternions using fuzzy PDC and fuzzy LQR controllers.

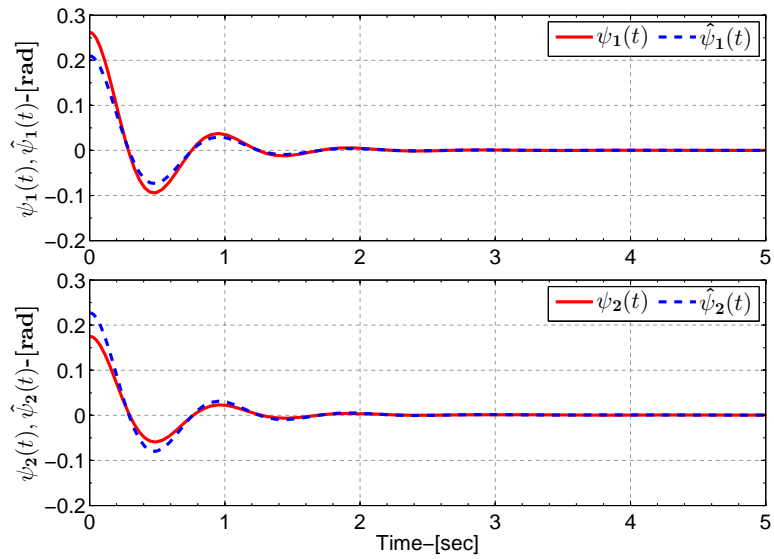


Fig. 4.6: Actual and estimated responses of the pendulum angles.

ducted with the initial conditions presented in the Table 3.3 and with the observer initial conditions presented in Table 4.1.

Figures 4.4 and 4.5 show the time history of the body angular velocities and quaternions,

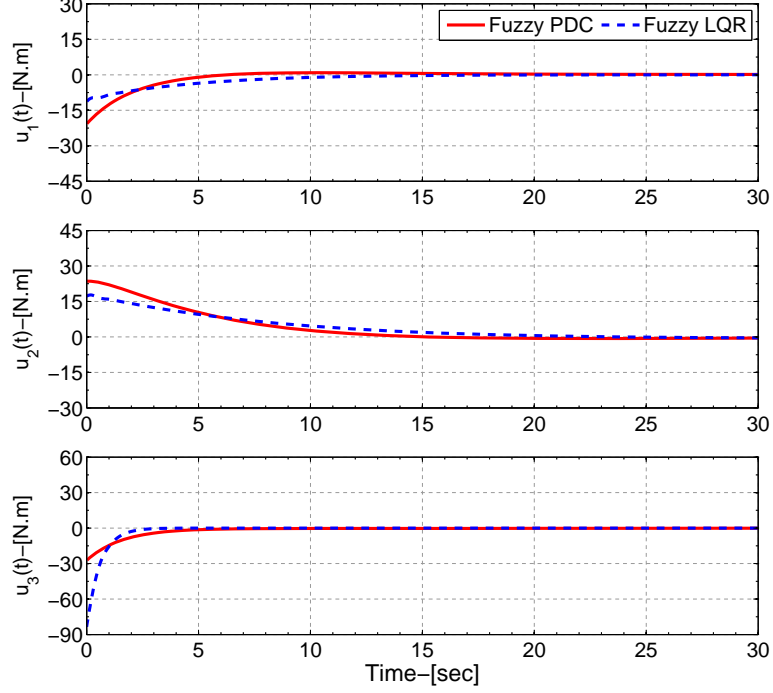


Fig. 4.7: Time responses of the control inputs using fuzzy PDC and fuzzy LQR controllers.

Table 4.1: Observer Initial Conditions

Parameter	Value	Units
$\hat{\psi}_1(0)$	$12\pi/180$	<i>rad</i>
$\hat{\psi}_2(0)$	$13\pi/180$	<i>rad</i>
$\hat{\dot{\psi}}_1(0)$	$2\pi/180$	<i>rad/s</i>
$\hat{\dot{\psi}}_2(0)$	$3\pi/180$	<i>rad/s</i>

respectively, both for the fuzzy PDC and fuzzy LQR controllers. The results show the fuzzy PDC has a smaller settling time and less overshoot compared to the fuzzy LQR. Figure 4.6 shows how the estimated states — the spherical pendulum angles — converge to their true values. The magnitude of each control input—which is the control moment about the body-fixed axis of spacecraft—are shown in Fig. 4.7. The plot shows that the fuzzy PDC satisfies the control input constraint $|u_i(t)| \leq 79 \text{ N.m}$, ($i = 1, 2, 3$) for all times while the fuzzy LQR attempts to use its maximum tolerable value for control input.

4.6.3 Robustness Evaluation

In this section we examine and compare the robustness of the fuzzy PDC and fuzzy LQR due to mass-moment-of-inertia uncertainties. Our numerical investigations show that the fuzzy

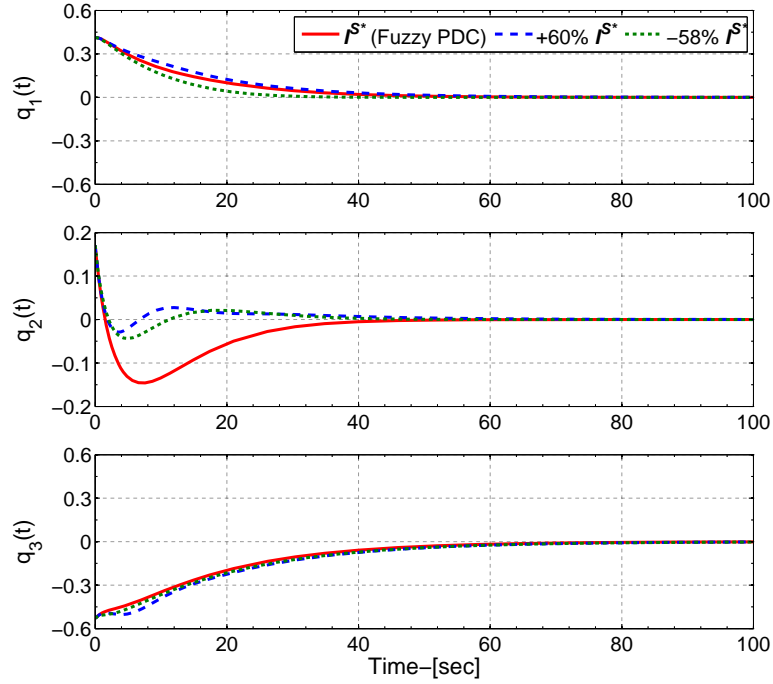


Fig. 4.8: The effect of uncertainty in the mass-moment-of-inertia on the time responses of quaternions using Fuzzy PDC controller.

PDC and fuzzy LQR controllers can stabilize the attitude of the spacecraft in the presence of about $\pm 60\%$ parameter uncertainties. It can be seen from Figs. 4.8 and 4.9 that the fuzzy PDC has less overshoot and faster response when compared to the proposed fuzzy LQR controller. We use the root-mean-square-error (RMSE) to quantitatively compare the performance of the controllers. The results for different mass-moment-of-inertia for the spacecraft angular velocity, ω , quaternions, q , and the control input, u , are summarized in Table 4.2. It can be seen that the error between the two controllers are very close when $0.42I^{S^*}$. On the other hand, when $1.6I^{S^*}$, the fuzzy PDC controller outperforms the fuzzy LQR.

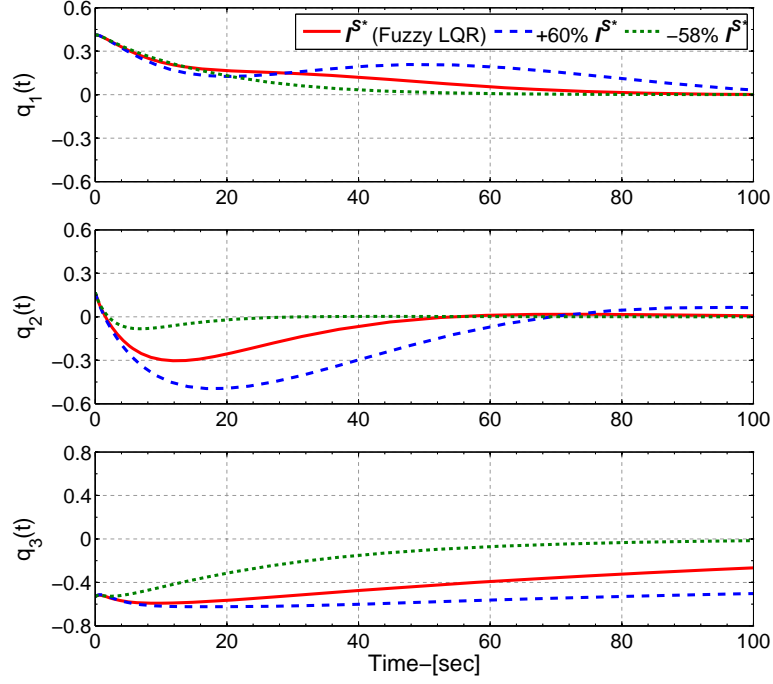


Fig. 4.9: The effect of uncertainty in the mass-moment-of-inertia on the time responses of quaternions using Fuzzy LQR controller.

Table 4.2: RMSE for states and control inputs using Fuzzy PDC and Fuzzy LQR

		Fuzzy PDC	Fuzzy LQR
ω	$0.42I^{S^*}$	0.0392	0.0359
	I^{S^*}	0.0483	0.0430
	$1.60I^{S^*}$	0.0488	0.0516
q	$0.42I^{S^*}$	0.2081	0.2629
	I^{S^*}	0.2123	0.4912
	$1.60I^{S^*}$	0.2271	0.6687
u	$0.42I^{S^*}$	3.2520	3.2259
	I^{S^*}	5.3343	6.0241
	$1.60I^{S^*}$	7.6595	8.4000

4.6.4 Robust-Optimal Simulation

In this section, we present the simulation results of proposed T-S robust-optimal fuzzy observer-based controller and compare it with fuzzy PDC and PID based on Ziegler-Nichols method.

For the numerical simulation, the inertia matrix of the spacecraft is taken as [25]

$$I^{S^*} = \text{diag}(540.97, 540.97, 173.5) \text{ kg.m}^2.$$

The $\text{diag}()$ function denotes a diagonal matrix. The physical parameters of the spacecraft and the spherical pendulum are given in Table 3.2. MATLAB /SIMULINK[®] is used to model and simulate the response of the open and closed-loop systems.

We follow the design procedure presented in the schematic diagrams 4.2. In section 3.5, we validated the developed T-S fuzzy model by comparing the open-loop response of all the states of the T-S fuzzy model with the nonlinear model, Eq. (2.27). After validation of the developed T-S fuzzy model, we use the model rules and construct the robust-optimal fuzzy controller Eq. (4.11). To reduce the duration of LMI solver, we choose the universe of discourses as: $z_\omega = [z_1, z_2, z_3] \in [-\pi/2, \pi/2] \text{ rad/s}$ and proceed with the eight model rules. Although, we note that open-loop validation deteriorated. The feedback and observer gains are found by solving the optimization problem with LMI constraints described in section 4.3 using the Matlab toolbox YALMIP [85] with SDPT3 solver. The simulation results of a closed-loop system are shown in Figs. 4.10– 4.13 with the initial conditions presented in Tables 3.3 and 4.1.

The uncertainty matrices for each rule in the T-S fuzzy model, Eq. (3.13), are defined as $D_a = 0.05 * \mathbb{J}_{11 \times 2}$, $D_b = 0.01 * \mathbb{J}_{11 \times 2}$, $E_a = 0.05 * \mathbb{J}_{2 \times 11}$, and $E_b = 0.01 * \mathbb{J}_{2 \times 11}$, where \mathbb{J} is the matrix of ones. The weighting matrix W and R in the quadratic performance function, Eq. (4.18), are obtained as follows:

$$W = \frac{1}{x_{max}^2} \mathbb{I}_{7 \times 7}, \quad R = 0.6 * \frac{1}{u_{max}^2} \mathbb{I}_{3 \times 3}, \quad (4.33)$$

where x_{max} is the highest tolerable value for the states, u_{max} is the highest tolerable value for the input, and \mathbb{I} is the identity matrix.

Figures 4.10 and 4.11 show the time history of the body angular velocities and quaternions in the N -frame, respectively. It can be seen that the closed-loop system could stabilize the

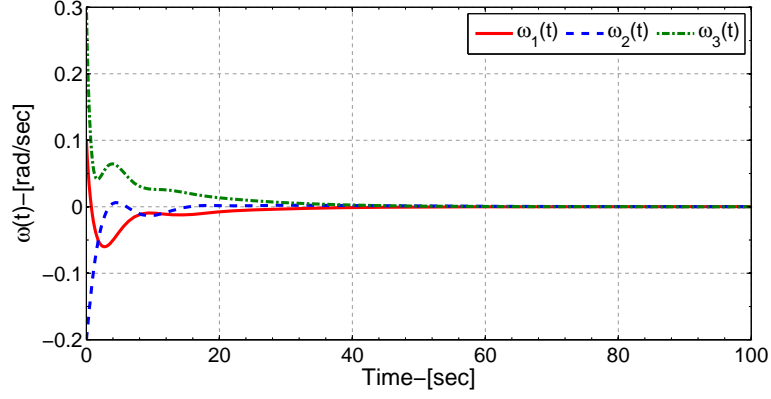


Fig. 4.10: Time response of the spacecraft angular velocity components.

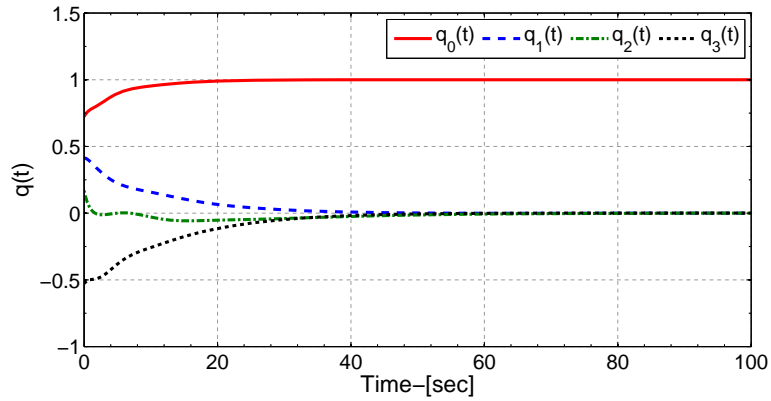


Fig. 4.11: Time response of the quaternions.

spacecraft attitude. As mentioned earlier, we assume that states of angular velocities and unit quaternion are available and therefore, the measurable output is defined as $y(t) = Cx$, where matrix $C = [\mathbb{I}_{3 \times 3} \ 0_{3 \times 8}; 0_{4 \times 7} \ \mathbb{I}_{4 \times 4}]$. A fuzzy observer described in section 3.3 is utilized to estimate the unavailable states corresponding to pendulum positions and angular rates. We apply the obtained fuzzy controller from Eq. (4.11) on the nonlinear model Eq. (2.27) as shown in Fig. 4.2. The actual (solid line) and estimated (dashed line) spherical pendulum angles are shown in Fig. 4.12. The results show that the angles and the estimation error go to zero rapidly.

In the LMIs, Eq. (4.16), we use the upper bound value for the control input as 79 N.m , which we found in the result of solving the optimization problem on actuator amplitude in our

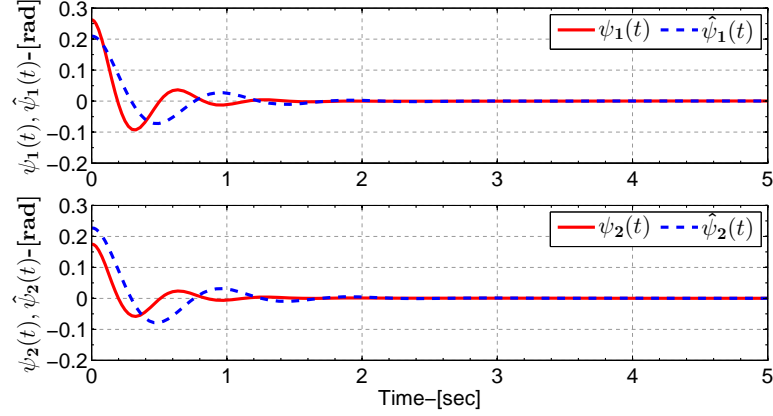


Fig. 4.12: Actual and estimated response of the pendulum angles.

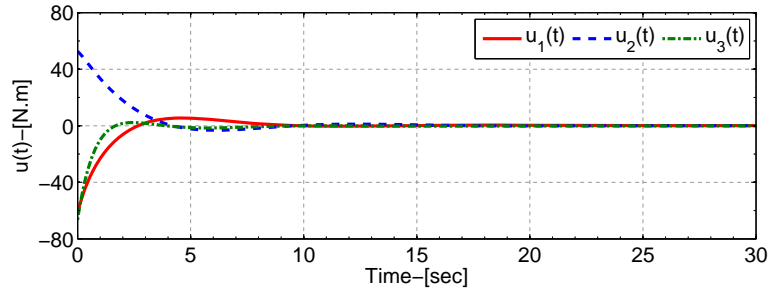


Fig. 4.13: Control inputs, $|u_i(t)| \leq 79 \text{ N.m}$, ($i = 1, 2, 3$).

previous work [86]. The magnitude of each control input—which is control moment about body-fixed axis of spacecraft—are shown in Fig. 4.13. The plot shows that the proposed control law satisfies the control input constraint $|u_i(t)| \leq 79 \text{ N.m}$, ($i = 1, 2, 3$) for all the times.

4.6.5 Performance Evaluation

We compare the effectiveness of the robust-optimal fuzzy PDC controller with a fuzzy PDC, fuzzy LQR and proportional-integral-derivative (PID) as a baseline controller.

The PID gains, described in Eq. (4.32), are tuned using the closed-loop Ziegler-Nichols method [88], and the results are shown in Table 4.3, where K_u and P_u are the ultimate gain and

Table 4.3: PID gains using closed-loop Ziegler-Nichols method

	K_P	K_I	K_D
	$0.6K_u$	$2K_P/P_u$	$K_PP_u/8$
u_1	47.4	4.278	131.298
u_2	47.4	4.107	136.749
u_3	47.4	6.996	80.284

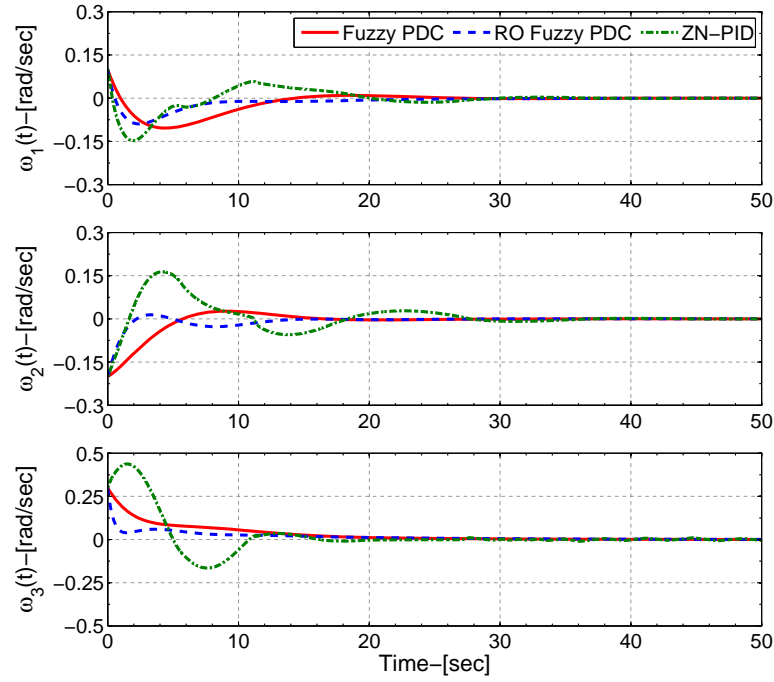


Fig. 4.14: Time responses of the spacecraft angular velocities using fuzzy PDC, robust-optimal fuzzy PDC and PID controllers.

ultimate period, respectively. The state responses and control inputs for robust-optimal control in comparison with fuzzy PDC and PID are presented in Figures 4.14, 4.15, and 4.16. The results show that the robust-optimal fuzzy PDC controller results satisfactory performance in the presence of system and actuator uncertainties. In comparison with PID controller, we see that fuzzy controllers have superiority over the PID controller.

In the end, as a performance evaluation measure we choose the root-mean-square-error (RMSE)

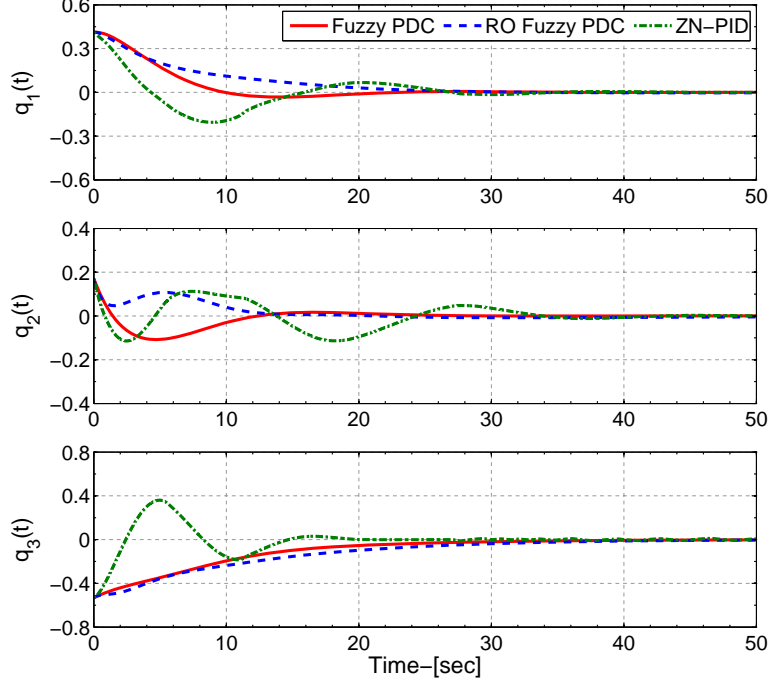


Fig. 4.15: Time responses of the quaternions using fuzzy PDC, robust-optimal fuzzy PDC and PID controllers.

in the following form:

$$f_{RMSE} = \sqrt{\frac{1}{T} \int_0^T [f_1^2(t) + f_2^2(t) + f_3^2(t)] dt}, \quad (4.34)$$

Table 4.4: RMSE for states and control inputs

	ω_{RMSE}	\mathbf{q}_{RMSE}	\mathbf{u}_{RMSE}
Fuzzy PDC	0.0483	0.2123	5.3343
Fuzzy LQR	0.0430	0.4912	6.0241
RO Fuzzy PDC	0.0178	0.0916	5.5934
ZN PID	0.0910	0.1172	8.5805

where f_{RMSE} can represent the root-mean-square-error for spacecraft angular velocity (ω_{RMSE}), quaternion (q_{RMSE}), and control input (u_{RMSE}) using the fuzzy PDC, fuzzy LQR, robust-optimal fuzzy control, and PID. The results are presented in Table 4.4. The RMSEs for the spacecraft angular velocities and attitude quaternions for the robust-optimal fuzzy con-

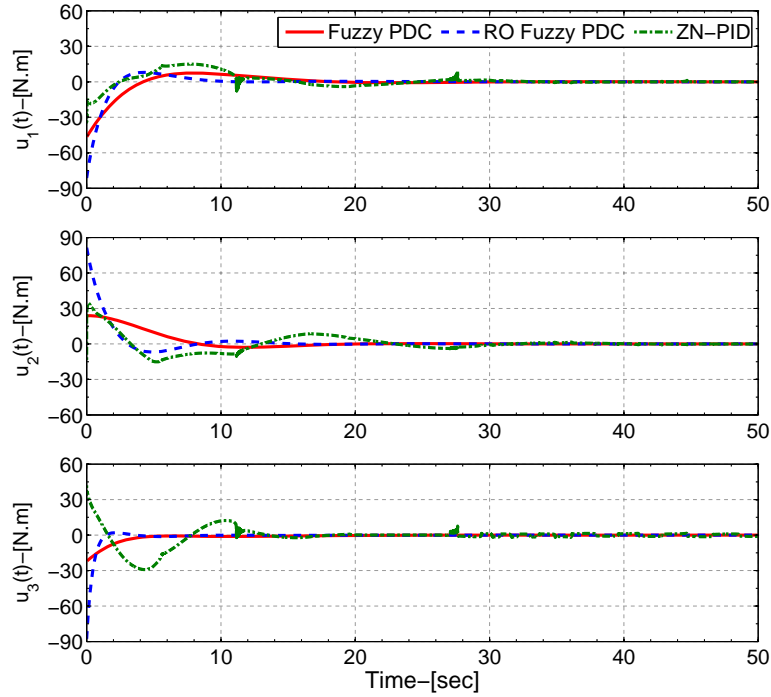


Fig. 4.16: Time responses of the control inputs using fuzzy PDC, robust-optimal fuzzy PDC and PID controllers.

troller are considerably lower than the RMSEs for the spacecraft angular velocities and attitude quaternions for the other controllers. Although, the RMSEs for the control inputs are about the same for both fuzzy PDC and robust-optimal fuzzy controllers, they are considerably lower for the fuzzy LQR and PID controllers. Based on numerical simulation results presented in Figures 4.4, 4.5, 4.7, 4.14, 4.15, and 4.16, and based on performance evaluation measure RMSE results presented in Tables 4.2 and 4.4, we conclude that the designed fuzzy controllers stabilize the attitude of the spacecraft with fuel sloshing with considerably better performance in the robust-optimal fuzzy controller case.

4.7 Design Case Studies

We study three design cases and compare them to the "nominal" case that we designed in previous section. In Case 1, the performance cost function is the upper bound of the norm

of initial condition, i.e. $\|x(0)\|$, where we assume that initial states are unknown, and the actuator amplitude and decay rate are known. Our objective here is to maximize the size of a controllable set of the nonlinear system. The modified LMIs for independent initial state condition is given in Eq. (4.9). Hence, the optimization problem is formulated as following:

$$\begin{aligned}
 & \underset{(G, Q, M_i, N_i)}{\text{Maximize:}} && J_1 = \beta^2, \\
 & \text{Subject to:} && \text{Eqs. (4.3), (4.4), (4.7), and (4.9)}.
 \end{aligned} \tag{4.35}$$

In Case 2, the objective is to minimize the actuator size while the upper bound on the initial

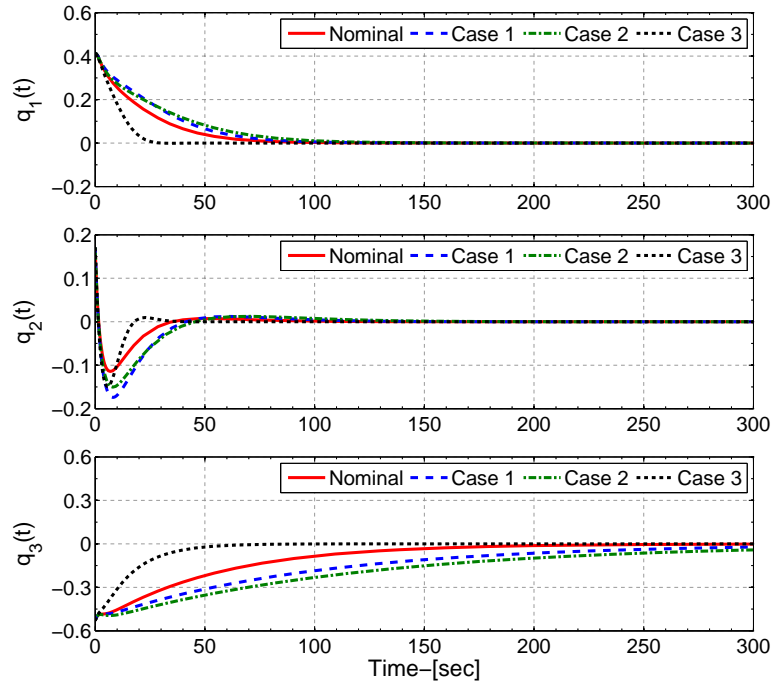


Fig. 4.17: Design on the responses of quaternions: Nominal, Case 1– $\max(\beta^2)$, Case 2– $\min(\alpha^2)$, Case 3– $\max(d)$.

states and decay rate are known. The modified LMIs for input bound constrains $|u_i(t)| \leq \alpha_i$, ($i = 1, 2, 3$) are given in Eq. (4.7). Defining $\alpha = [\alpha_1, \alpha_2, \alpha_3]^T$, the optimization problem

is formulated as following:

$$\begin{aligned}
 & \underset{(G,Q,M_i,N_i)}{\text{Minimize:}} && J_2 = \alpha^T R \alpha, \quad R = R^T > 0, \\
 & \text{Subject to:} && \text{Eqs. (4.3), (4.4), (4.7), and (4.9)}.
 \end{aligned} \tag{4.36}$$

Finally, in Case 3, the objective is to improve the response time by maximizing the decay rate, d , given the upper bound on the initial states and actuator amplitude. The optimization problem in this case can be formulated as following:

$$\begin{aligned}
 & \underset{(G,Q,M_i,N_i)}{\text{Maximize:}} && J_3 = d, \\
 & \text{Subject to:} && \text{Eqs. (4.3), (4.4), (4.7), and (4.9)}.
 \end{aligned} \tag{4.37}$$

Note that for the nominal model we have $\beta = 3$, $\alpha_i = 200 \text{ N.m}$, ($i = 1, 2, 3$), and $d = 0.01$.

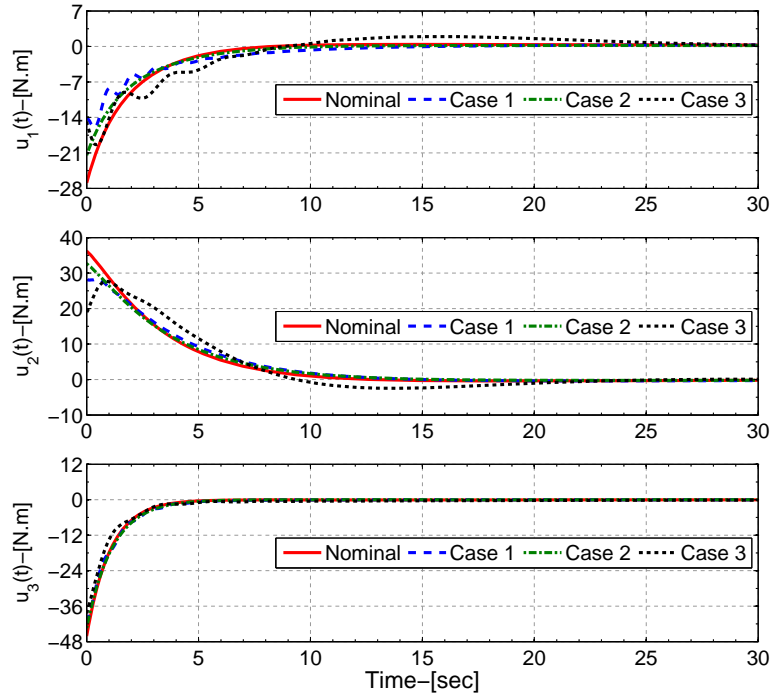


Fig. 4.18: Design on the responses of input control: Nominal, Case 1– $\max(\beta^2)$, Case 2– $\min(\alpha^2)$, Case 3– $\max(d)$.

We use the Matlab toolbox YALMIP [85] with SDPT3 solver to solve the optimization

problems. We found that for case 1, the largest bound on the β is 4.818 and for case 2, the largest bound on the α is 149.756 *N.m*. Assuming all α_i are equal and $R = \text{diag}(1, 1, 1)$. In case 3, the maximum decay rate is 0.178. The time history of quaternions and input control for each optimization problem along with the nominal case are shown in Figs. 4.17 and 4.18, respectively. The results shows that the performance of the designed controller for case 3 has a better performance in compare to the nominal and the other two cases. Also, as we expected, case 2 has the worst performance due to reduction in control authority.

CHAPTER 5

Modeling and Analysis of Spacecraft with Fuel Sloshing in High-G Maneuvers

5.1 Introduction

In this chapter, we derive the equations of motion of spinning spacecraft with partially-filled, multiple-tanks, a nutation damper, and momentum wheels in the high-g environment. We model the fuel sloshing in each tank by means of two spherical pendulums with torsional dampers at hinge points. Using the Kane's method, the nonlinear equations of motion of a spacecraft containing liquid fuel stores are derived. The developed model is an extension of the existing models in the literature [20, 27, 36]. Derived equations of motion of spacecraft are numerically solved, and the effects of the slosh-model parameters on the spacecraft nutation angle are investigated. We note that the spacecraft is said to be in a "high-g" environment when it is under high acceleration provided by the main engine and the surface tension forces of liquid in tanks do not significantly affect the propellant motion during main engine burns [36, 37].

5.2 Modeling of Spacecraft with Fuel Sloshing

5.2.1 Model Description

Let us consider a spin-stabilized spacecraft with partially-filled multiple spherical fuel tanks. Three momentum wheels, W_1, W_2, W_3 , are aligned with the gyrostat (spacecraft+momentum wheels) principal axes, g_1, g_2 , and g_3 , as shown in Fig. 5.1. The gyrostat, G , is a fictitious rigid body that has the mass distribution of the combined system of spacecraft body, B , and the wheels, but moves like B , while the rotors spin with respect to B frame. [28] We define inertial, body (gyrostat) and pendulum fixed-frames as the reference frames by N, G , and P , respectively. The inertial frame N corresponds to the Earth center. G^* is the center-of-mass, and I^{G^*} is the central principal moment-of-inertia of the gyrostat. The nutation damper is represented by a mass, m_Q , supported by a spring of stiffness, σ , and damping coefficient, δ .

We adopt two spherical pendulums as the mechanical analogy model of high-g propellant sloshing in the gyrostat [36]. Each pendulum mass, m_{ij} ($i = 1, 2$ shows the pendulum number, and $j = 1, \dots, S$ shows the tank number), represents the first two modes of sloshing in each tank, correspondingly, and the remaining fluid mass, m_{0j} , is attached along the tank centerline as a static body. The model of spherical tank j with spherical pendulums is presented in Fig. 5.2. O_j is defined as an empty-tank centroid. Pendulums with fixed lengths are defined by l_{ij} and are hinged at point O_{ij} along the tank centerline off the gyrostat main axis. The locations of pendulum hinges and static body are referenced to the center of the empty tank by h_{0j} , and h_{ij} . The presented model must preserve the static and dynamic properties of the liquid [14]. In other words, the total fuel mass in each tank must be equal to the sum of all masses in the pendulum model, and the center of the mass of the model must be at the same elevation as the liquid. Therefore, we can write

$$m_{0j} + m_{1j} + m_{2j} = m_{fj}, \quad (j = 1, \dots, S), \quad (5.1)$$

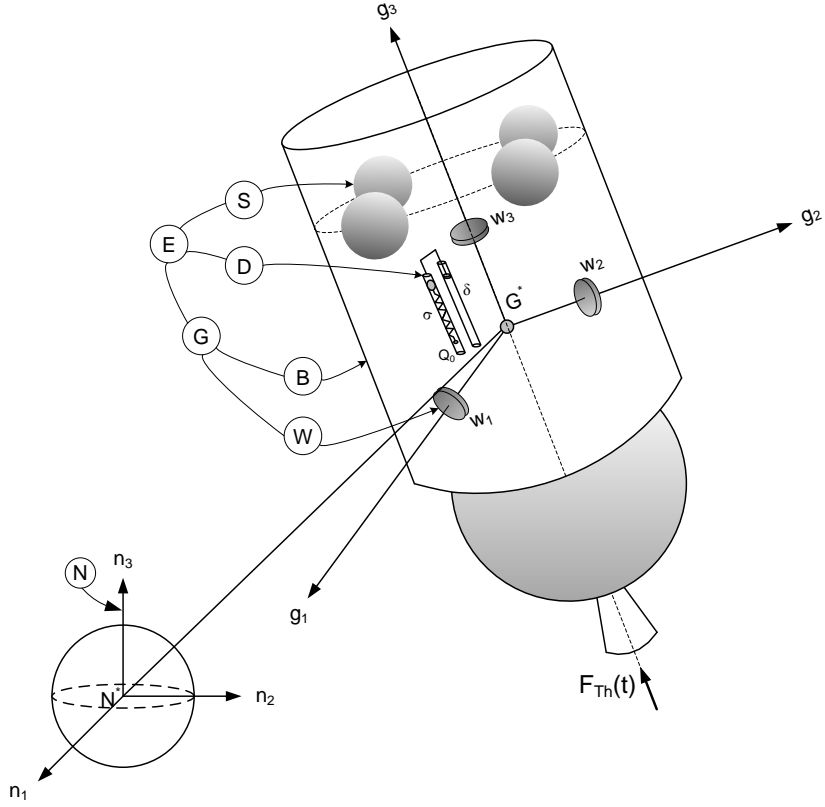


Fig. 5.1: A gyrostat model with multiple, partially-filled, spherical tanks.

$$m_{0j}h_{0j} = m_{1j}(h_{1j} - l_{1j}) + m_{2j}(h_{2j} - l_{2j}), \quad (j = 1, \dots, S). \quad (5.2)$$

We choose the generalized speeds, u_k , as follows:

$$u_k = {}^N V^{G^*} \cdot \hat{g}_k, \quad (k = 1, 2, 3), \quad (5.3)$$

$$u_{3+k} = {}^N \omega^G \cdot \hat{g}_k, \quad (k = 1, 2, 3), \quad (5.4)$$

$$u_{3+4k} = \dot{\alpha}_{1k}, \quad (k = 1, \dots, S), \quad (5.5)$$

$$u_{4+4k} = \dot{\beta}_{1k}, \quad (k = 1, \dots, S), \quad (5.6)$$

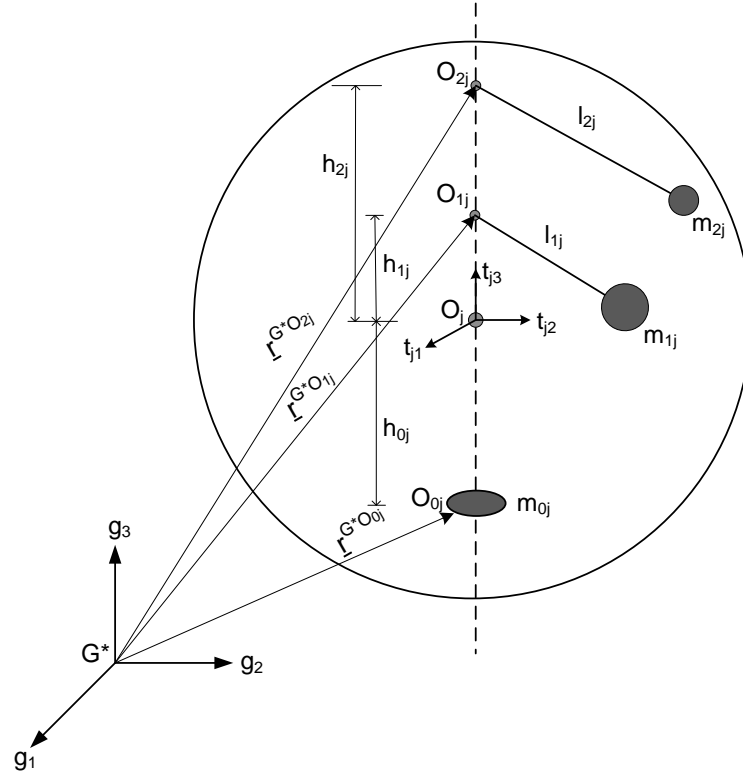


Fig. 5.2: Equivalent model of fuel sloshing in spherical tank j for high- g environment.

$$u_{5+4k} = \dot{\alpha}_{2k}, \quad (k = 1, \dots, S), \quad (5.7)$$

$$u_{6+4k} = \dot{\beta}_{2k}, \quad (k = 1, \dots, S), \quad (5.8)$$

$$u_{7+4k} = \dot{q}, \quad (k = S), \quad (5.9)$$

where S is the number of tanks. The components of the velocity of the center of mass G^* with respect to inertial frame N are defined by $u_k (k = 1, 2, 3)$, and the components of the angular velocity of the gyrostat with respect to frame N are defined by $u_{3+k} (k = 1, 2, 3)$. The angles α_{ij} and β_{ij} represent the relative orientation of the massless rod of the spherical pendulum in the tank j as shown in Fig. 5.3, and $\dot{\alpha}_{ij}$ and $\dot{\beta}_{ij}$ are the corresponding generalized speeds. In

Eq. (5.9), q is the displacement of the mass particle, m_Q . The angular speed of momentum wheels $W_k (k = 1, 2, 3)$ with respect to the gyrostat frame G are not included in generalized speeds as the motion of the momentum wheels are prescribed in gyrostat. The number of degrees of freedom is $7 + 4S$.

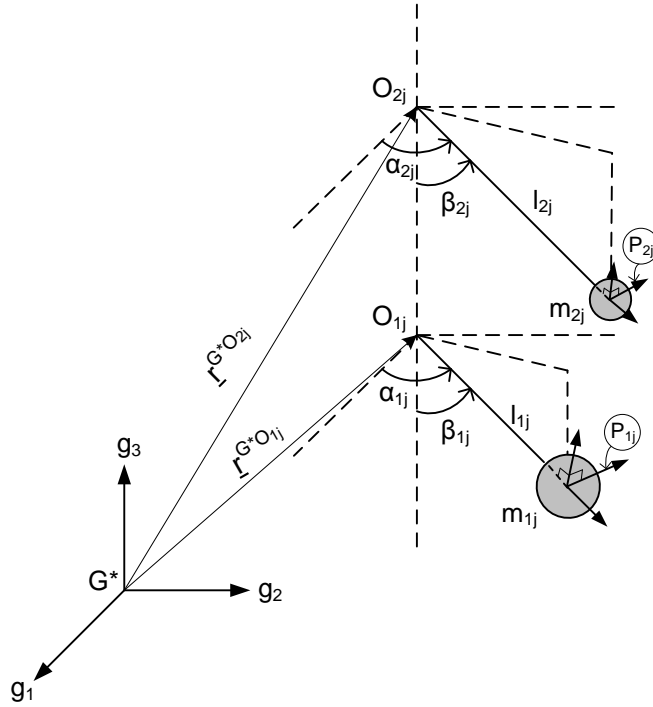


Fig. 5.3: Angles α_{ij} and β_{ij} represent the relative orientation of the spherical pendulum with respect to the G -frame.

5.2.2 Equations of Motion

Now, we are going to derive the equations of motion of the presented model using the Kane's method. The velocity of point G^* , angular velocity of the gyrostat, angular velocities of the pendulums with respect to inertial frame N can be written as

$${}^N V^{G^*} = u_1 \hat{g}_1 + u_2 \hat{g}_2 + u_3 \hat{g}_3, \quad (5.10)$$

$${}^N \omega^G = u_4 \hat{g}_1 + u_5 \hat{g}_2 + u_6 \hat{g}_3, \quad (5.11)$$

$${}^N\omega^{P_{ij}} = {}^N\omega^G + {}^G\omega^{P_{ij}}, \quad (i = 1, 2; j = 1, \dots, S), \quad (5.12)$$

where ${}^G\omega^{P_{ij}}$ is the angular velocity of the P_{ij} frame with respect to the G frame.

Angular velocity of the static body m_{0j} in each tank with respect to the inertial frame N is the same as the angular velocity of the gyrostat with respect to the inertial frame N .

The acceleration of point G^* with respect to the inertial frame, N , can be obtained as

$${}^N a^{G^*} = \frac{{}^G d}{{}^G dt} {}^N V^{G^*} + {}^N \omega^G \times {}^N V^{G^*}, \quad (5.13)$$

where the first term in Eq. (5.13) represents the time-derivative of the velocity vector in the G frame. The acceleration of point G^* can be written as

$${}^N a^{G^*} = (\dot{u}_1 + Z_1)\hat{g}_1 + (\dot{u}_2 + Z_2)\hat{g}_2 + (\dot{u}_3 + Z_3)\hat{g}_3. \quad (5.14)$$

Here Z_1 , Z_2 , and Z_3 are defined as

$$Z_1 \triangleq u_5 u_3 - u_6 u_2, \quad (5.15)$$

$$Z_2 \triangleq u_6 u_1 - u_4 u_3, \quad (5.16)$$

$$Z_3 \triangleq u_4 u_2 - u_5 u_1. \quad (5.17)$$

Using Fig. 5.3, we can show the transformation matrix from the gyrostat frame, G , to the pendulum frame P_{ij} as

$${}^{P_{ij}} R^G(\alpha_{ij}, \pi/2 - \beta_{ij}) = R_2(\pi/2 - \beta_{ij}) R_3(\alpha_{ij}), \quad (5.18)$$

$${}^{P_{ij}}R^G(\alpha_{ij}, \pi/2 - \beta_{ij}) = \begin{bmatrix} c\alpha_{ij}s\beta_{ij} & s\alpha_{ij}s\beta_{ij} & -c\beta_{ij} \\ -s\alpha_{ij} & c\alpha_{ij} & 0 \\ c\alpha_{ij}c\beta_{ij} & s\alpha_{ij}c\beta_{ij} & s\beta_{ij} \end{bmatrix}, \quad (5.19)$$

where c and s denote the cosine and sine functions, respectively. Using the transformation matrix, Eq. (5.19), ${}^G\omega^{P_{ij}}$ can be written in vector form as

$${}^G\omega^{P_{ij}} = \dot{\alpha}_{ij} \hat{g}_3 + \dot{\beta}_{ij}s\alpha_{ij} \hat{g}_1 - \dot{\beta}_{ij}c\alpha_{ij} \hat{g}_2, \quad (i = 1, 2; j = 1, \dots, S), \quad (5.20)$$

and using Eq. (5.12), the ${}^N\omega^{P_{1j}}$ and ${}^N\omega^{P_{2j}}$ are determined by

$${}^N\omega^{P_{1j}} = (u_4 + u_{4+4j}s\alpha_{1j}) \hat{g}_1 + (u_5 - u_{4+4j}c\alpha_{1j}) \hat{g}_2 + (u_6 + u_{3+4j}) \hat{g}_3, \quad (5.21)$$

$${}^N\omega^{P_{2j}} = (u_4 + u_{6+4j}s\alpha_{2j}) \hat{g}_1 + (u_5 - u_{6+4j}c\alpha_{2j}) \hat{g}_2 + (u_6 + u_{5+4j}) \hat{g}_3. \quad (5.22)$$

Therefore, the velocity of the pendulum mass m_{ij} with respect to inertial frame N can be determined as

$${}^N V^{m_{ij}} = {}^N V^{G^*} + {}^N \omega^G \times r^{G^*O_{ij}} + {}^N \omega^{P_{ij}} \times r^{O_{ij}m_{ij}}. \quad (5.23)$$

After simplification, we get

$$\begin{aligned} {}^N V^{m_{1j}} = & \{u_1 + u_5 r_{1j,3} - u_6 r_{1j,2} - l_{1j} c\beta_{1j} u_5 + l_{1j} c\beta_{1j} u_{4+4j} c\alpha_{1j} - \\ & l_{1j} s\alpha_{1j} s\beta_{1j} u_6 - l_{1j} s\alpha_{1j} s\beta_{1j} u_{3+4j}\} \hat{g}_1 + \{u_2 + u_6 r_{1j,1} - u_4 r_{1j,3} + \\ & + l_{1j} c\alpha_{1j} s\beta_{1j} u_6 + l_{1j} c\alpha_{1j} s\beta_{1j} u_{3+4j} + l_{1j} c\beta_{1j} u_4 + l_{1j} s\alpha_{1j} c\beta_{1j} u_{4+4j}\} \hat{g}_2 + \\ & + \{u_3 + u_4 r_{1j,2} - u_5 r_{1j,1} + l_{1j} s\alpha_{1j} s\beta_{1j} u_4 + l_{1j} s^2 \alpha_{1j} s\beta_{1j} u_{4+4j} - l_{1j} c\alpha_{1j} s\beta_{1j} u_5 + \\ & l_{1j} c^2 \alpha_{1j} s\beta_{1j} u_{4+4j}\} \hat{g}_3, \end{aligned} \quad (5.24)$$

and

$$\begin{aligned}
{}^N V^{m_{2j}} = & \{u_1 + u_5 r_{2j,3} - u_6 r_{2j,2} - l_{2j} c \beta_{2j} u_5 + l_{2j} c \beta_{2j} u_{6+4j} c \alpha_{2j} - \\
& l_{2j} s \alpha_{2j} s \beta_{2j} u_6 - l_{2j} s \alpha_{2j} s \beta_{2j} u_{5+4j}\} \hat{g}_1 + \{u_2 + u_6 r_{2j,1} - u_4 r_{2j,3} + \\
& + l_{2j} c \alpha_{2j} s \beta_{2j} u_6 + l_{2j} c \alpha_{2j} s \beta_{2j} u_{5+4j} + l_{2j} c \beta_{2j} u_4 + l_{2j} s \alpha_{2j} c \beta_{2j} u_{6+4j}\} \hat{g}_2 + \\
& + \{u_3 + u_4 r_{2j,2} - u_5 r_{2j,1} + l_{2j} s \alpha_{2j} s \beta_{2j} u_4 + l_{2j} s^2 \alpha_{2j} s \beta_{2j} u_{6+4j} - l_{2j} c \alpha_{2j} s \beta_{2j} u_5 + \\
& l_{2j} c^2 \alpha_{2j} s \beta_{2j} u_{6+4j}\} \hat{g}_3.
\end{aligned} \tag{5.25}$$

The acceleration of the pendulum mass m_{ij} with respect to inertial frame N is

$$\begin{aligned}
{}^N a^{m_{ij}} = & {}^N a^{G^*} + \frac{G d}{dt} {}^N \omega^G \times r^{G^* O_{ij}} + {}^N \omega^G \times \frac{G d}{dt} r^{G^* O_{ij}} + {}^N \omega^G \times ({}^N \omega^G \times r^{G^* O_{ij}}) + \\
& + \frac{P_{ij} d}{dt} {}^N \omega^{P_{ij}} \times r^{O_{ij} m_{ij}} + {}^N \omega^{P_{ij}} \times P_{ij} V^{m_{ij}} + {}^N \omega^{P_{ij}} \times ({}^N \omega^{P_{ij}} \times r^{O_{ij} m_{ij}}),
\end{aligned} \tag{5.26}$$

and the velocity and acceleration of the static body m_{0j} with respect to inertial frame N will be

$${}^N V^{m_{0j}} = {}^N V^{G^*} + {}^N \omega^G \times r^{G^* O_{0j}}, \tag{5.27}$$

$${}^N a^{m_{0j}} = {}^N a^{G^*} + \frac{G d}{dt} {}^N \omega^G \times r^{G^* O_{0j}} + {}^N \omega^G \times ({}^N \omega^G \times r^{G^* O_{0j}}). \tag{5.28}$$

Further, we assume that the nutation damper is attached at a Q_0 point fixed in G frame. If we denote the distance between G^* and Q_0 on the \hat{g}_1 axis by z_Q , the distance between G^* and Q_0 on the \hat{g}_3 axis by d , and the displacement and velocity of the nutation damper mass point with respect to the damper fixed-frame N , with q , and \dot{q} , respectively, the velocities of the Q and Q_0 will be

$${}^N V^Q = {}^N V^{G^*} + {}^N \omega^G \times (z_Q \hat{g}_1 + q \hat{g}_3) + \dot{q} \hat{g}_3, \tag{5.29}$$

$${}^N V^{Q_0} = {}^N V^{G^*} + {}^N \omega^G \times (z_Q \hat{g}_1 - d \hat{g}_3). \quad (5.30)$$

Correspondingly, we obtain the accelerations of the point Q and Q_0 , in the following forms:

$${}^N a^Q = \frac{{}^G d}{dt} {}^N V^Q + {}^N \omega^G \times {}^N V^Q, \quad (5.31)$$

$${}^N a^{Q_0} = \frac{{}^G d}{dt} {}^N V^{Q_0} + {}^N \omega^G \times {}^N V^{Q_0}, \quad (5.32)$$

as

$${}^N a^Q = (\dot{u}_1 + q\dot{u}_5 + Z_7)\hat{g}_1 + (\dot{u}_2 - q\dot{u}_4 + z_Q\dot{u}_6 + Z_8)\hat{g}_2 + (\dot{u}_3 - z_Q\dot{u}_5 + \dot{u}_{7+4k} + Z_9)\hat{g}_3, \quad (5.33)$$

$${}^N a^{Q_0} = (\dot{u}_1 - d\dot{u}_5 + Z_{10})\hat{g}_1 + (\dot{u}_2 + d\dot{u}_4 + z_Q\dot{u}_6 + Z_{11})\hat{g}_2 + (\dot{u}_3 - z_Q\dot{u}_5 + Z_{12})\hat{g}_3, \quad (5.34)$$

where Z -s are defined as

$$Z_7 \triangleq Z_1 - z_Q u_5^2 + q u_4 u_6 - z_Q u_6^2 + 2u_{7+4k} u_5, \quad (5.35)$$

$$Z_8 \triangleq Z_2 + z_Q u_4 u_5 + q u_5 u_6 - 2u_{7+4k} u_4, \quad (5.36)$$

$$Z_9 \triangleq Z_3 - q u_4^2 - q u_5^2 + z_Q u_4 u_6, \quad (5.37)$$

$$Z_{10} \triangleq Z_1 - z_Q u_5^2 - d u_4 u_6 - z_Q u_6^2, \quad (5.38)$$

$$Z_{11} \triangleq Z_2 + z_Q u_4 u_5 - d u_5 u_6, \quad (5.39)$$

$$Z_{12} \triangleq Z_3 + d u_4^2 + d u_5^2 + z_Q u_4 u_6. \quad (5.40)$$

Using the above equations we can calculate the partial velocities and partial angular velocities.

Thereafter, we can derive the dynamical equations of the motion of the gyrostator with fuel

sloshing which simply state that the sum of the generalized inertia and active forces is zero for each generalized coordinate. Defining generalized inertia and active forces by F_r^* and F_r , respectively, Kane's equations can be written as [29]

$$F_r + F_r^* = 0, \quad (r = 1, \dots, 7 + 4S). \quad (5.41)$$

Negative generalized inertia force is determined by

$$\begin{aligned} -F_r^* = & F_{G^*}^* \cdot {}^N V_r^{G^*} + T_G^* \cdot {}^N \omega_r^G + \sum_{i=0}^2 \sum_{j=1}^S F_{m_{ij}}^* \cdot {}^N V_r^{m_{ij}} + \sum_{k=1}^3 T_k^* \cdot {}^N \omega_r^G + \\ & + F_Q^* \cdot {}^N V_r^Q, \quad (r = 1, \dots, 7 + 4S), \end{aligned} \quad (5.42)$$

where

$$F_{G^*}^* = m_G \cdot {}^N a^{G^*}, \quad (5.43)$$

$$F_{m_{ij}}^* = m_{ij} \cdot {}^N a^{m_{ij}}, \quad (5.44)$$

$$F_Q^* = m_Q \cdot {}^N a^Q, \quad (5.45)$$

$$T_G^* = I^{G^*} \cdot {}^N \alpha^G + {}^N \omega^G \times I^{G^*} \cdot {}^N \omega^G, \quad (5.46)$$

$$T_k^* = I_k^{W_k^*} \cdot {}^G \alpha^{W_k} + {}^N \omega^G \times I_k^{W_k^*} \cdot {}^G \omega^{W_k}, \quad (k = 1, 2, 3). \quad (5.47)$$

It can be shown that generalized inertia forces, $-F_r^*$, can be written in matrix form as

$$-F^* = M\dot{U} + C, \quad (5.48)$$

where

$$\dot{U} = [\dot{u}_1, \dot{u}_2, \dots, \dot{u}_{7+4k}]^T, \quad (5.49)$$

and

$$C = [c_1, c_2, \dots, c_{7+4k}]^T. \quad (5.50)$$

The elements of vectors C and matrix M are listed in the Appendix (A.2).

The generalized active force is determined by

$$\begin{aligned} F_r = & F_{gG} \cdot {}^N V_r^{G^*} + M_{gG} \cdot {}^N \omega_r^G - \sum_{k=1}^3 T_k \cdot {}^N \omega_r^G + \sum_{i=0}^2 \sum_{j=1}^S F_{gm_{ij}} \cdot {}^N V_r^{m_{ij}} - \\ & - \sum_{i=1}^2 \sum_{j=1}^S T_{fm_{ij}} \cdot {}^N \omega_r^G + \sum_{i=1}^2 \sum_{j=1}^S T_{fm_{ij}} \cdot {}^N \omega_r^{P_{ij}} + F_{Th} \cdot {}^N V_r^F + T_{Th} \cdot {}^N \omega_r^G + \\ & + F_{gQ} \cdot {}^N V_r^Q - (\sigma q + \delta \dot{q}) \cdot ({}^N V_r^Q - {}^N V_r^{Q_0}), \quad (r = 1, \dots, 7 + 4S), \end{aligned} \quad (5.51)$$

where F_{gG} is the gravitational force on the gyrost in the body-fixed frame, M_{gG} is the gravitational torque on the gyrost, T_k is the torque on momentum wheel k , $F_{gm_{ij}}$ is the gravitational force on each pendulum, $T_{fm_{ij}}$ is the linear viscous torque models on pendulums m_{ij} , F_{Th} is the thrust force on the gyrost applied at point F , T_{Th} is the thrust torque on the gyrost, F_{gQ} is the gravitational force on point mass Q , and Q_0 is a fixed point in the G frame. Equation (5.51) is valid when the gyrost mass loss is zero or negligible in compare to its total mass. In our case, the thrust force is generated by the upper-stage solid rocket motor. Therefore, the gyrost mass is constant. Knowing the position vector of the point of thrust application, we can determine the partial velocity ${}^N V_r^F$.

The linear viscous torque models on pendulums are given by

$$T_{fm_{ij}} = (-C_{\beta_{ij}} l_{ij}^2 \dot{\beta}_{ij} s \alpha_{ij}, C_{\beta_{ij}} l_{ij}^2 \dot{\beta}_{ij} c \alpha_{ij}, -C_{\alpha_{ij}} l_{ij}^2 \dot{\alpha}_{ij} s \beta_{ij}^2), \quad (5.52)$$

where $C_{\alpha_{ij}}$ and $C_{\beta_{ij}}$ are constants. We note that the pendulum is not spring-restrained as the spring represents the surface tension forces, which are zero in high-g model. As described in section 2.3, the model is in high-g if the spacecraft acceleration that is provided by the main

engine is large enough so that surface tension forces do not significantly affect the propellant motion during main engine burn. For example, upper-stage solid rocket motor STAR 37 produces about 47,85 kN thrust, which makes the Bond number to be much higher than 1, $Bo \gg 1$.

Thus, we obtain the dynamical equations of motion for the gyrostatt with spherical pendulums:

$$M\dot{U} + C = F, \quad (5.53)$$

or

$$\dot{U} = M^{-1}(F - C). \quad (5.54)$$

The elements of vectors C and F , and matrix M are listed in the Appendix (A.2). Equation (5.54) consists of highly nonlinear ordinary differential equations.

5.2.3 The Kinematic Equations

To avoid the singularities of Euler angles, we use the Modified Rodrigues Parameters (MRPs) to describe the attitude motion of the gyrostatt in the inertial frame. Using the definition of MRPs in terms of principal rotation elements, the MRPs are defined as

$${}^N\sigma^G = \tan\left(\frac{\Phi}{4}\right)\hat{e}, \quad (5.55)$$

where the components of ${}^N\sigma^G$ are given by $\{\sigma_1, \sigma_2, \sigma_3\}^T$. In Eq. (5.55), Φ is the principal angle, \hat{e} is a unit vector which shows the direction of the Euler (or Principal) axis.

The kinematic equations in terms of MRPs, in the matrix form, are given by

$${}^N\dot{\sigma}^G = \frac{1}{4}B(\sigma) {}^N\omega^G, \quad (5.56)$$

where

$$B(\sigma) = \begin{bmatrix} 1 - \sigma^2 + 2\sigma_1^2 & 2(\sigma_2\sigma_1 - \sigma_3) & 2(\sigma_1\sigma_3 + \sigma_2) \\ 2(\sigma_2\sigma_1 + \sigma_3) & 1 - \sigma^2 + 2\sigma_2^2 & 2(\sigma_3\sigma_2 - \sigma_1) \\ 2(\sigma_3\sigma_1 - \sigma_2) & 2(\sigma_3\sigma_2 + \sigma_1) & 1 - \sigma^2 + 2\sigma_3^2 \end{bmatrix} \quad (5.57)$$

and $\sigma = \|\sigma^G\|_2$.

We choose a 1-2-3 (Yaw, Pitch, Roll) Euler angle sequence to visualize the attitude motion of the gyrost. Comparing the rotation matrix written in terms of MRPs and the 1-2-3 Euler angle sequence transformation matrix [83] given by

$${}^N R_{123}^G(\psi, \theta, \phi) = \begin{bmatrix} c\theta c\phi & -c\theta s\phi & s\theta \\ s\psi s\theta c\phi + c\psi s\phi & -s\psi s\theta s\phi + c\psi c\phi & -c\theta s\psi \\ -c\psi s\theta c\phi + s\psi s\phi & c\psi s\theta s\phi + c\psi c\phi & c\theta c\psi \end{bmatrix}, \quad (5.58)$$

we can find the relation between this Euler angle sequence and MRPs as follows:

$$\begin{aligned} \psi &= -\arctan \left[\frac{8\sigma_2\sigma_3 - 4\sigma_1(1 - \sigma^2)}{4(-\sigma_1^2 - \sigma_2^2 + \sigma_3^2) + (1 - \sigma^2)^2} \right] \\ \theta &= \arcsin \left[\frac{8\sigma_1\sigma_3 + 4\sigma_2(1 - \sigma^2)}{(1 + \sigma^2)^2} \right] \\ \phi &= -\arctan \left[\frac{8\sigma_1\sigma_3 - 4\sigma_3(1 - \sigma^2)}{4(\sigma_1^2 - \sigma_2^2 - \sigma_3^2) + (1 - \sigma^2)^2} \right], \end{aligned} \quad (5.59)$$

where $-90^\circ \leq \psi, \theta, \phi \leq 90^\circ$. This set of Euler angles is singular at $\theta = \pm 90^\circ$.

Kinematic differential equations for 1-2-3 Euler angle sequence is

$$\begin{Bmatrix} \dot{\psi} \\ \dot{\theta} \\ \dot{\phi} \end{Bmatrix} = \begin{bmatrix} c\phi/c\theta & -s\phi/c\theta & 0 \\ s\phi & c\phi & 0 \\ -s\theta c\phi/c\theta & s\theta s\phi/c\theta & 1 \end{bmatrix} \begin{Bmatrix} u_4 \\ u_5 \\ u_6 \end{Bmatrix} \quad (5.60)$$

The set of Eq. (5.54) along with the kinematic equations, Eq. (5.56), constitute a mathemati-

cal model of the system.

5.3 Analysis of Spacecraft with Fuel Sloshing in High-G Maneuvers

5.3.1 Nutation Angle

Nutation angle, Θ , is defined as the angle between the total angular momentum vector, H , and the spin axis of the gyrostat. If the gyrostat is spinning about \hat{g}_3 axis, then Θ is determined as

$$\Theta = \cos^{-1} \left(\hat{g}_3 \cdot \frac{H^{E/E^*}}{|H^{E/E^*}|} \right). \quad (5.61)$$

The total angular momentum is the sum of the angular momentums of the spacecraft, wheels, nutation damper, and pendulums:

$$\begin{aligned} H^{E/E^*} = & I^G \cdot {}^N \omega^G + m_G r^{E^*G^*} \times {}^N V^{G^*} + m_Q r^{E^*Q} \times {}^N V^Q + \\ & + \sum_{k=1}^3 I^{W_k} \cdot {}^G \omega^{W_k} + \sum_{i=0}^2 \sum_{j=1}^S (m_{ij} r^{E^*m_{ij}} \times {}^N V^{m_{ij}}), \end{aligned} \quad (5.62)$$

where E^* denotes the mass center of the whole system formed by the gyrostat, nutation damper, and the pendulums. The position vectors are given by

$$r^{G^*Q} = q\hat{g}_3 + z_Q\hat{g}_1, \quad (5.63)$$

$$r^{G^*m_{ij}} = r^{G^*O_{ij}} + r^{O_{ij}m_{ij}}, \quad (5.64)$$

$$r^{E^*Q} = r^{E^*G^*} + r^{G^*Q}, \quad (5.65)$$

$$r^{E^*m_{ij}} = r^{E^*G^*} + r^{G^*m_{ij}}, \quad (5.66)$$

and

$$r^{E^*G^*} = -\frac{m_Q r^{G^*Q} + \sum_{i=0}^2 \sum_{j=1}^S m_{ij} r^{G^*m_{ij}}}{m_G + m_Q + \sum_{i=0}^2 \sum_{j=1}^S m_{ij}}. \quad (5.67)$$

5.3.2 Dynamic Analysis

We use Mathematica[®] to check our derivation and to solve numerically the equations of motion and kinematic equations, (5.54)–(5.56). From now on, we use the words "gyrostat" and "spacecraft" interchangeably. To reduce the computational time, we assume the spacecraft has one tank and fuel sloshing is described by two spherical pendulums, i.e. ($S = 1; i = 1, 2$). In addition, we assume all the gravitational forces and the thrust force are zero. The appendix includes all coefficients from equations of motion for this special case. The spherical pendulum and nutation damper parameters are listed in Table 5.1.

Table 5.1: The spherical pendulum and nutation damper parameters

Parameter	Value	Units
m_G	5274.40	<i>kg</i>
m_{01}	338.44	<i>kg</i>
m_{11}	164	<i>kg</i>
m_{21}	25	<i>kg</i>
l_{11}, l_{21}	0.15	<i>m</i>
h_0	0.05	<i>m</i>
h_1	0.20	<i>m</i>
h_2	0.50	<i>kg</i>
$C_{\alpha_{ij}} C_{\beta_{ij}}$	26.66	<i>N.s/m</i>
m_Q	52.74	<i>kg</i>
z_Q	1	<i>m</i>
δ	105	<i>N.s/m</i>
σ	52.74	<i>N/m</i>

The inertia matrices of the gyrostat and momentum wheels are

$$[I^{G^*}] = \text{diag}(1375.7, 1292.5, 1402.4) \text{ kg.m}^2 \quad (5.68)$$

$$I^{W_1^*} = I^{W_2^*} = I^{W_3^*} = I^W = 0.17 \text{ kg.m}^2 \quad (5.69)$$

The initial conditions used in the simulation are presented in Table 5.2.

Table 5.2: Initial Conditions for spherical-spherical pendulum case

Parameter	Value	Units
$u_1(0)$	0	rad/s
$u_2(0)$	0	rad/s
$u_3(0)$	0	rad/s
$u_4(0)$	0.03	rad/s
$u_5(0)$	0.02	rad/s
$u_6(0)$	20	rpm
$\sigma_1(0)$	0.2	
$\sigma_2(0)$	-0.3	
$\sigma_3(0)$	0.1	
$\alpha_{11}(0)$	$\pi/2$	rad
$\alpha_{21}(0)$	$\pi/2$	rad
$\dot{\alpha}_{11}(0)$	$\pi/2$	rad/s
$\dot{\alpha}_{21}(0)$	$\pi/2$	rad/s
$\beta_{11}(0)$	$\pi/180$	rad
$\beta_{21}(0)$	$\pi/180$	rad
$\dot{\beta}_{11}(0)$	$2\pi/180$	rad/s
$\dot{\beta}_{21}(0)$	$2\pi/180$	rad/s
$q(0)$	0.01	m
$\dot{q}(0)$	0	m/s

In further we study the following maneuvers: 1) Spinning about the maximum moment-of-inertia axis, 2) Spinning about the minimum moment-of-inertia axis and 3) Reorientation maneuver.

Case 1 - Spinning about the maximum moment-of-inertia axis.

Let us assume that the spacecraft has a constant spin rate of 20 rpm around its maximum

moment-of-inertia, \hat{g}_3 axis, and zero initial angular velocity around the other axes, i.e. $\omega_0 = (0, 0, 20)$ rpm. Fig. 5.4 shows the components of angular velocity of the spacecraft for the spherical-spherical pendulum model. The effect of spherical-spherical pendulum model on

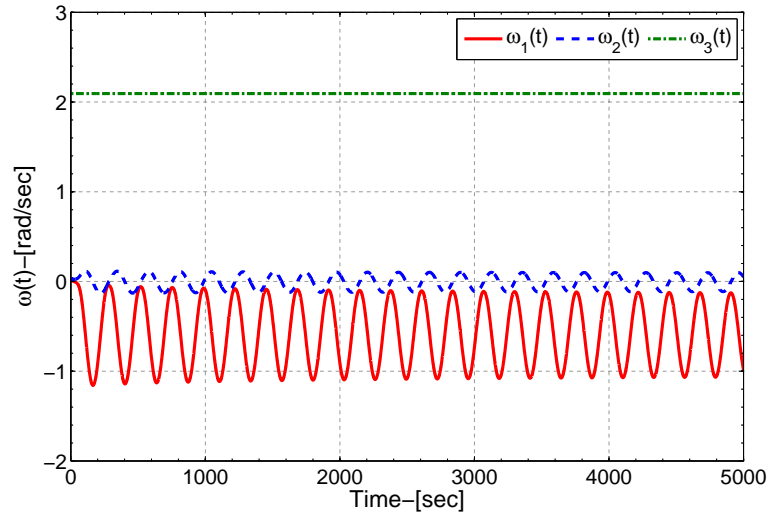


Fig. 5.4: The time history of spacecraft angular velocity components with spherical-spherical pendulum model (Case 1).

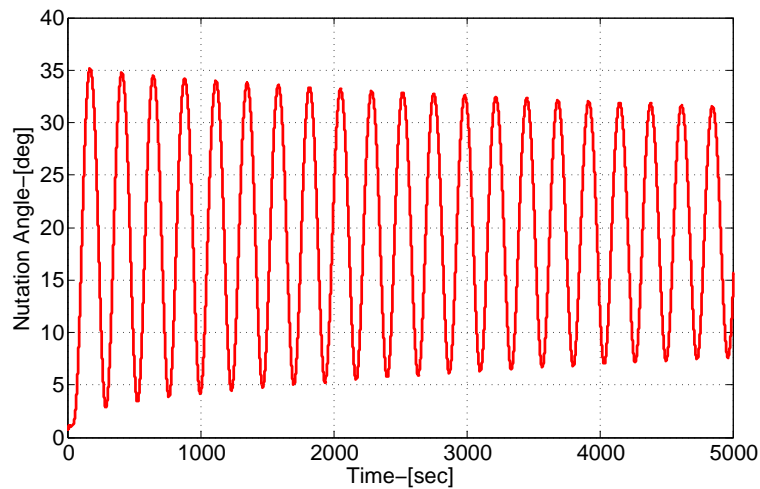


Fig. 5.5: Nutation angle for spherical-spherical pendulum model (Case 1).

the spacecraft nutation angle is shown in Fig. 5.5. It can be easily seen that the average nutation angle of the spacecraft for the spherical-spherical model is higher, although, it does not grow.

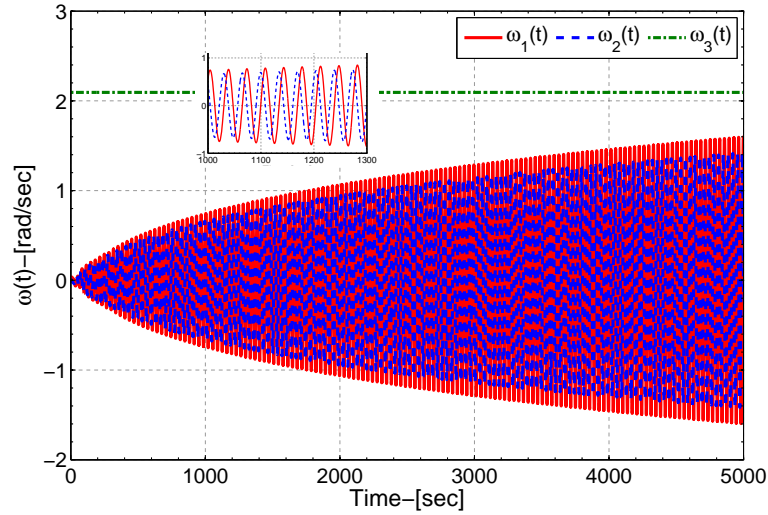


Fig. 5.6: The time history of spacecraft angular velocity components with spherical-spherical pendulum model (Case 2).

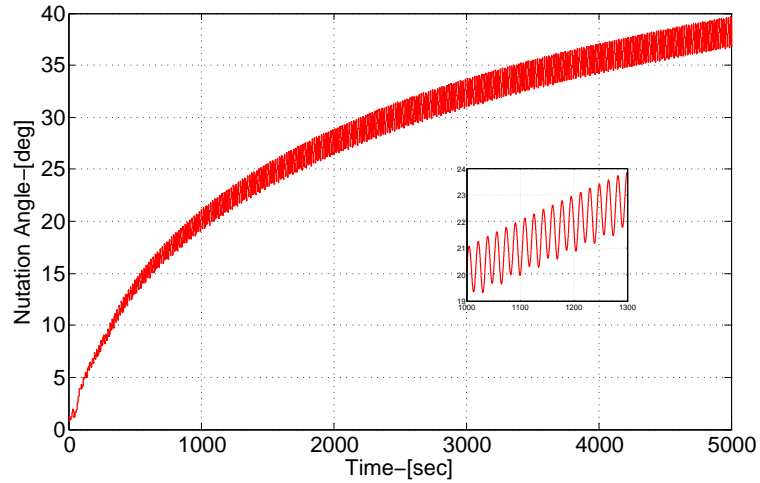


Fig. 5.7: Nutation angle for spherical-spherical pendulum model (Case 2).

Case 2 - Spinning about the minimum moment-of-inertia axis.

Now, we assume that the spacecraft has a constant spin rate of 20 *rpm* around its minimum moment-of-inertia, \hat{g}_2 axis, and zero initial angular velocity around the other axes, i.e. $\omega_0 = (0, 20, 0)$ *rpm*. Fig. 5.6 shows the components of angular velocity of the spacecraft for the spherical-spherical pendulum model.

The effect of spherical-spherical pendulum model on the spacecraft nutation angle is shown

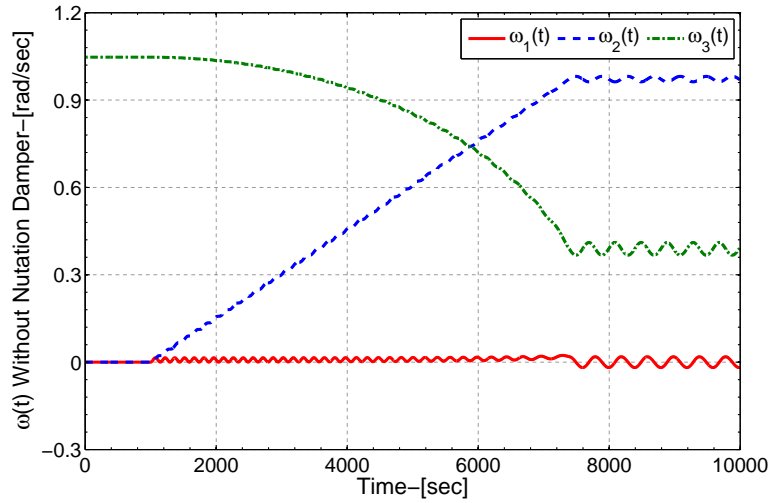


Fig. 5.8: Case 2-The time history of spacecraft angular velocity components with an empty tank and without nutation damper.

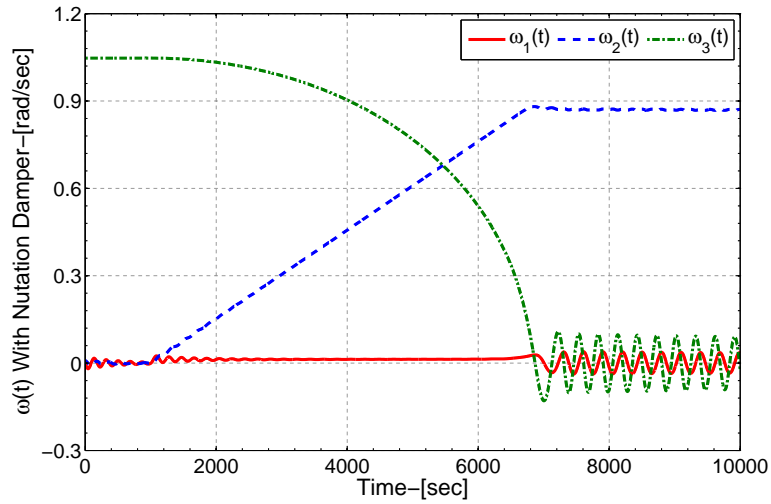


Fig. 5.9: Case 2-The time history of spacecraft angular velocity components with an empty tank and with nutation damper.

in Fig. 5.7. It can be easily seen that the average nutation angle of the spacecraft for the spherical-spherical model is eventually growing.

Case 3 - Reorientation Maneuver Analysis.

In this case, we assume the spacecraft has an initial spin rate of 10 *rpm* around its maximum moment-of-inertia axis, \hat{g}_3 axis, and zero around other axes. i.e. $\omega_0 = (0, 0, 10)$ *rpm*. We

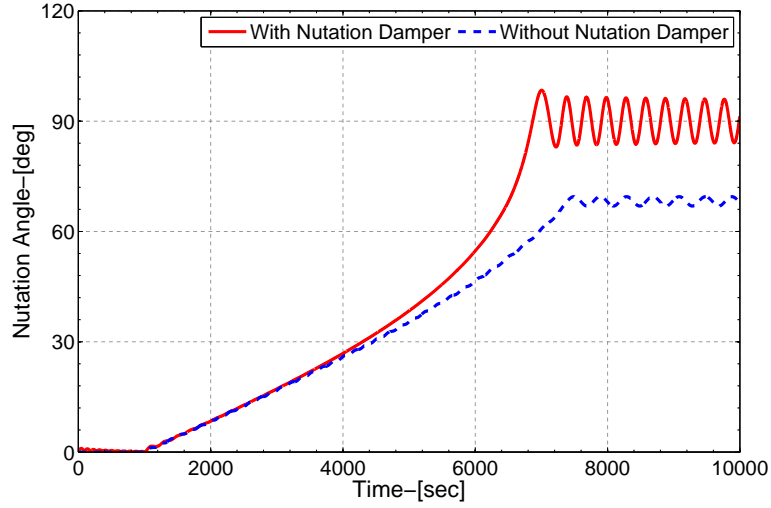


Fig. 5.10: Case 2-The effect of nutation damper on spacecraft nutation angle with empty tank.

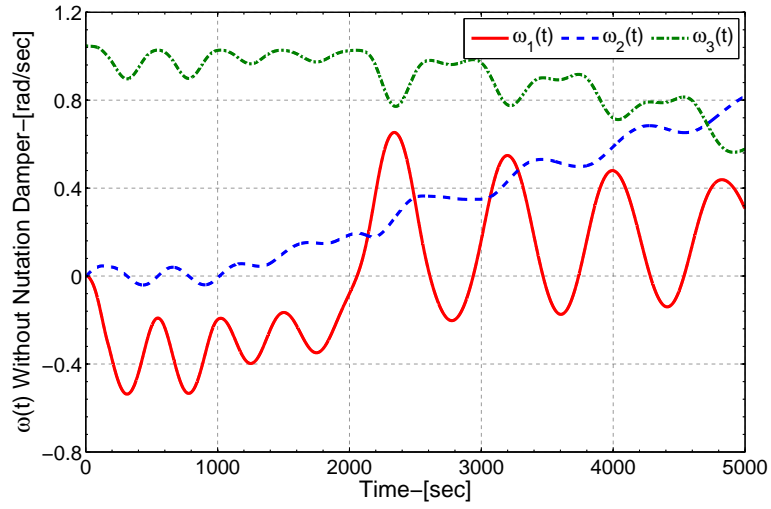


Fig. 5.11: Case 2-The time history of spacecraft angular velocity components with partially-filled tank and without nutation damper.

also assume the third momentum wheel, along the body \hat{g}_2 axis, spins up according to the following piecewise function [26]:

$$G_{\omega}W_2 = \begin{cases} 0 & 0 \leq t < 1,000 \\ 0.9375(t - 1000) & 1,000 \leq t < 7,400 \\ 6,000 & 7,400 \leq t \leq 10,000 \end{cases} \quad (5.70)$$

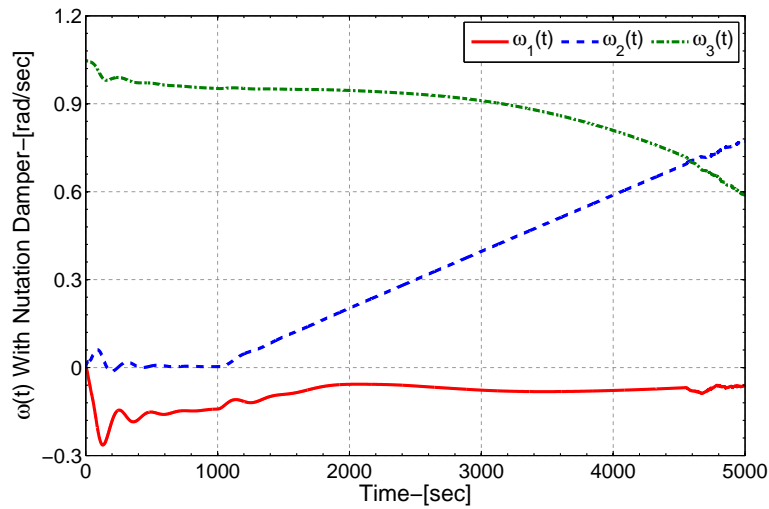


Fig. 5.12: Case 2-The time history of spacecraft angular velocity components with partially-filled tank and with nutation damper.

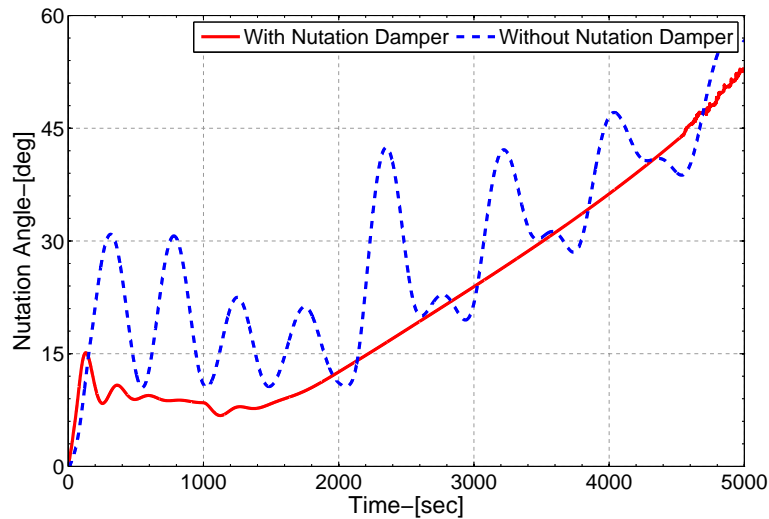


Fig. 5.13: Case 2-The effect of nutation damper on spacecraft nutation angle with partially-filled tank.

Figures 5.8– 5.10 show the effect of nutation damper on the angular velocity and nutation angle of the spacecraft with an empty tank during reorientation maneuver, respectively. As we expected, the nutation damper will damp the oscillations and causes the spacecraft to spin about the \hat{g}_2 axis. It can be seen that the nutation angle will oscillate with a small amplitude about 90° . Similarly, the nutation damper has the same effect on the spacecraft when its fuel tank is partially-filled, as shown in Figs. 5.11– 5.13.

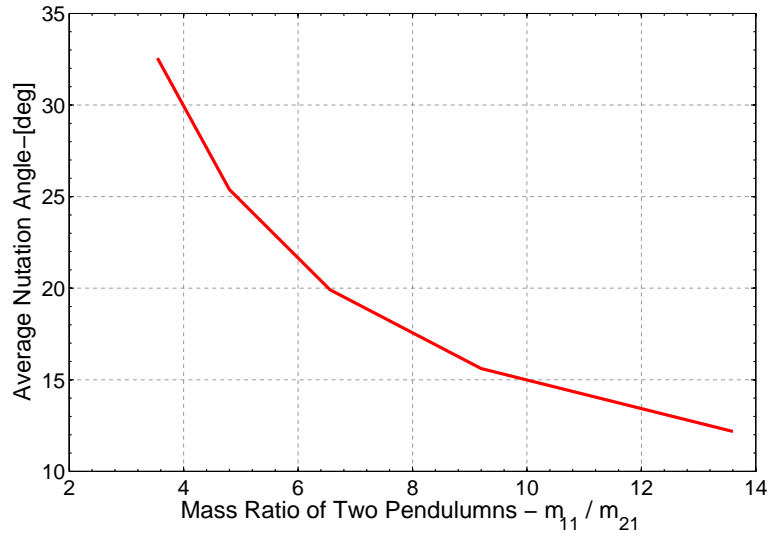


Fig. 5.14: Case 1-The effect of pendulum mass-ratio on the spacecraft nutation angle.

Moreover, by using Eqs. 5.1 and 5.2, we investigate the effect of change in the mass-ratio, m_{11}/m_{21} , of the spherical-spherical pendulum model on the spacecraft nutation angle, see Fig. 5.14. It can be seen that the average nutation angle decreases as the mass-ratio increases.

CHAPTER 6

Conclusions and Future Work

6.1 Conclusions

In the first part of the research, three fuzzy controllers for attitude stabilization of a spacecraft with a partially-filled tank are presented and compared. The spherical pendulum model is adopted to capture the behavior of the spacecraft with a partially-filled tank. The nonlinear T-S fuzzy model is built and validated based on the weighted sum of the local linear models. The first controller is a fuzzy PDC controller with a minimum upper bound control input. The second controller is a fuzzy LQR which uses the premises of the T-S model, and the controller and observer gains for each rule are obtained by solving the corresponding algebraic Riccati equations. The third controller is the robust-optimal fuzzy-model-based controller with a minimum upper bound control input. The stability, performance, and robustness of controllers are examined via numerical simulations. The simulation results show that the fuzzy PDC exhibits better performance and robustness compared to the fuzzy LQR, and the robust-optimal fuzzy PDC is robust in the presence of system and actuator uncertainties. Fuzzy PDC and robust-optimal fuzzy PDC exhibit better performance compared to the baseline PID controller. The proposed T-S controllers are nonlinear controllers with a simple structure and, therefore, easy for implementation.

In the second part of the research, we extended the existing models of spinning spacecraft with fuel sloshing in the literature. The equations of motion for a spinning spacecraft with

constant mass properties, three momentum wheels, one nutation damper, and S number of partially-filled tanks were derived using the Kane's method. As suggested in the literature, a two spherical pendulum model is adopted to capture the behavior of spacecraft with fuel sloshing during high-g maneuvers. Numerical simulations were performed to validate the behavior of the spacecraft for standard maneuvers.

6.2 Recommendations for Future Work

Below we present recommendations that can improve and extend the research conducted in this dissertation:

1. Conduct an experiment to verify the stability, performance, and robustness of the developed controllers.
2. Design a robust-optimal fuzzy tracking controller for flexible spacecraft with fuel sloshing.
3. Design a thrust vector controller based on T-S model for spacecraft with fuel sloshing.
4. Utilize computational fluid dynamics (CFD) instead of mechanical analogy models with control analysis to get a more accurate model.

APPENDIX A

A.1 The Elements of Matrix M and Vectors E and F in case of one tank with one pendulum

We notice that the matrix M in Eq. (2.24) is a symmetric matrix with the lower half written explicitly as:

$$M = \begin{bmatrix} m_{1,1} & * & * & * & * \\ m_{2,1} & m_{2,2} & * & * & * \\ m_{3,1} & m_{3,2} & m_{3,3} & * & * \\ m_{4,1} & m_{4,2} & m_{4,3} & m_{4,4} & * \\ m_{5,1} & m_{5,2} & m_{5,3} & m_{5,4} & m_{5,5} \end{bmatrix}, \quad (\text{A-1})$$

where * denote the transposed elements for symmetric positions. The nonzero elements of the matrix M are:

$$m_{1,1} = m_0 r_0^2 - l_p m_p c \psi_2 (r_p - l_p c \psi_2) + r_p m_p (r_p - l_p c \psi_2) + l_p^2 m_p s^2 \psi_1 s^2 \psi_2 + I_1, \quad (\text{A-2})$$

$$m_{2,1} = -l_p^2 m_p s \psi_1 c \psi_1 s^2 \psi_2, \quad (\text{A-3})$$

$$m_{2,2} = m_0 r_0^2 - l_p m_p c \psi_2 (r_p - l_p c \psi_2) + r_p m_p (r_p - l_p c \psi_2) + l_p^2 m_p c^2 \psi_1 s^2 \psi_2 + I_2, \quad (\text{A-4})$$

$$m_{3,1} = l_p m_p c \psi_1 s \psi_2 (l_p c \psi_2 - r_p), \quad (\text{A-5})$$

$$m_{3,2} = -l_p m_p s \psi_1 s \psi_2 (r_p - l_p c \psi_2), \quad (\text{A-6})$$

$$m_{3,3} = l_p^2 m_p s^2 \psi_2 + I_3, \quad (\text{A-7})$$

$$m_{4,1} = l_p m_p c \psi_1 s \psi_2 (-r_p + l_p c \psi_2), \quad (\text{A-8})$$

$$m_{4,2} = -l_p m_p s \psi_1 s \psi_2 (r_p - l_p c \psi_2), \quad (\text{A-9})$$

$$m_{4,3} = m_{4,4} = l_p^2 m_p s^2 \psi_2, \quad (\text{A-10})$$

$$m_{5,1} = l_p m_p s \psi_1 c \psi_2 (-r_p + l_p c \psi_2) + l_p^2 m_p s \psi_1 s^2 \psi_2, \quad (\text{A-11})$$

$$m_{5,2} = l_p m_p c \psi_1 c \psi_2 (r_p - l_p c \psi_2) - l_p^2 m_p c \psi_1 s^2 \psi_2, \quad (\text{A-12})$$

$$m_{5,5} = l_p^2 m_p, \quad (\text{A-13})$$

where r_0 and r_p are the locations of the pendulum hinge and static body described in section 2.4. I_1 , I_2 , and I_3 are the components of the inertia matrix of the spacecraft $I^{S^*/S}$.

The elements of the vector E in Eq. (2.24) are:

$$e_1 = I_3 g_3 g_2 - I_2 g_2 g_3 - m_0 r_0^2 g_2 g_3 + m_p (l_p c \psi_2 - r_p) Z_{51} + l_p m_p s \psi_1 s \psi_2 Z_{61}, \quad (\text{A-14})$$

$$e_2 = -I_3 g_3 g_1 + I_1 g_1 g_3 + m_0 r_0^2 g_1 g_3 + m_p (-l_p c \psi_2 + r_p) Z_{41} - l_p m_p c \psi_1 s \psi_2 Z_{61}, \quad (\text{A-15})$$

$$e_3 = I_2 g_2 g_1 - I_1 g_1 g_2 - l_p m_p s \psi_1 s \psi_2 Z_{41} + l_p m_p c \psi_1 s \psi_2 Z_{51}, \quad (\text{A-16})$$

$$e_4 = -l_p m_p s \psi_1 s \psi_2 Z_{41} + l_p m_p c \psi_1 s \psi_2 Z_{51}, \quad (\text{A-17})$$

$$e_5 = l_p m_p c \psi_1 c \psi_2 Z_{41} + l_p m_p c \psi_2 s \psi_1 Z_{51} + l_p m_p s \psi_2 Z_{61}. \quad (\text{A-18})$$

The expressions for Z_{i1} , ($i = 4, 5, 6$) are found as:

$$Z_{41} = r_p g_4 g_6 + (-g_4(\dot{\psi}_1 + g_6) - \dot{\psi}_2 s \psi_1 (2\dot{\psi}_1 + g_6)) l_p c \psi_2 + \frac{1}{2} (-\dot{\psi}_2 s (2\psi_1) g_4 + 3\dot{\psi}_2 g_5 + c(2\psi_1) \dot{\psi}_2 g_5 + 2s\psi_1 g_4 g_5 - 2c\psi_1 (\dot{\psi}_2^2 + g_5^2 + (\dot{\psi}_1 + g_6)^2)) l_p s \psi_2, \quad (\text{A-19})$$

$$Z_{51} = r_p g_5 g_6 + (-g_5(\dot{\psi}_1 + g_6) + \dot{\psi}_2 c \psi_1 (2\dot{\psi}_1 + g_6)) l_p c \psi_2 + \frac{1}{2} (-3\dot{\psi}_2 g_4 + \dot{\psi}_2 g_4 c(2\psi_1) + \dot{\psi}_2 g_5 s(2\psi_1) + 2c\psi_1 g_4 g_5 - 2s\psi_1 (\dot{\psi}_2^2 + g_4^2 + (\dot{\psi}_1 + g_6)^2)) l_p s \psi_2, \quad (\text{A-20})$$

$$Z_{61} = -(g_4^2 + g_5^2) r_p + (1 + 2s\psi_1 g_4 - 2c\psi_1 g_5) \dot{\psi}_2 c \psi_2 l_p + (g_4^2 + g_5^2) c \psi_2 l_p + (\dot{\psi}_1 + g_6) (c\psi_1 g_4 + s\psi_1 g_5) s \psi_2 l_p. \quad (\text{A-21})$$

The generalized active force can be written from Eq. (2.24) in the following vector form:

$$F = \begin{bmatrix} F_1 \\ F_2 \\ F_3 \\ F_4 \\ F_5 \end{bmatrix} = \begin{bmatrix} u_1 \\ u_2 \\ u_3 \\ -(D_{\psi_1} + K_{\psi_1}) l_p^2 g_4 s^2 \psi_2 \\ -(D_{\psi_2} + K_{\psi_2}) l_p^2 g_5 \end{bmatrix}. \quad (\text{A-22})$$

The 11×1 vector E' in Eq. (2.30) is

$$E' = [-e_1, -e_2, -e_3, F_4 - e_4, F_5 - e_5, \dot{\psi}_1, \dot{\psi}_2, \dot{q}_0, \dot{q}_1, \dot{q}_2, \dot{q}_3]^T. \quad (\text{A-23})$$

$$m_{9,1} = -l_{21}m_{21}s\alpha_{21}s\beta_{21}, \quad (\text{A-30})$$

$$m_{10,1} = l_{21}m_{21}c\alpha_{21}c\beta_{21}, \quad (\text{A-31})$$

$$m_{4,2} = -m_{5,1}, \quad (\text{A-32})$$

$$m_{6,2} = l_{11}m_{11}c\alpha_{11}s\beta_{11} + l_{21}m_{21}c\alpha_{21}s\beta_{21} + m_Q z_Q, \quad (\text{A-33})$$

$$m_{7,2} = l_{11}m_{11}c\alpha_{11}s\beta_{11}, \quad (\text{A-34})$$

$$m_{8,2} = l_{11}m_{11}c\beta_{11}s\alpha_{11}, \quad (\text{A-35})$$

$$m_{9,2} = l_{21}m_{21}c\alpha_{21}s\beta_{21}, \quad (\text{A-36})$$

$$m_{10,2} = l_{21}m_{21}c\beta_{21}s\alpha_{21}, \quad (\text{A-37})$$

$$m_{4,3} = -m_{6,1}, \quad (\text{A-38})$$

$$m_{5,3} = -m_{6,2}, \quad (\text{A-39})$$

$$m_{8,3} = l_{11}m_{11}s\beta_{11}, \quad (\text{A-40})$$

$$m_{10,3} = l_{21}m_{21}s\beta_{21}, \quad (\text{A-41})$$

$$m_{11,3} = m_Q, \quad (\text{A-42})$$

$$\begin{aligned} m_{4,4} = & m_{01}r_{03}^2 + l_{11}m_{11}c\beta_{11}(-r_{13} + l_{11}c\beta_{11}) - r_{13}m_{11}(-r_{13} + l_{11}c\beta_{11}) + \\ & l_{21}m_{21}c\beta_{21}(-r_{23} + l_{21}c\beta_{21}) - r_{23}m_{21}(-r_{23} + l_{21}c\beta_{21}) + \\ & + l_{11}^2 m_{11} s\alpha_{11}^2 s\beta_{11}^2 + l_{21}^2 m_{21} s\alpha_{21}^2 s\beta_{21}^2 + \\ & + m_Q q^2 + I_{11}, \end{aligned} \quad (\text{A-43})$$

$$m_{5,4} = -l_{11}^2 m_{11} s\alpha_{11} c\alpha_{11} s\beta_{11}^2 - l_{21}^2 m_{21} s\alpha_{21} c\alpha_{21} s\beta_{21}^2 + I_{12}, \quad (\text{A-44})$$

$$m_{6,4} = l_{11}m_{11}c\alpha_{11}s\beta_{11}(l_{11}c\beta_{11} - r_{13}) + l_{21}m_{21}c\alpha_{21}s\beta_{21}(l_{21}c\beta_{21} - r_{23}) - m_Q z_Q q + I_{13}, \quad (\text{A-45})$$

$$m_{7,4} = l_{11}m_{11}c\alpha_{11}s\beta_{11}(-r_{13} + l_{11}c\beta_{11}), \quad (\text{A-46})$$

$$m_{8,4} = l_{11}m_{11}s\alpha_{11}c\beta_{11}(-r_{13} + l_{11}c\beta_{11}) + l_{11}^2 m_{11}s\alpha_{11}s\beta_{11}^2, \quad (\text{A-47})$$

$$m_{9,4} = l_{21}m_{21}c\alpha_{21}s\beta_{21}(-r_{23} + l_{21}c\beta_{21}), \quad (\text{A-48})$$

$$m_{10,4} = l_{21}m_{21}s\alpha_{21}c\beta_{21}(-r_{23} + l_{21}c\beta_{21}) + l_{21}^2 m_{21}s\alpha_{21}s\beta_{21}^2, \quad (\text{A-49})$$

$$\begin{aligned} m_{5,5} = & m_{01}r_{03}^2 - l_{11}m_{11}c\beta_{11}(r_{13} - l_{11}c\beta_{11}) + r_{13}m_{11}(r_{13} - l_{11}c\beta_{11}) - \\ & - l_{21}m_{21}c\beta_{21}(r_{23} - l_{21}c\beta_{21}) + r_{23}m_{21}(r_{23} - l_{21}c\beta_{21}) + \\ & + l_{11}^2 m_{11}c\alpha_{11}^2 s\beta_{11}^2 + l_{21}^2 m_{21}c\alpha_{21}^2 s\beta_{21}^2 + \\ & + m_Q z_Q^2 + m_Q q^2 + I_{22}, \end{aligned} \quad (\text{A-50})$$

$$m_{6,5} = -l_{11}m_{11}s\alpha_{11}s\beta_{11}(r_{13} - l_{11}c\beta_{11}) - l_{21}m_{21}s\alpha_{21}s\beta_{21}(r_{23} - l_{21}c\beta_{21}) + I_{23}, \quad (\text{A-51})$$

$$m_{7,5} = -l_{11}m_{11}s\alpha_{11}s\beta_{11}(r_{13} - l_{11}c\beta_{11}), \quad (\text{A-52})$$

$$m_{8,5} = l_{11}m_{11}c\alpha_{11}c\beta_{11}(r_{13} - l_{11}c\beta_{11}) - l_{11}^2 m_{11}c\alpha_{11}s\beta_{11}^2, \quad (\text{A-53})$$

$$m_{9,5} = -l_{21}m_{21}s\alpha_{21}s\beta_{21}(r_{23} - l_{21}c\beta_{21}), \quad (\text{A-54})$$

$$m_{10,5} = l_{21}m_{21}c\alpha_{21}c\beta_{21}(r_{23} - l_{21}c\beta_{21}) - l_{21}^2 m_{21}c\alpha_{21}s\beta_{21}^2, \quad (\text{A-55})$$

$$m_{11,5} = -m_Q z_Q, \quad (\text{A-56})$$

$$m_{6,6} = l_{11}^2 m_{11}s\beta_{11}^2 + l_{21}^2 m_{21}s\beta_{21}^2 + m_Q q^2 + I_{33}, \quad (\text{A-57})$$

$$m_{7,6} = m_{7,7} = l_{11}^2 m_{11}s\beta_{11}^2, \quad (\text{A-58})$$

$$m_{9,6} = m_{9,9} = l_{21}^2 m_{21}s\beta_{21}^2, \quad (\text{A-59})$$

$$m_{8,8} = l_{11}^2 m_{11}, \quad (\text{A-60})$$

$$m_{10,10} = l_{21}^2 m_{21}, \quad (\text{A-61})$$

$$m_{11,11} = m_Q. \quad (\text{A-62})$$

The elements of vector C in Eq. (5.48) are as follows:

$$c_1 = m_{01} r_{03} u_4 u_6 + (m_G + m_{01}) Z_1 + m_{11} Z_{41} + m_{21} Z_{42} + m_Q Z_7, \quad (\text{A-63})$$

$$c_2 = m_{01} r_{03} u_5 u_6 + (m_G + m_{01}) Z_2 + m_{11} Z_{51} + m_{21} Z_{52} + m_Q Z_8, \quad (\text{A-64})$$

$$c_3 = -m_{01} r_{03} (u_4^2 + u_5^2) + (m_G + m_{01}) Z_3 + m_{11} Z_{61} + m_{21} Z_{62} + m_Q Z_9, \quad (\text{A-65})$$

$$\begin{aligned} c_4 = & Z_{15} u_5 - Z_{14} u_6 - m_{01} r_{03}^2 u_5 u_6 - m_{01} r_{03} Z_2 + \\ & + m_{11} (l_{11} c\beta_{11} - r_{13}) Z_{51} + m_{21} (l_{21} c\beta_{21} - r_{23}) Z_{52} + l_{11} m_{11} s\alpha_{11} s\beta_{11} Z_{61} + \\ & + l_{21} m_{21} s\alpha_{21} s\beta_{21} Z_{62} - m_Q q Z_8 + I^W (G_\alpha^{W_1} - G_\omega^{W_2} u_6 + G_\omega^{W_3} u_5), \end{aligned} \quad (\text{A-66})$$

$$\begin{aligned} c_5 = & -Z_{15} u_4 + Z_{13} u_6 + m_{01} r_{03}^2 u_4 u_6 + m_{01} r_{03} Z_1 + \\ & + m_{11} (-l_{11} c\beta_{11} + r_{13}) Z_{41} + m_{21} (-l_{21} c\beta_{21} + r_{23}) Z_{42} - l_{11} m_{11} c\alpha_{11} s\beta_{11} Z_{61} - \\ & - l_{21} m_{21} c\alpha_{21} s\beta_{21} Z_{62} - m_Q q Z_7 - m_Q z_Q Z_9 + I^W (G_\alpha^{W_2} + G_\omega^{W_1} u_6 - G_\omega^{W_3} u_4), \end{aligned} \quad (\text{A-67})$$

$$\begin{aligned} c_6 = & Z_{14} u_4 - Z_{13} u_5 - l_{11} m_{11} s\alpha_{11} s\beta_{11} Z_{41} - l_{21} m_{21} s\alpha_{21} s\beta_{21} Z_{42} + l_{11} m_{11} c\alpha_{11} s\beta_{11} Z_{51} + \\ & + l_{21} m_{21} c\alpha_{21} s\beta_{21} Z_{52} + m_Q z_Q Z_8 + I^W (G_\alpha^{W_3} - G_\omega^{W_1} u_5 + G_\omega^{W_2} u_4), \end{aligned} \quad (\text{A-68})$$

$$c_7 = -l_{11} m_{11} s\alpha_{11} s\beta_{11} Z_{41} + l_{11} m_{11} c\alpha_{11} s\beta_{11} Z_{51}, \quad (\text{A-69})$$

$$c_8 = l_{11} m_{11} c\alpha_{11} c\beta_{11} Z_{41} + l_{11} m_{11} c\beta_{11} s\alpha_{11} Z_{51} + l_{11} m_{11} s\beta_{11} Z_{61}, \quad (\text{A-70})$$

$$c_9 = -l_{21} m_{21} s\alpha_{21} s\beta_{21} Z_{42} + l_{21} m_{21} c\alpha_{21} s\beta_{21} Z_{52}, \quad (\text{A-71})$$

$$c_{10} = l_{21}m_{21}c\alpha_{21}c\beta_{21}Z_{42} + l_{21}m_{21}c\beta_{21}s\alpha_{21}Z_{52} + l_{21}m_{21}s\beta_{21}Z_{62}, \quad (\text{A-72})$$

$$c_{11} = m_Q Z_9, \quad (\text{A-73})$$

where

$$Z_{13} \triangleq I_{11}u_4 + I_{12}u_5 + I_{13}u_6, \quad (\text{A-74})$$

$$Z_{14} \triangleq I_{12}u_4 + I_{22}u_5 + I_{23}u_6, \quad (\text{A-75})$$

$$Z_{15} \triangleq I_{13}u_4 + I_{23}u_5 + I_{33}u_6. \quad (\text{A-76})$$

The generalized active force can be written from Eq. (5.48) in the following vector form:

$$\{F\} = \begin{bmatrix} F_{gG_1} + F_{gm_{01}} + F_{gm_{11}} + F_{gm_{21}} + F_{gQ_1} \\ F_{gG_2} + F_{gm_{02}} + F_{gm_{12}} + F_{gm_{22}} + F_{gQ_2} \\ F_{gG_3} + F_{gm_{03}} + F_{gm_{13}} + F_{gm_{23}} + F_{gQ_3} \\ F_4 \\ F_5 \\ F_6 \\ F_7 \\ F_8 \\ F_9 \\ F_{10} \\ -\sigma q - \delta \dot{q} + F_{gQ_3} \end{bmatrix}, \quad (\text{A-77})$$

where

$$\begin{aligned} F_4 = & M_{gG_1} - T_1 - T_2 - T_3 - F_{gm_{02}}r_{03} + F_{gm_{12}}(-r_{13} + l_{11}c\beta_{11}) + \\ & + F_{gm_{22}}(-r_{23} + l_{21}c\beta_{21}) + F_{gm_{13}}l_{11}s\alpha_{11}s\beta_{11} + F_{gm_{23}}l_{21}s\alpha_{21}s\beta_{21} - \\ & - F_{gQ_2}q + (d + q)(\sigma q + \delta \dot{q}), \end{aligned} \quad (\text{A-78})$$

$$\begin{aligned}
F_5 = & M_{gG_2} - T_1 - T_2 - T_3 + F_{gm_01}r_{03} + F_{gm_{11}}(r_{13} - l_{11}c\beta_{11}) + \\
& + F_{gm_{21}}(r_{23} - l_{21}c\beta_{21}) - F_{gm_{13}}l_{11}c\alpha_{11}s\beta_{11} - F_{gm_{23}}l_{21}c\alpha_{21}s\beta_{21} + \\
& + F_{gQ_1}q - F_{gQ_3}z_Q - (d + q)(\sigma q + \delta\dot{q}),
\end{aligned} \tag{A-79}$$

$$\begin{aligned}
F_6 = & M_{gG_3} - T_1 - T_2 - T_3 + F_{gm_{12}}l_{11}c\alpha_{11}s\beta_{11} - F_{gm_{11}}l_{11}s\alpha_{11}s\beta_{11} + \\
& + F_{gm_{22}}l_{21}c\alpha_{21}s\beta_{21} - F_{gm_{21}}l_{21}s\alpha_{21}s\beta_{21} + F_{gQ_2}z_Q,
\end{aligned} \tag{A-80}$$

$$F_7 = F_{gm_{12}}l_{11}c\alpha_{11}s\beta_{11} - F_{gm_{11}}l_{11}s\alpha_{11}s\beta_{11} - C_{\alpha_{11}}l_{11}^2u_7s\beta_{11}^2, \tag{A-81}$$

$$F_8 = F_{gm_{11}}l_{11}c\alpha_{11}c\beta_{11} + F_{gm_{12}}l_{11}s\alpha_{11}c\beta_{11} + F_{gm_{13}}l_{11}s\beta_{11} - C_{\beta_{11}}l_{11}^2u_8, \tag{A-82}$$

$$F_9 = F_{gm_{22}}l_{21}c\alpha_{21}s\beta_{21} - F_{gm_{21}}l_{21}s\alpha_{21}s\beta_{21} - C_{\alpha_{21}}l_{21}^2u_9s\beta_{21}^2, \tag{A-83}$$

$$F_{10} = F_{gm_{21}}l_{21}c\alpha_{21}c\beta_{21} + F_{gm_{22}}l_{21}s\alpha_{21}c\beta_{21} + F_{gm_{23}}l_{21}s\beta_{21} - C_{\beta_{21}}l_{21}^2u_{10}. \tag{A-84}$$

Bibliography

- [1] Scholl, H. F., Pinson, L. D., and Stephens, D. G., Investigation of Slosh Anomaly in Apollo Lunar Module Propellant Gage, NASA-TM-X-2362, L-7757, 1971.
- [2] O'Hern, E., Baddeley, V., and Rekowski, J., Analysis of Effects of Fluid Energy Dissipation on Spinning Satellite Control Dynamics, *AIAA Guidance and Control Conference*, AIAA 72-886, 1972.
- [3] Slabinski, V. J., Intelsat IV In-Orbit Liquid Slosh Tests and Problems in the Theoretical Analysis of the Data, *Proc. Conf. Attitude Control of Space Vehicles: Technological and Dynamical Problems Associated with the Presence of Liquids*, Toulouse, France, ESA SP-129, 1977, pp. 87–102.
- [4] Agrawal, B. N., Dynamic Characteristics of Liquid Motion in Partially Filled Tanks of a Spinning Spacecraft, *Journal of Guidance, Control, and Dynamics*, Vol. 16, No. 4, 1993, pp. 636–640.
- [5] Strikwerda, T. E., Ray, J. C., Haley, D. R., and O'Shaughnessy, D. J., NEAR Shoemaker: Major Anomaly Survival, Delayed Rendezvous and Mission Success, *Proc. Conf. Attitude Control of Space Vehicles: Technological and Dynamical Problems Associated with the Presence of Liquids*, in *Guidance and Control 2001*, R.D. Culp and C.N. Schira, Eds. San Diego, CA: Univelt, 2001, pp. 597–614.
- [6] Sances, D., Gangadharan, S., Sudermann, J., and Marsell, B., CFD Fuel Slosh Modeling of Fluid-Structure Interaction in Spacecraft Propellant Tanks with Diaphragms,

51st, AIAA/ASME/ASME/ASCE/AHS/ASC Structures, Structural Dynamics and Materials Conference, Orlando, FL, Vol. 8, 2010, pp. 6009-6017.

- [7] Mason, P. and Starin, S. R., The Effects of Propellant Slosh Dynamics on the Solar Dynamics Observatory, *AIAA Guidance, Navigation, and Control Conference*, Portland, OR, Vol. 10, 2011, pp. 8768–8790.
- [8] Nan, M., Junfeng, L., and Tianshu, W., Equivalent Mechanical Model of Large-Amplitude Liquid Sloshing Under Time-Dependent Lateral Excitations in Low-Gravity Conditions, *Journal of Sound and Vibration*, Vol. 386, 2017, pp. 421–432.
- [9] Sidi, M. J., *Spacecraft Dynamics and Control*, Cambridge Aerospace Series, Cambridge University Press, 1997.
- [10] Wertz, J. R., *Spacecraft Attitude Determination and Control*, Kluwer Academic Press, 1978.
- [11] Deep Space 1: Technology Validation Reports, Jet Propulsion Laboratory, CA, 1999, Available: https://www.jpl.nasa.gov/news/press_kits/ds1launch.pdf
- [12] DELTA II: Payload Planners Guide, United Launch Alliance, Colorado, 2006. Available: <https://www.ulalaunch.com/docs/default-source/rockets/deltaiipayloadplannersguide2007.pdf>
- [13] Atlas V Launch Services: User's Guide, United Launch Alliance, Colorado, 2010, Available: <https://www.ulalaunch.com/docs/default-source/rockets/atlasvusersguide2010.pdf>
- [14] Dodge, F. T., The New Dynamic Behavior of Liquids in Moving Container, *Tech. Rep. NASA SP-106*, Southwest Research Institute, San Antonio, TX, 2000.

- [15] Ibrahim, R. A., *Liquid Sloshing Dynamics, Theory and Applications*, Cambridge University Press, 2005.
- [16] Flandro, G. A., Leloudis, M., and Roach, R., *Flow Induced Nutation Instability in Spinning Solid Propellant Rockets, AD-A222 504*, Wasatch Research and Engineering, Inc., 1990.
- [17] Man, G. K. and Eke, F. O., *Effects of Payload Motions on the Nutational Stability of the Galileo Spacecraft, Journal of Guidance, Control, and Dynamics*, Vol. 8, No. 6, 1985, pp. 683–688.
- [18] Mingori, D. L. and Yam, Y., *Nutational Instability of a Spinning Spacecraft with Internal Mass Motion and Axial Thrust, AAS 86-2271, AIAA/AAS Astrodynamics Conference*, Williamsburg, VA, 1986, pp. 367–375.
- [19] Or, A. C., *Rotor-Pendulum Model for the Perigee Assist Module Nutation Anomaly, Journal of Guidance, Control, and Dynamics*, Vol. 15, No. 2, 1992, pp. 297–303.
- [20] Hill D. E., Baumgarten, J. R., and Miller, J. T., *Dynamic Simulation of Spin-Stabilized Spacecraft with Sloshing Fluid Stores, Journal of Guidance, Control and Dynamics*, Vol. 11, No. 6, 1988, pp. 597–599.
- [21] Baumgarten, J. R., Flugrad, D. R., and Prusa, J. M., *Investigation of Liquid Sloshing in Spin-Stabilized Satellites, Tech. Rep. ISU-ERI-Ames-90401*, Iowa State University, Ames, IA, 1989.
- [22] Cochran, J. E. and Kang, J. Y., *Nonlinear Stability Analysis of the Attitude Motion of a Spin-Stabilized Upper Stage, AAS 91-109, 1st AAS/AIAA Annual Spaceflight Mechanics Meeting*, Vol. 1, 1991, pp. 345–364.
- [23] Kang, J. Y. and Cochran, J. E., *Resonant Motion of a Spin-Stabilized Thrusting Spacecraft, Journal of Guidance, Control, and Dynamics*, Vol. 27, No. 3, 2004, pp. 356–364.

- [24] Quadrelli, M. B., Modeling and Analysis for Nutation Time Constant Determination of On-Axis Diaphragm Tanks on Spinners: Application to the Deep Space One Spacecraft, *Spaceflight Mechanics 2003*, AIAA, Ponce, Puerto Rico, Vol. 114, No. 2, 2003, pp. 835–854.
- [25] Quadrelli, M. B., Nutation Time Constant Determination of On-Axis Diaphragm Tanks on Spinner Spacecraft, *Journal of Spacecraft and Rockets*, Vol. 42, No. 3, 2005, pp. 530–542.
- [26] Kang, J. Y. and Lee, S., Attitude Acquisition of a Satellite with a Partially Filled Liquid Tank, *Journal of Guidance, Control, and Dynamics*, Vol. 31, No. 3, 2008, pp. 790–793.
- [27] Ayoubi, M. A., Goodarzi, F. A., and Banerjee, A., Attitude Motion of a Spinning Spacecraft with Fuel Sloshing and Nutation Damping, *Journal of the Astronautical Sciences*, Vol. 58, No. 4, 2011, pp. 551–568.
- [28] Kane, T. R., Likins, P., and Levinson, D. A., *Spacecraft Dynamics*, Mc Graw-Hill, Inc., 1983.
- [29] Kane, T. R. and Levinson, D. A., *Dynamics Theory and Applications*, Mc Graw-Hill, Inc., 1985.
- [30] Banerjee, A. K., Contributions of Multibody Dynamics to Space Flight: A Brief Review, *Journal of Guidance, Control, and Dynamics*, Vol. 26, No. 3, 2003, pp. 385–394.
- [31] Abramson, N. H., Further Studies of Liquid Sloshing in Rocket Propellant Tanks, *Tech. Rep. Project 02-1072*, Southwest Research Institute, 1965.
- [32] Abramson, N. H., The Dynamic Behavior of Liquids in Moving Containers with Applications to Space Vehicle Technology, *Tech. Rep. NASA SP-106*, Southwest Research Institute, 1966.

- [33] Dodge, F. T., Green, S. T., and Kana, D. D., Fluid Management Technology: Liquid Slosh Dynamics and Control, *Tech. Rep. Project 04-2453*, Southwest Research Institute, 1991.
- [34] Roberts, J. R., Basurto, E. R., and Chen, P.-Y., Slosh Design Handbook 1, *Northrop Space Lab, NASA Technical Report No. 27, Contract NAS 8-11111*, 1966.
- [35] Kana, D. D., Validated Spherical Pendulum Model for Rotary Liquid Slosh, *Journal of Spacecraft and Rockets*, Vol. 26, 1989, pp. 188–195.
- [36] Enright, P. J. and Wong, E. C., Propellant Slosh Models for the Cassini Spacecraft, *AIAA. Inc. with permission Jet Propulsion Laboratory*, California Institute of Technology, Pasadena, CA, 1994.
- [37] Wong, E. C. and Breckenridge, W. G., An Attitude Control Design for the Cassini Spacecraft, *Tech. Rep., AIAA. Inc. with permission Jet Propulsion Laboratory*, California Institute of Technology, Pasadena, CA, 1990.
- [38] Nan, M., Junfeng, L., and Tianshu, B. Z., Large-Amplitude Sloshing Analysis and Equivalent Mechanical Modeling in Spherical Tanks of Spacecraft, *Journal of Spacecraft and Rockets*, Vol. 53, No. 3, 2016, pp. 500–506.
- [39] Navabi, M. and Davoodi, A., 3D Multi-Pendulum Model of Slosh Dynamics in a Spacecraft, *Proceedings of 8th International Conference on Recent Advances in Space Technologies (RAST) IEEE*, 2017, pp. 259–262.
- [40] Hill D. E. and Baumgarten, J. R., Control of Spin-Stabilized Spacecraft with Sloshing Fluid Stores, *Journal of Dynamic Systems, Measurement, and Control*, Vol. 114, No. 4, 1992, pp. 728–731.

- [41] Cho, S., McClamrocht, N. H., and Reyhanoglu, M., Feedback Control of a Space Vehicle with Unactuated Fuel Slosh Dynamics, *AIAA Guidance, Navigation, and Control Conference and Exhibit*, Denver, CO, Vol. 1, 2000, pp. 1–6.
- [42] Shageer, H. and Tao, G., Modeling and Adaptive Control of Spacecraft with Fuel Slosh: Overview and Case Studies, *AIAA Guidance, Navigation, and Control Conference and Exhibit*, Denver, CO, 2007.
- [43] Reyhanoglu, M. and Hervas, J. R., Nonlinear Control of a Spacecraft with Multiple Fuel Slosh Modes, *50th IEEE Conference on Decision and Control and European Control Conference (CDC-ECC)*, Orlando, FL, USA, 2011.
- [44] Reyhanoglu, M., Maneuvering Control Problems for a Spacecraft with Unactuated Fuel Slosh Dynamics, *Proceedings of IEEE Conference on Control Application*, Vol. 1, 2003, pp. 695–699.
- [45] Hervas, J. R. and Reyhanoglu, M., Thrust-Vector Control of a Three-Axis Stabilized Upper-Stage Rocket with Fuel Slosh Dynamics, *Acta Astronautica*, Vol. 98, 2014, pp. 120–127.
- [46] Zhang, H. and Wang, Z., Attitude Control and Sloshing Suppression for Liquid-Filled Spacecraft in the Presence of Sinusoidal Disturbance, *Journal of Sound and Vibration*, Vol. 383, 2016, pp. 64–75.
- [47] Deng, M. L. and Yue, B. Z., Nonlinear Model and Attitude Dynamics of Flexible Spacecraft with Large Amplitude Slosh, *Acta Astronautica*, Vol. 133, 2017, pp. 111–120.
- [48] Deng, M. L. and Yue, B. Z., Attitude Dynamics and Control of Spacecraft with Multiple Liquid Propellant Tanks in Press, *Journal of Aerospace Engineering*, Vol. 29, No. 6, 2016, pp. 04016042-1–11.

- [49] Takagi, T. and Sugeno, M., Fuzzy Identification of Systems and its Applications to Modeling and Control, *IEEE Transactions on Systems, Man, and Cybernetics*, Vol. 15, 1985, pp. 116–132.
- [50] Sugeno, M. and Kang, T., Fuzzy Modeling and Control of Multilayer Incinerator, *Fuzzy Sets and Systems*, No. 18, 1986, pp. 329–346.
- [51] Tanaka, K. and Sugeno, M., Stability Analysis and Design of Fuzzy Control Systems, *Fuzzy Sets and Systems*, Vol. 45, No. 2, 1992, pp. 135–156.
- [52] Tanaka, K. and Wang, H. O., Fuzzy Control Systems Design and Analysis: A Linear Matrix Inequality Approach, John Wiley & Sons, New York, 2001.
- [53] Boyd, S., Ghaoui, L. El, Feron, E., and Balakrishnan, V., *Linear Matrix Inequalities in Systems and Control Theory*, SIAM, Philadelphia, PA, 1994.
- [54] Zečević, A. I. and Šiljak, D. D., Control of Complex Systems: Structural Constraints and Uncertainty, Springer, Berlin, 2010.
- [55] Wang, H. O., Tanaka, K., and Griffin, M., Parallel Distributed Compensation of Non-linear Systems by Takagi-Sugeno Fuzzy Model, *International Joint Conference of the Fourth IEEE International Conference on Fuzzy Systems and The Second International Fuzzy Engineering Symposium*, Vol. 2, No. 20–24, 1995, pp. 531–538.
- [56] Li, J., Wang, H. O., Niemann, D., and Tanaka, K., Dynamic Parallel Distributed Compensation for Takagi-Sugeno Fuzzy Systems: An LMI Approach, *Information Sciences*, Vol. 123, No. 3-4, 2000, pp. 201–221.
- [57] Feng, G., A Survey on Analysis and Design of Model-Based Fuzzy Control Systems, *IEEE Transactions on Fuzzy Systems*, Vol. 14, No. 5, 2006, pp. 676–697.

- [58] Song, B., Ma, G., Li, Ch., and Lv, J., Quaternion-Based Fuzzy Attitude Regulation of a Rigid Spacecraft, *Proceedings of the 6th World Congress on Intelligent Control and Automation, IEEE*, 2006, pp. 8434–8438.
- [59] Ayoubi, M. A. and Sendi, C., Fuzzy-Logic Attitude Control of Spacecraft with Retargeting Flexible Antenna, *AIAA Guidance, Navigation, and Control Conference*, Boston, Massachusetts, August 19-22, 2013.
- [60] Ayoubi, M. A. and Sendi, C., Takagi-Sugeno Fuzzy Model-Based Control of Spacecraft with Flexible Appendage, *Journal of Astronautical Sciences*, Vol. 61, No. 1, 2014, pp. 40–59.
- [61] Sendi, C. and Ayoubi, M. A., Robust-Optimal Fuzzy Model-Based Control of Flexible Spacecraft with Actuator Constraint, *Journal of Dynamic Systems, Measurement, and Control*, Vol. 138, No. 9, 2016.
- [62] Baculi, J. and Ayoubi, M. A., Fuzzy Attitude Control of Solar Sail via Linear Matrix Inequalities, *Acta Astronautica*, Vol. 138, 2017, pp. 233–241.
- [63] Mazmanyanyan, L. and Ayoubi, M. A., Takagi-Sugeno Fuzzy Model-Based Attitude Control of Spacecraft with Partially-Filled Fuel Tanks, *AIAA/AAS Astrodynamics Specialist Conference*, San Diego, California, August 4–7, 2014, Vol. 2, pp. 1227–1240.
- [64] Yang, Y., Analytic LQR Design for Spacecraft Control System Based on Quaternion Model, *Journal of Aerospace Engineering*, Vol. 25, No. 3, 2012, pp. 448–453.
- [65] Driankov, D., Palm, R., and Rehfuss, U., A Takagi-Sugeno Fuzzy Gain-Scheduler, *Proceedings of the Fifth IEEE International Conference on Fuzzy Systems*, 1996, pp. 1053–1059.

- [66] Applebaum, E., Fuzzy Gain Scheduling for Flutter Suppression in Unmanned Aerial Vehicles, *International Conference-North American Fuzzy Information Processing Society, IEEE*, Chicago, IL, 2003, pp. 323–328.
- [67] Li, A., Yang, L., Zhang, J., and He, Ch., LQR and Fuzzy Gain-Scheduling Based Attitude Controller for RLV within Large Operating Envelope, *2014 IEEE International Conference on Control Science and Systems Engineering (CCSSE)*, 2014, pp. 51–56.
- [68] Jie, M. and Yang, X., Fuzzy Reaching Law Sliding Mode Controller for Spacecraft Attitude Control, *2014 International Conference on Mechatronics and Control (ICMC), IEEE*, 2014, pp. 1084–1089.
- [69] Chen, B. S., Tseng, C. S., and Uang, H. J., Robustness Design of Nonlinear Dynamic Systems via Fuzzy Linear Control, *IEEE Transactions on Fuzzy Systems*, Vol. 7, No. 5, 1999, pp. 571–585.
- [70] Tanaka, K., Taniguchi, T., and Wang, H. O., Robust and Optimal Fuzzy Control: A Linear Matrix Inequality Approach, *1999 International Federation of Automatic Control IFAC, World Congress, Beijing, July 1999*, pp. 213–218.
- [71] Park, Y., Tahk, M.-J., and Park, J., Optimal Stabilization of Takagi-Sugeno Fuzzy Systems with Application to Spacecraft Control, *Journal of Guidance, Control, and Dynamics*, Vol. 24, No. 4, 2001, pp. 767–777.
- [72] Ousaloo, H. S., Attitude Control of a Small Satellite with Uncertainly Dynamic Model using Fuzzy Logic Strategy, *2011 2nd International Conference on Control, Instrumentation and Automation, Shiraz*, 2011, pp. 68–73.
- [73] Zhang, X. and Zeng, M., Multi-Objective Control of Spacecraft Attitude Maneuver Based on Takagi-Sugeno Fuzzy Model, *CEAI*, Vol. 14, No. 1, 2012, pp. 31–36.

- [74] Kane, T. R., Dynamics of Nonholonomic systems, *Trans. ASME, Journal of Applied Mechanics*, Vol. 28, No. 4, 1961, pp. 574–578.
- [75] Jourdain, P. E. B., Note on an Analogue at Gauss Principle of Least Constraint, *Quarterly Journal on Pure Applied Mathematics*, Vol. 40, 1909, pp. 153–197.
- [76] Kane, T. R., and Levinson, D. A., Formulation of Equations of Motion for Complex Spacecraft, *Journal of Guidance, Control, and Dynamics*, Vol. 3, No. 2, 1980, pp. 99–112.
- [77] Huston, R. L., *Multibody Dynamics*, Butterworth-Heinemann, Boston, 1990.
- [78] Josephs, H. and Huston, R. L., *Dynamics of Mechanical Systems*, 2002.
- [79] Kane, T. R., Partial Rates of Change of Position and of Orientation, *Bulletin of Mechanical Engineering Education*, Vol. 11, No. 17, 1960, pp. 17–24.
- [80] Zhukovskii, N. E., On the Motion of a Rigid Body Having Cavities Filled with a Homogeneous Liquid, *Collected Works*, Vol. 29, 1936.
- [81] Okhotsimskidi, E., Theory of the Motion of a Body With Cavities Partially Filled with a Liquid, NASA TT F-33, 1960.
- [82] Mazmanyán, L. and Ayoubi, M. A., Attitude Motion of a Spinning Spacecraft with Fuel Sloshing in High-G Maneuvers, *AAS/AIAA Astrodynamics Specialist Conference*, Hilton Head, South Carolina, 2013, Vol. 150, pp. 793–812.
- [83] Schaub, H. and Junkins, J. L., *Analytical Mechanics of Aerospace Systems*, AIAA Education Series, 2002.
- [84] Gahinet, P., Nemirovski, A., Laub, A. J., and Chilali, M., *LMI Control Toolbox*, Math Works, 1995.

- [85] Löfberg, J., YALMIP: A Toolbox for Modeling and Optimization in MATLAB, *In Proceedings of the IEEE International Symposium on Computer Aided Control System Design*, Taipei, Taiwan, 2004, pp. 284–289.
- [86] Mazmnyan, L. and Ayoubi, M. A., Fuzzy Attitude Control of Spacecraft with Fuel Sloshing via Linear Matrix Inequalities, *IEEE Transactions on Aerospace and Electronic Systems*, 2018. Available: <http://dx.doi.org/10.1109/TAES.2018.2820419>
- [87] Franklin, G. F., Powell, J. D., and Emami-Naeini, A., *Feedback Control of Dynamic Systems*, Prentice Hall, Upper Saddle River, NJ, 4th edition, 2002.
- [88] Ogata, K., *Modern Control Engineering*, Fifth Edition, Prentice. Hall, 2010.
- [89] Nesterov, Y. and Nemirovskii, A., *Interior-Point Polynomial Algorithms in Convex Programming*, SIAM, Philadelphia, Pennsylvania, 1994.
- [90] Toh, K. C., Todd, M. J., and Tutuncu, R. H., SDPT3 – A Matlab Software Package for Semidefinite Programming, *Optimization Methods and Software*, Vol. 11/12, 1999, pp. 545–581.
- [91] Tutuncu, R. H., Toh, K. C., and Todd, M. J., Solving Semidefinite-Quadratic-Linear Programs using SDPT3, *Mathematical Programming*, Vol. 95, 2003, pp. 189–217.
- [92] Mehrotra, S., On the Implementation of a Primal-Dual Interior Point Method, *SIAM Journal on Optimization*, Vol. 2, 1992, pp. 575–601.
- [93] Hervas, J. R. and Reyhanoglu, M., Observer-Based Nonlinear Control of Space Vehicles with Multi-Mass Fuel Slosh Dynamics, *2014 IEEE 23rd International Symposium on Industrial Electronics (ISIE)*, 2014, pp. 178–182.
- [94] Marsell, B., Griffin, D., Schallhorn, P., and Roth, J., High Accuracy Liquid Propellant Slosh Predictions Using an Integrated CFD and Controls Analysis Interface, Document

ID 20120010782. Cocoa Beach, FL: NASA Kennedy Space Center; Pasadena, CA: Jet Propulsion Laboratory, 2012.

[95] Vandenberghe, L. and Boyd, S., Semidefinite Programming, *SIAM Review*, Vol. 38, No. 1, 1996, pp. 49–95.

[96] Mazmanyán, L. and Ayoubi, M. A., Robust and Optimal Rule-Based Attitude Control of Spacecraft with Partially-Filled Tanks, To be presented at the *AAS/AIAA Astrodynamics Specialist Conference*, Snowbird, Utah, 2018.

Vita

Lilit Mazmanyanyan earned her Bachelor's, Master's and Candidate of Physical and Mathematical Sciences degrees in the Faculty of Mathematics and Mechanics at Yerevan State University (YSU) in Armenia. Afterwards, she was a junior researcher at YSU in differential game theory applied to elastic bodies. Meantime, Lilit completed her Master of Engineering degree in Industrial Engineering & Systems Management at American University of Armenia (AUA). Later, she was a research associate in sequencing and scheduling and lecturer in industrial engineering and systems management at AUA. Recently, she completed her internship in Stinger Ghaffarian Technologies (SGT) at NASA Ames Research Center, Intelligent Systems Division. Currently, Lilit is Ph.D. Candidate in the Department of Mechanical Engineering at Santa Clara University. She is a Packard Research Engineering Fellow. Her current research interest includes spacecraft dynamics and nonlinear, optimal and intelligent control.

Publications and presentations:

- 1 Mazmanyanyan, L. and Ayoubi, M. A., Fuzzy Attitude Control of Spacecraft with Fuel Sloshing via Linear Matrix Inequalities, *IEEE Transactions on Aerospace and Electronic Systems*, 2018. Available: <http://dx.doi.org/10.1109/TAES.2018.2820419>
- 2 Mazmanyanyan, L. and Ayoubi, M. A., Robust and Optimal Rule-Based Attitude Control of Spacecraft with Partially-Filled Tanks, To be presented at the *AAS/AIAA Astrodynamics Specialist Conference*, Snowbird, Utah, 2018.
- 3 Mazmanyanyan, L. and Ayoubi, M. A., Takagi-Sugeno Fuzzy Model-Based Attitude Control of Spacecraft with Partially-Filled Fuel Tanks, *AIAA/AAS Astrodynamics Specialist*

Conference, San Diego, California, August 4–7, 2014, Vol. 2, pp. 1227–1240.

- 4 Mazmanyán, L. and Ayoubi, M. A., Attitude Motion of a Spinning Spacecraft with Fuel Sloshing in High-G Maneuvers, *AAS/AIAA Astrodynamics Specialist Conference*, Hilton Head, South Carolina, 2013, Vol. 150, pp. 793–812.